Novel Microwave Passive Devices For Dual-Band Applications

WONG, Fai Leung

A Thesis Submitted in Partial Fulfillment
of the Requirements for the Degree of
Doctor of Philosophy
in
Electronic Engineering

The Chinese University of Hong Kong
July 2011

ProQuest LLC.
789 East Eisenhower Parkway
P.O. Box 1346
Ann Arbor, MI 48106 - 1346

Abstract

Microwave passive couplers are widely used in microwave and millimeter-wave applications and communication systems. Common examples are branch line coupler, rat race coupler, power divider, and crossover junction. They are used for the dividing, combining and re-directing of signal power.

Very often, a passive coupler utilizes simple quarter-wavelength transmission lines for implementation which will lead to narrow-band operation. Therefore, it is difficult to deploy such circuit for wide-band or multi-band applications. Multi-section topologies may be used to broaden the operating bandwidth, with which the major drawbacks are enlarged circuit size and the requirement of extreme high (or low) branch-line characteristic impedances. Both are not attractive for mass and low cost production. Conventional design approaches are, therefore, not suitable for modern communication systems with multi-band operation.

For size miniaturization and cost reduction, the design of dual band devices has become an emerging research area in recent years. A desirable dual-band solution should offer size compactness, high performance (e.g. low insertion loss) and compatible with conventional printed circuit broad (PCB) technology, especially microstrip lines.

In this research, several new devices, including rat-race coupler, power divider and crossover junction, capable of operating at dual frequency bands are proposed. These structures involve only simple branch-line sections and a minimal number of shunt stubs. All characteristic impedances are ranged from 20 Ω to 100 Ω. Most designs can

operate with wide frequency spacing between the two bands. These designs offer low insertion loss as well as good return loss performances, and are small in size, in compared to the broadband approach. For design purposes, explicit closed-form equations are derived for the evaluation of circuit parameters. In addition, the usable range of these devices with respect to frequency band separation is examined. For verification, various prototypes are constructed by using microstrip technology and in-house fabrication facilities. Both simulated and measured results are presented and compared with state-of-the-art examples.

摘要

被動式耦合器被廣泛應用於微波和毫米波通訊領域中。常見的被動式耦合器包括分支綫耦合器、鼠徑耦合器、Wilkinson 功率放大器及交越接合。它們可用作結合、分解或轉移訊號。

被動式耦合器一般由四分之一波長的傳輸線組成，所以頻率帶寬較窄，因此很難應用於寬帶的通訊系統中。儘管多段式被動耦合器頻率帶寬較大，但電路尺寸會相應增大，而且個別的分支線特徵阻抗太小／大，不利於大量低成本生產。傳統的被動耦合器，不可能用於雙波段、甚至多波段的應用。

由於能降低設計尺寸和增加頻率帶寬，雙帶耦合器的設計成爲了近年來新興的研究方向。一個良好的雙帶耦合器設計應該具備：尺吋小、高效能（例如：低損耗）和可以傳統印刷電路版技術生產，尤其是微帶線。

這篇論文提出了數款新穎的雙帶設計，包括鼠徑耦合器、功率分配器和交越接合。它們均只由簡單的傳輸線，加插額外的分流支段組成。所有傳輸線的特性阻抗由 20 歐姆至 100 歐姆之間，而大部分設計均能在運作頻率相距很濶的條件下工作。比較傳統的設計，所有雙帶耦合器都具有低損耗、高端口隔離度及高回波損耗、與尺寸較小的特性。

另外，新提出的功率分配器通過使用雙帶轉換器代替四分之一波長傳輸線，達致在兩個頻段提供 3 分貝的功率分配。最後，雙波段交越接合是一個全新的結構，與傳統的單頻帶的大小相若，但能夠在雙頻帶工作。

本論文提供了所有數學分析和設計方程式的推導步驟，並審視了各個設計的有效運作頻帶的範圍。同時，爲了核實理論，幾個設計透過微帶線技術製造，並進行驗證，展示、比較模擬仿真結果和測量結果。

Table of Contents

List of figures

Acknowledgement

It is indeed true that completing a PhD degree is not easy. The whole process was always full of frustrations, puzzles and loneliness. Striking a balance between my PhD degree, research work and full time job was the biggest challenge. Frankly speaking, I could not pass through all the hardships and the achievement would not have become a reality without support from all.

I would like to take this opportunity to thank my supervisor, Professor Michael Cheng, for his guidance and patience given to me during my study. Professor Cheng was my supervisor of final year project during undergraduate and MPhil degree as well. He always enlightened me with his advices and suggestions when I got confused with my research work. It is generous of him to keep an eye on my research progress when I worked outside school. I am really appreciated with his generous support.

I would like to express my gratitude to Professor Keli Wu, the other teacher in microwave laboratory for his valuable comments.

In addition, I am indebted to my colleagues, for their support and company: Carlos Law, Ka-fai Chang, Leo Fung, Tony Cheng, Kitty Leung, Anita Yim and Au-yeung Chung Fai. We worked together in the laboratory and shared tears and joys in research life.

Last but not least, I would like to thank my parents for their unlimited support and love.

Chapter 1. Introduction

Passive couplers are useful components for the realization of microwave systems. Some passive couplers can combine or divide signals with certain phase relationship, like branch line couplers, rat race couplers and Wilkinson power dividers. On the other hand, some devices are used to re-direct a small portion or the whole of the input power, such as directional couplers and crossover junctions. Couplers are widely used in the design of microwave circuits, including balanced amplifiers, double-balanced mixers, modulators and antenna array [1].

There are numerous technologies for the construction of passive couplers, including waveguide, stripline, coaxial lines, microstrip, etc. The choice of realization method depends on applications, cost, and required performance. Among these methods, microstrip is a very popular planar technology as it can offer low fabrication cost, ease of construction, and compatibility with other active circuits to form highly integrated microwave circuits and sub-systems.

Nonetheless, a passive coupler usually composes of sections of quarter-wavelength transmission lines which lead to bulky size. The situation is even worse when the coupler is designed for low frequency operation. In addition, couplers based upon simple quarter-wavelength transmission lines usually exhibit narrow bandwidth

(~20%) and therefore its applications to wideband and multi-band systems are greatly limited. The introduction of multi-section structure may help to enlarge the bandwidth of such devices, but at the expense of circuit size.

Much effort has been devoted to improve the design and performance of couplers, including size reduction [2-4] and bandwidth enhancement [5-7]. In recent years, dual-band or multi-band couplers have also been proposed for use in modern communication systems due to their small size and ability to handle signals located at widely separated frequency bands. Various dual-band designs have been introduced, including branch line couplers [8-10], rat race couplers [11-13], and Wilkinson power dividers [14-16]. The most common techniques for achieving dual-band operation involve the adoption of shunt stubs, coupled lines, or artificial transmission lines.

1.1. Rat race coupler

Rat race coupler (also known as rat race hybrid or 180° hybrid) is one of the most popular passive devices used in the design of microwave circuits or systems. The conventional rat race coupler design is generally a four-port network, which consists of three section of 90° and one section of 270° branch-lines, as depicted in Figure 1-1. The total circumference of such a coupler is one and a half wavelength long.

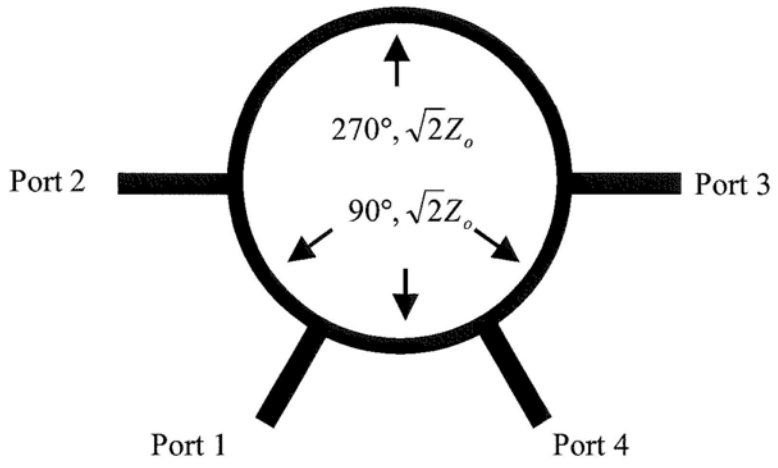

Figure 1-1: Conventional rat race coupler design

This coupler is often used for power division. When port 1 is defined as the input port, power is split into two in-phase components at port 2 and port 4 respectively, and no power is delivered to port 3. On the other hand, when port 3 is the input port, output power is equally split between port 2 and port 4, with out-of phase relationship. Port 1, in this case, becomes the isolated port.

In addition, a rat race coupler can be used for power combining, too. When microwave signals are injected into port 1 and port 3, they are superimposed and the sum (difference) of the signals will appear at port 2 (4). In general, a rat race coupler exhibits the following input-output relationships over the frequency band of interest:

$$|S_{21}| = |S_{41}| = |S_{23}| = |S_{43}| = \frac{1}{\sqrt{2}} \tag{1.1}$$

$$\angle S_{21} - \angle S_{41} = 0^\circ \tag{1.2}$$

$$\angle S_{23} - \angle S_{43} = 180^\circ \tag{1.3}$$

$$S_{11} = S_{22} = S_{33} = S_{44} = 0 \tag{1.4}$$

$$S_{13} = S_{31} = 0 \tag{1.5}$$

The corresponding S- matrix of a rat race coupler can be expressed by (1.6).

$$[S]_{rrh} = \frac{1}{j\sqrt{2}} \begin{bmatrix} 0 & 1 & 1 & 0 \\ 1 & 0 & 0 & -1 \\ 1 & 0 & 0 & 1 \\ 0 & -1 & 1 & 0 \end{bmatrix} \tag{1.6}$$

Figure 1-2 shows the general 4-port network representation (with line-of-symmetry XX`) of a rat-race coupler and Figure 1-3 illustrates the corresponding even- and odd-mode circuits. For the sake of analysis, the coupler is assumed to be lossless and reciprocal, and the port impedance is denoted as Z_0. Referring to the even and odd mode circuits, the s-parameters of the rat-race coupler can therefore be derived and expressed in terms of $\Gamma_{e,o}$, $T_{e,o}$ and $\tau_{e,o}$ as follows:

$$S_{11} = \frac{1}{2}(\Gamma_e + \Gamma_o) \tag{1.7}$$

$$S_{21} = \frac{1}{2}(T_e + T_o) \tag{1.8}$$

$$S_{31} = \frac{1}{2}(T_e - T_o) \tag{1.9}$$

$$S_{41} = \frac{1}{2}(\Gamma_e - \Gamma_o) \tag{1.10}$$

$$S_{22} = \frac{1}{2}(\tau_e + \tau_o) \tag{1.11}$$

$$S_{23} = \frac{1}{2}(\tau_e - \tau_o) \tag{1.12}$$

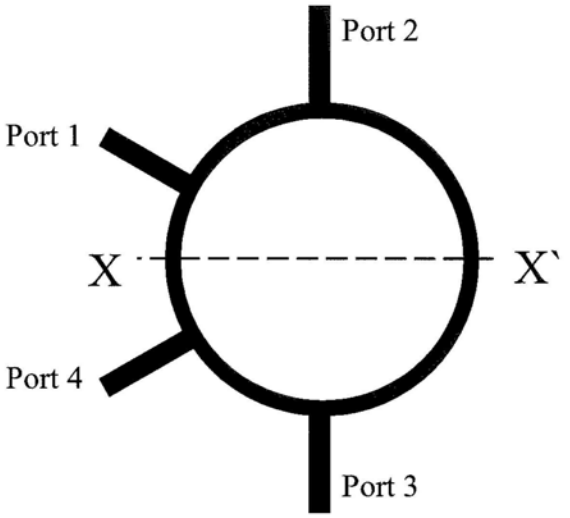

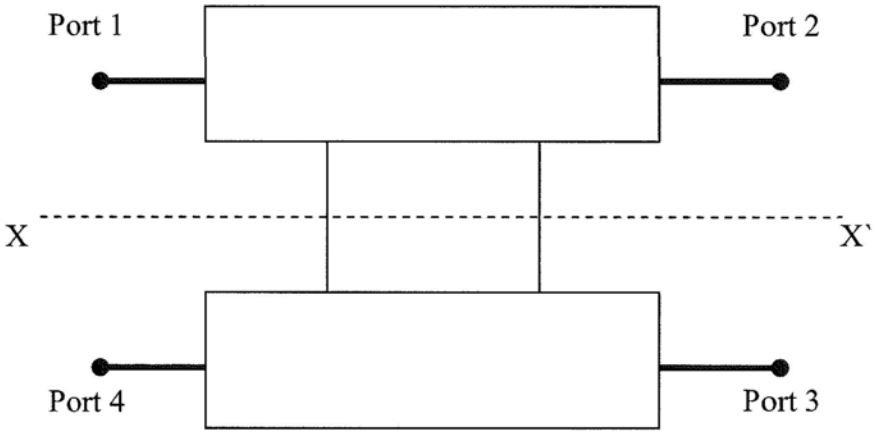

Figure 1-2: Rat race coupler for even-odd mode analysis with line of symmetry XX`

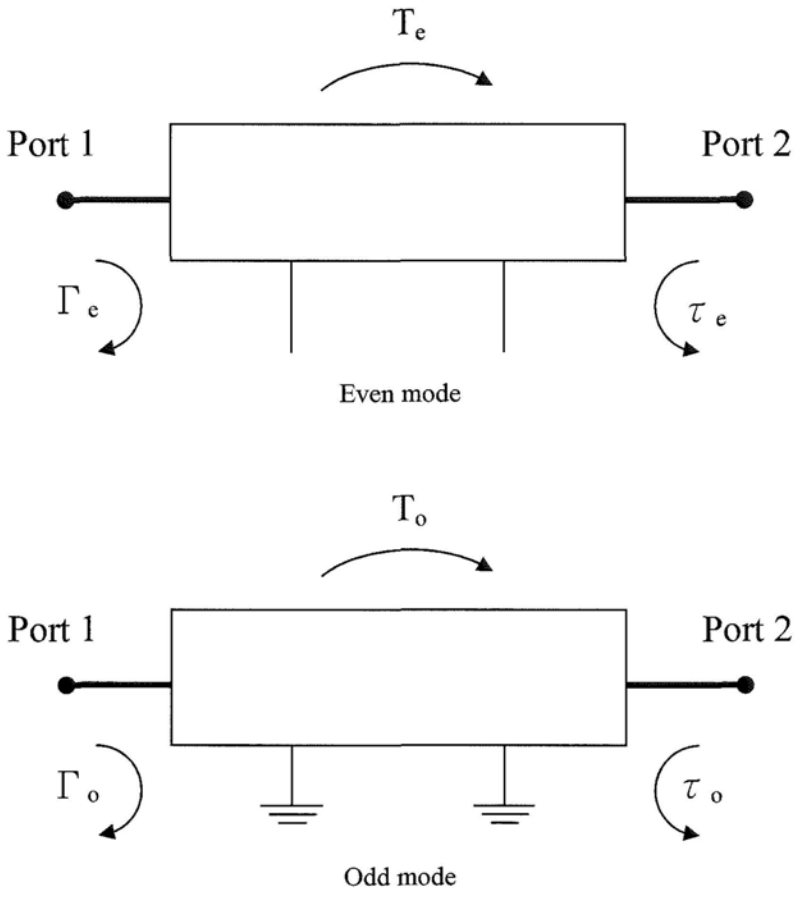

Figure 1-3: Reduced networks for even-odd mode analysis.

For illustration, Figure 1-4 to 1-8 show the simulated responses of a conventional rat-race coupler, with centre frequency of 1 GHz. The insertion loss of both output ports is -3dB at 1 GHz. When the tolerances of gain imbalance ($|S_{21} / S_{41}|$, $|S_{23} / S_{43}|$) and phase imbalance are set equal to ±0.5dB and ±5° respectively, the corresponding bandwidth is found to be about 16%. The absolute bandwidths of return loss (S_{11} and S_{22}) and port isolation (S_{31}) are approximately 280MHz and 320MHz, respectively, for a minimal requirement of 20dB.

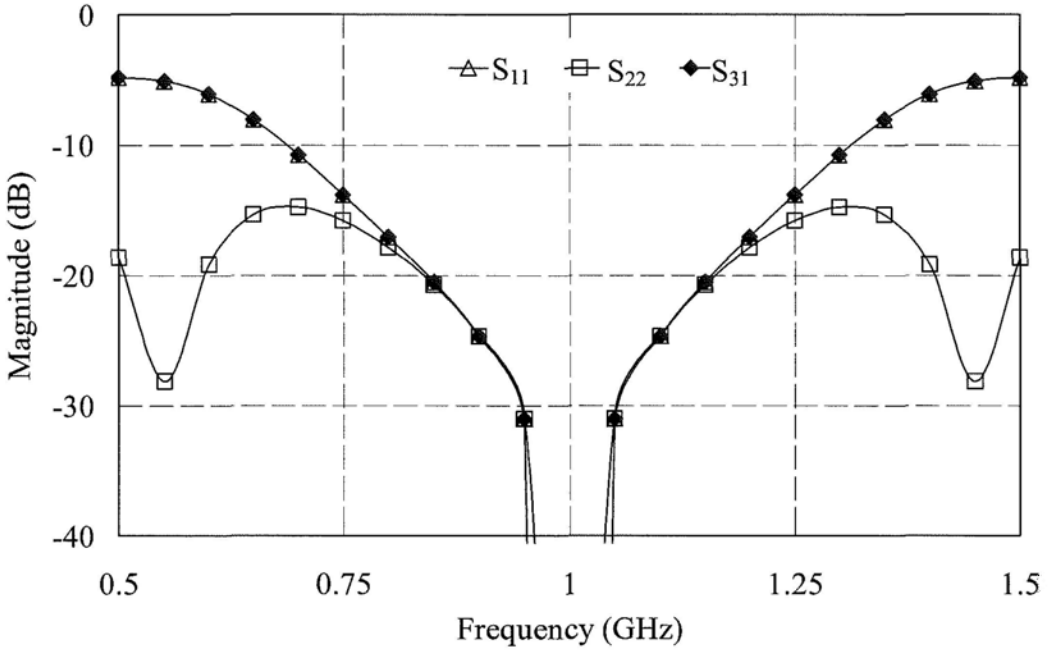

Figure 1-4: Simulated return loss and port isolation.

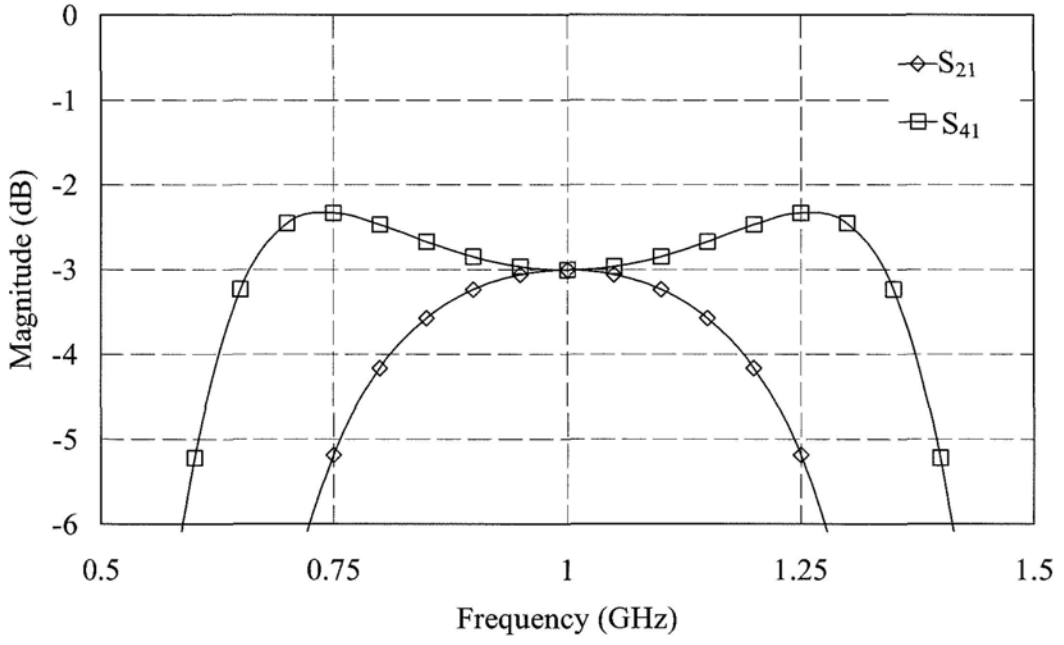

Figure 1-5: Simulated insertion loss of in-phase outputs.

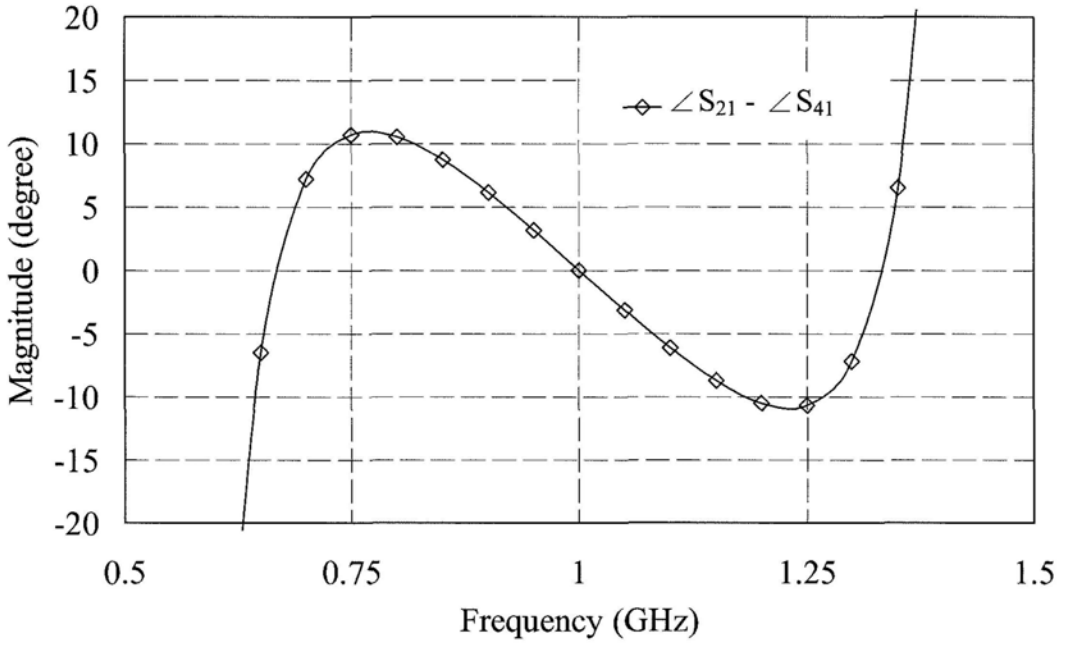

Figure 1-6: Simulated phase response of in-phase outputs.

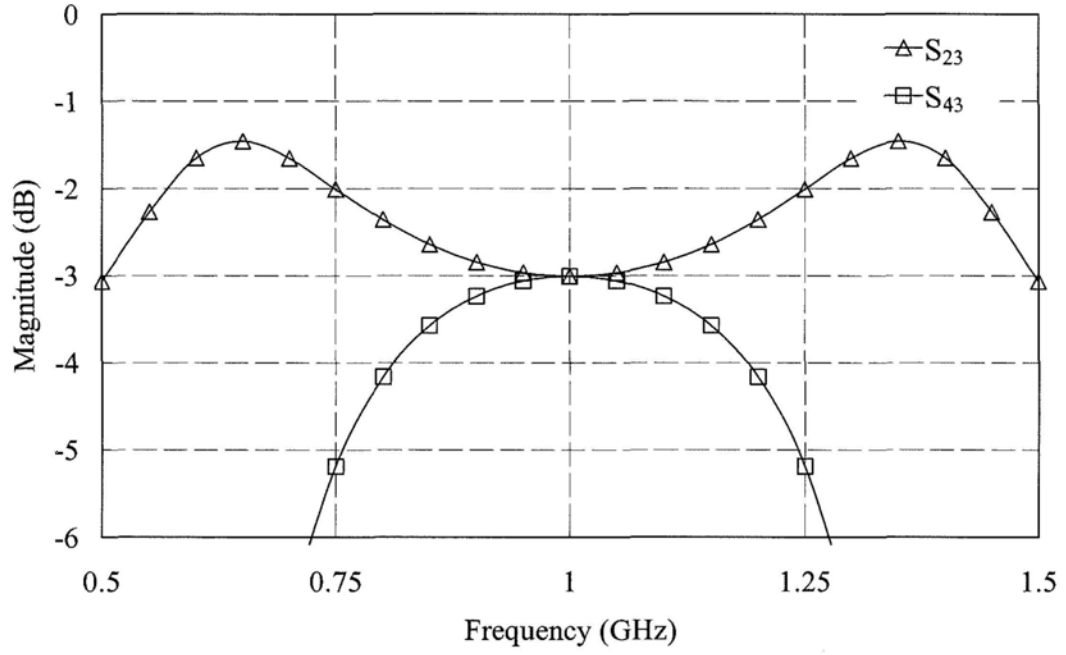

Figure 1-7: Simulated insertion loss of anti-phase outputs.

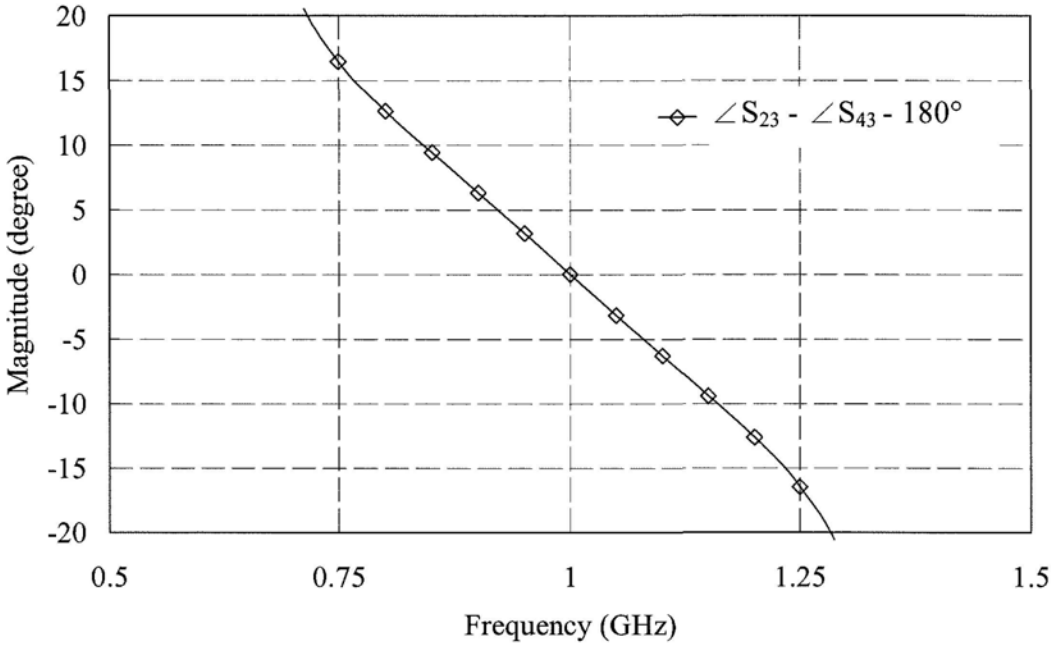

Figure 1-8: Simulated phase response of anti-phase outputs.

1.2. Wilkinson power divider

Wilkinson power divider, which was first invented in 1960s [24], is one of the most popular microwave devices for offering power dividing function. It features high return loss at all ports, high isolation between the two output ports, and low insertion loss. Besides the standard design, there are other power divider structures that can offer unequal power division [25-27] or multiple output ports [28-29].

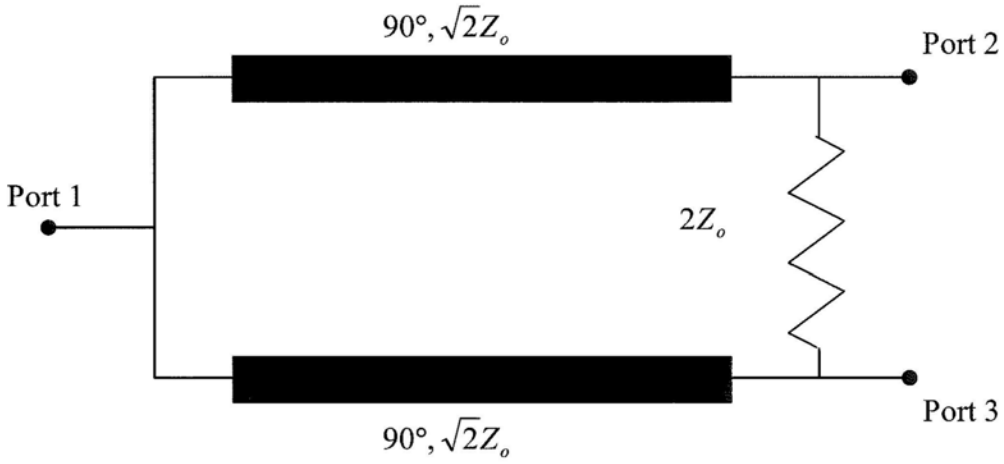

Figure 1-9: Conventional Wilkinson power divider design

Figure 1-9 shows the standard Wilkinson power divider design with two output ports and 3dB power division. Such three-port network is made of two quarter-wavelength branch-lines, with characteristic impedance of $\sqrt{2}Z_o$, and an internal resistor of $2Z_o$ for achieving good isolation between output ports.

To analyze the power divider network, even-odd mode formulation is applied to Figure 1-10 with line of symmetry XX`.

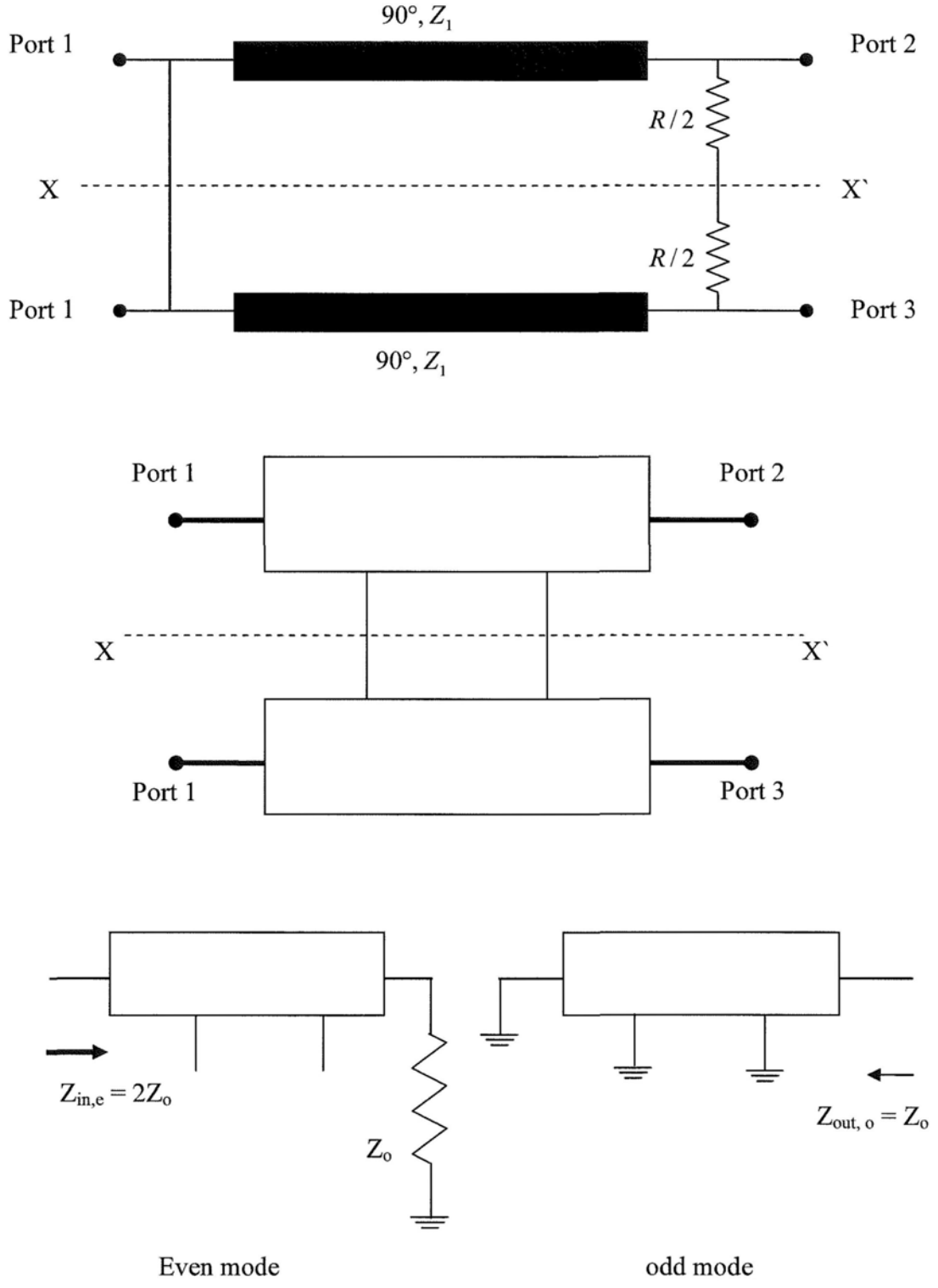

Figure 1-10: Wilkinson power divider - even and odd mode analysis.

Under the assumptions of perfect return loss and port isolation, the input impedance (even-mode) and output impedance (odd-mode) of the two half-circuits can simply be expressed by:

$$Z_{in,e} = 2Z_o \tag{1.13}$$

$$Z_{out,o} = Z_o \tag{1.14}$$

The corresponding s-parameters are given by:

$$[S]_{wpd} = \frac{1}{j\sqrt{2}}\begin{bmatrix} 0 & 1 & 1 \\ 1 & 0 & 0 \\ 1 & 0 & 0 \end{bmatrix} \tag{1.15}$$

Figure 1-11 shows the simulated responses of a conventional Wilkinson power divider with operating frequency of 1 GHz. Due to the relatively flat and low insertion loss performance, the operating bandwidth of the divider is thus mainly determined by the return loss and port isolation curves. Based on a minimal port isolation and return loss of 20dB, the available bandwidth of the divider is approximately 380 MHz, or 38%.

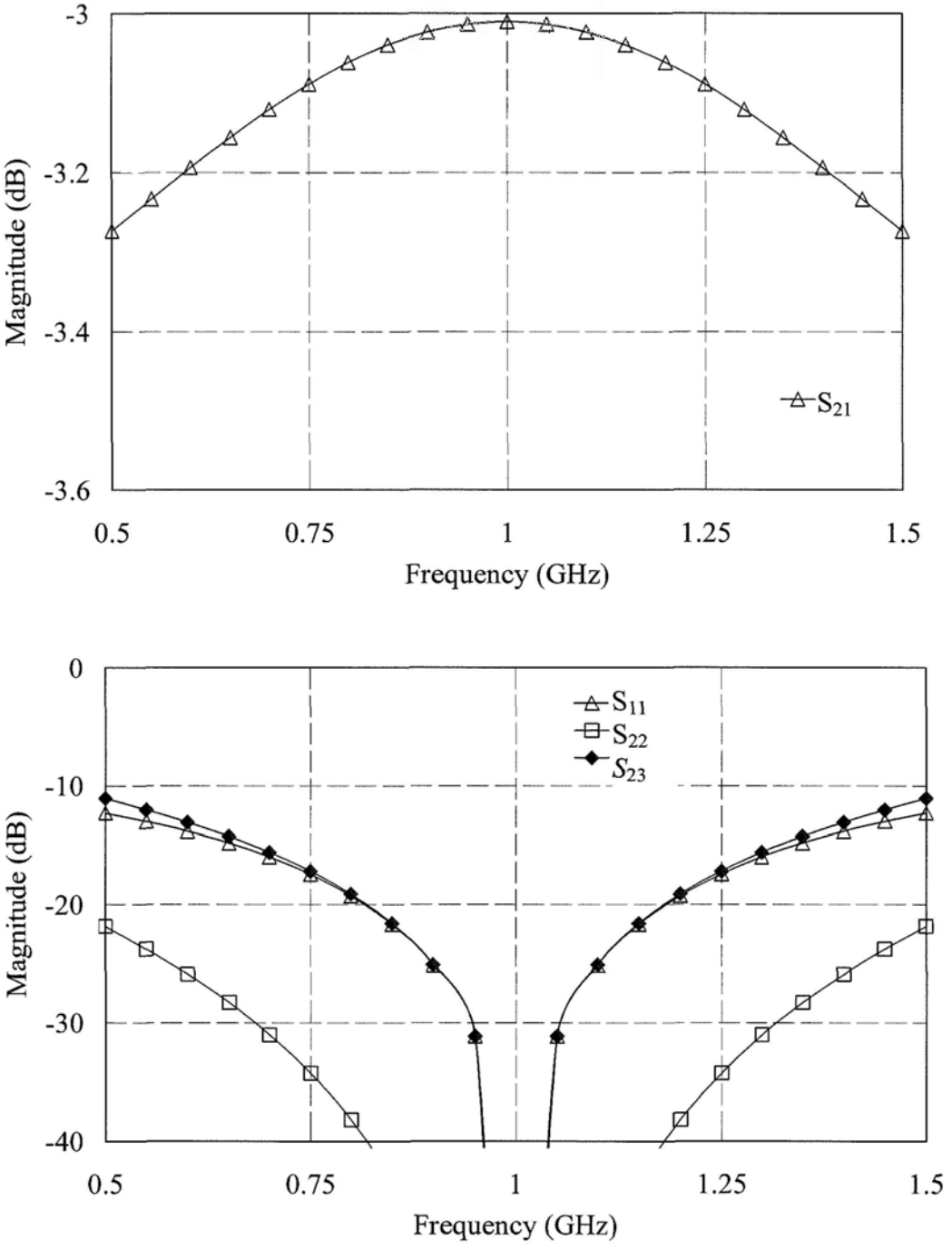

Figure 1-11: Simulated insertion loss, return loss and port isolation of conventional Wilkinson power dividers

1.3. Crossover junction

A crossover junction is one of the most fundamental components in microwave integrated circuit design. It may be employed in the design of a Butler matrix [30] for a switched-beam antenna array. The crossover of signal paths is usually realized by an air-bridge (bond-wire) or an underpass (different metallization in a multi-layer substrate). These non-planar approaches will certainly increase the fabrication cost. For a fully planar implementation, several crossover structures have been proposed in the past years including cascaded hybrid [31], "window" type 0-dB directional couplers [32-33], and symmetric four-port junctions [34-35].

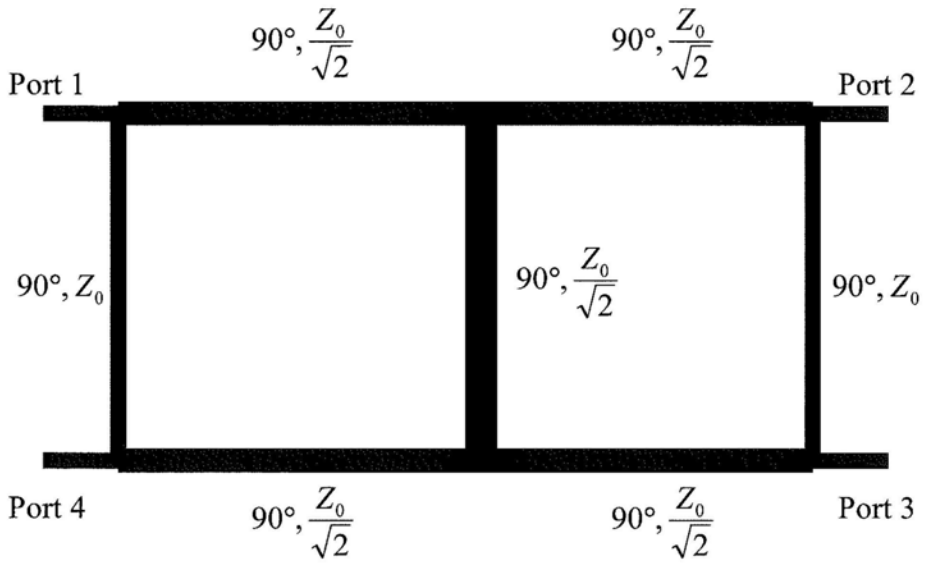

Figure 1-12: Standard crossover junction realized by cascaded-hybrid

Figure 1-12 illustrates the topology of a crossover junction realized by cascading two conventional branch line couplers. The size of this four-port network is double of the

convention branch line coupler, with a total circumference of one and a half wavelengths. Theoretically, all input power (port 1) is re-directed to port 3 (opposite port) with no power appearing at port 2 and port 4. The S-parameter matrix of a crossover junction is defined by (1.16).

$$[S]_{cj} = j\begin{bmatrix} 0 & 0 & 1 & 0 \\ 0 & 0 & 0 & 1 \\ 1 & 0 & 0 & 0 \\ 0 & 1 & 0 & 0 \end{bmatrix} \tag{1.16}$$

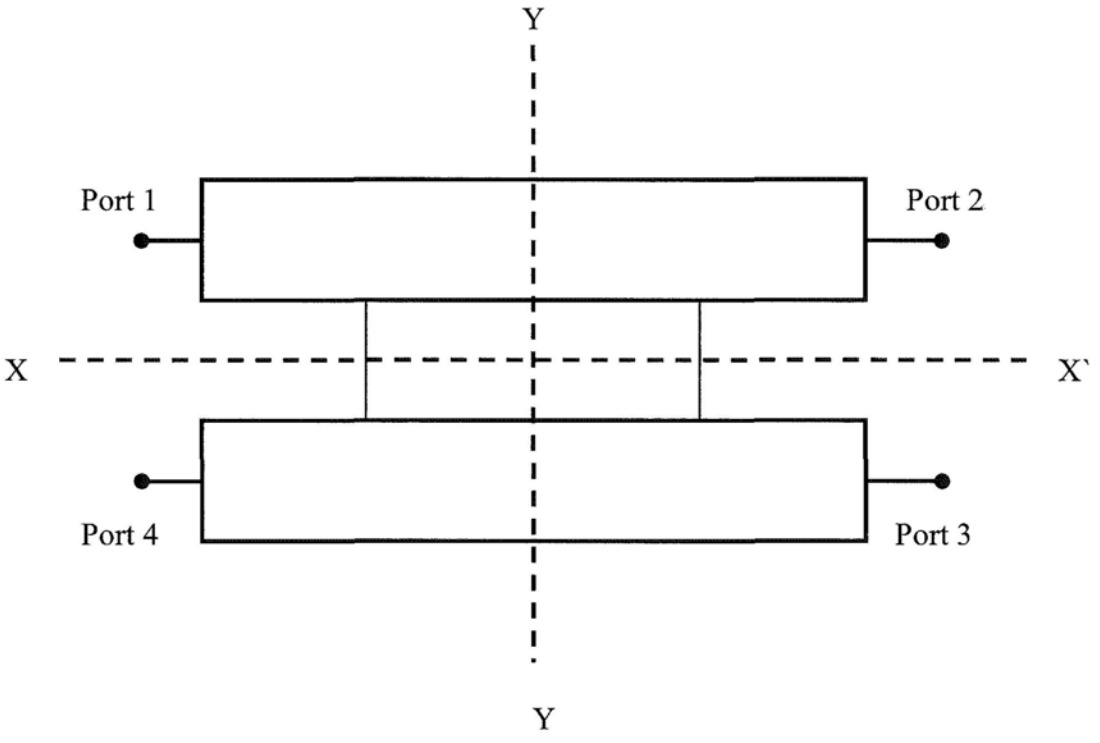

Figure 1-13: Crossover junction with bi-symmetry XX` and YY` for even-odd mode analysis

Figure 1-13 depicts, respectively, the 4-port representation (with bi-symmetry) and even-odd mode circuits of a crossover junction, For analysis purposes, the junction is

assumed to be lossless and reciprocal, with port impedance Z_0.

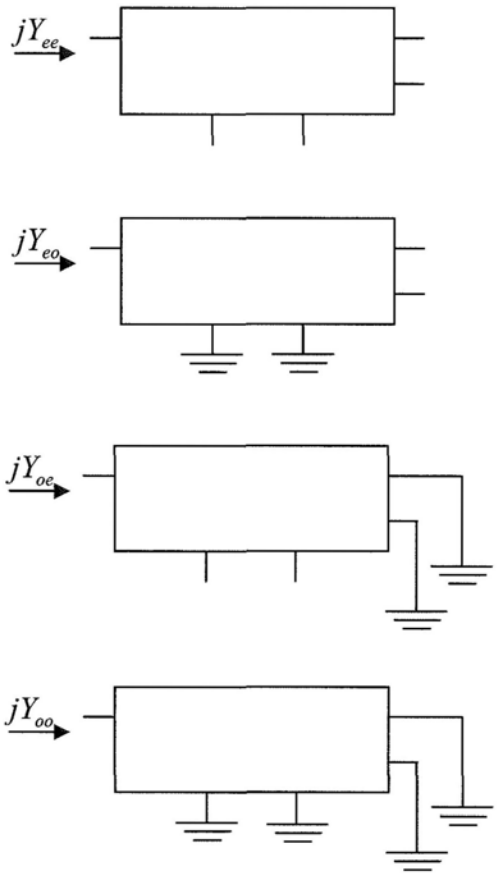

Figure 1-14: Reduced networks for analysis

Subsequently, the s-parameters of a crossover can now be expressed, in terms of the reflection coefficients of the corresponding even/ odd mode networks, as follows:

$$S_{11} = \frac{\tau_{ee} + \tau_{eo} + \tau_{oe} + \tau_{oo}}{4} \tag{1.17}$$

$$S_{21} = \frac{\tau_{ee} - \tau_{eo} + \tau_{oe} - \tau_{oo}}{4} \tag{1.18}$$

$$S_{31} = \frac{\tau_{ee} - \tau_{eo} - \tau_{oe} + \tau_{oo}}{4} \tag{1.19}$$

$$S_{41} = \frac{\tau_{ee} + \tau_{eo} - \tau_{oe} - \tau_{oo}}{4} \tag{1.20}$$

The reflection coefficients of the reduced networks are defined by:

$$\tau_{ee} = \frac{1 + jY_{ee}Z_o}{1 - jY_{ee}Z_o} \tag{1.21}$$

$$\tau_{eo} = \frac{1 - jY_{eo}Z_o}{1 + jY_{eo}Z_o} \tag{1.22}$$

$$\tau_{oe} = \frac{1 - jY_{oe}Z_o}{1 + jY_{oe}Z_o} \tag{1.23}$$

$$\tau_{oo} = \frac{1 + jY_{oo}Z_o}{1 - jY_{oo}Z_o} \tag{1.24}$$

A crossover junction operating at 1 GHz is designed and simulated by ADS (Figure 1-15). The insertion loss (from port 1 to port 3) is theoretically 0dB, and the operating bandwidth is found to be about 160 MHz for a maximum tolerance of 0.5dB. The bandwidths of all return loss performances are roughly the same, and approximately equal to 150 MHz based on a minimal requirement of 20dB. However, the bandwidth of port isolation (from port 1 to port 4, and port 1 to port 3) is relatively lower (~ 50MHz).

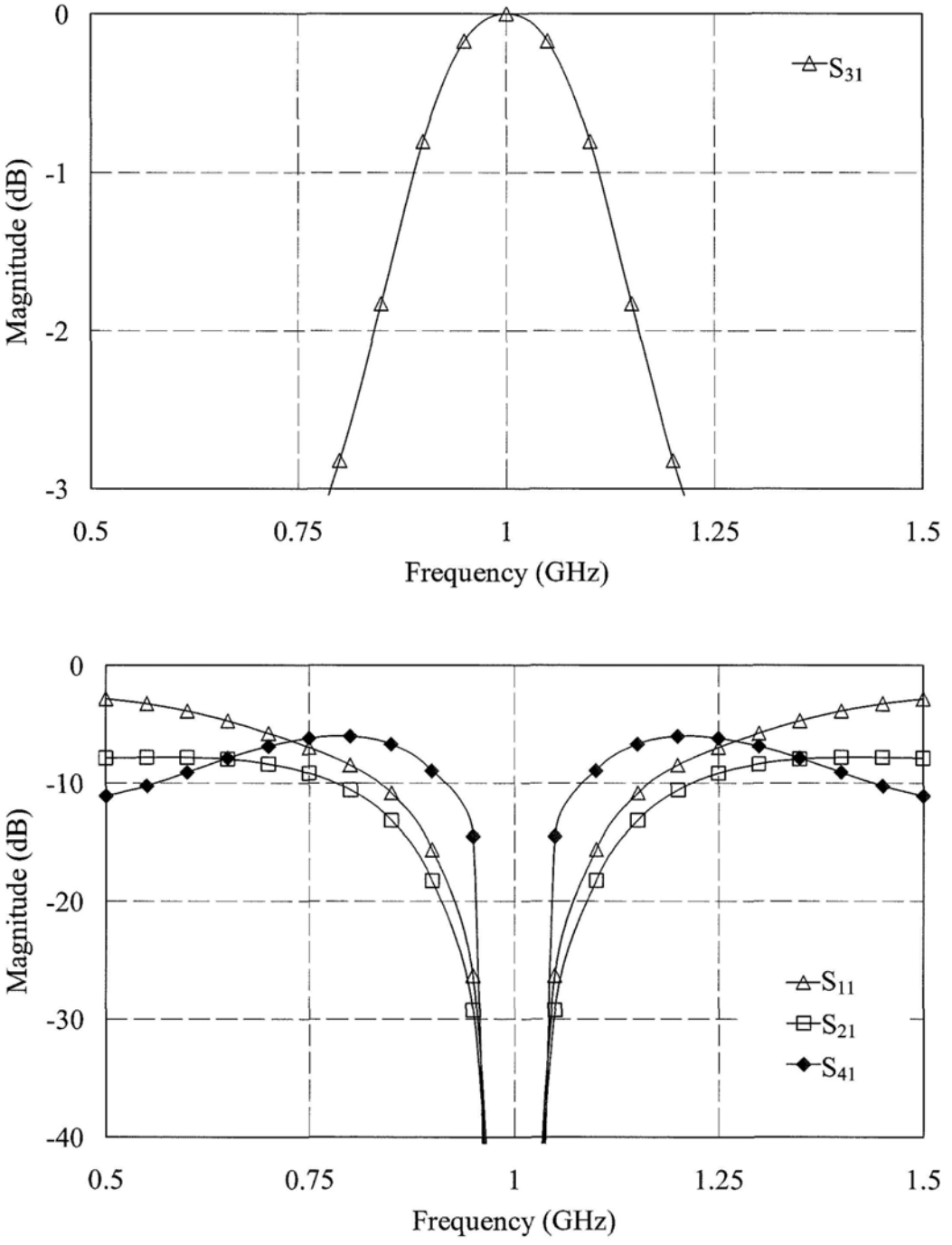

Figure 1-15: Simulated return loss, port isolation and insertion loss of a crossover junction.

1.4. Motivation of the research

Due to historical reasons, modern communication systems often operate at more than one frequency bands, like mobile applications (850MHz, 1800MHz and 2GHz). Although a wideband design may be deployed, it is certainly not an attractive system because of the following reasons:

- If a wideband device is used to cover two widely separated frequency bands, a large fractional bandwidth requirement will be needed. For example, assuming a wideband device is used to support a dual band application operating at 800 MHz and 1.2 GHz, a fractional bandwidth of, roughly 40% ($\frac{1.2\,GHz - 0.8\,GHz}{1\,GHz}$) is therefore required. This situation is even worse when the two frequency bands get further apart.
- A wideband device usually occupies more substrate area, which may lead to a increased fabrication cost and circuit size. In addition, a multi-section topology usually employs branch-line of extreme characteristic impedances. In practice, these circuits are more difficult to be realized by conventional fabrication technology due to the small width of strip conductors.
- A wideband device exhibits a flat frequency response over the entire operating band, and is unable to suppress unwanted signals with frequencies lying between the two designated bands.

Consequently, new microwave devices with compact size, dual frequency operation and inter-band rejection are more desirable for modern communication systems.

In this thesis, several dual-band devices are introduced including rat race couplers, power divider and crossover junction. They feature low insertion loss, easy to fabricate, and compactness in compared to the conventional circuits. Chapter 2 reviews some of the recent works reported by others. Chapter 3 to 5 provides the detailed design and performance study of the proposed dual-band circuits (rat-race couplers, power divider and crossover). The derivation of the closed-form design equations is presented. Simulation results of the proposed designs are given to verify the design equations and to examine the applicable range of operating frequencies. To accommodate the parasitic effects of junction discontinuities, comprehensive layout simulation based upon a full-wave electromagnetic solver is also incorporated. For experimental verification, the proposed circuits were fabricated using Duroid substrate, with dielectric constant of 3.38 and thickness of 0.8 mm. Circuit performance was characterized by scattering-parameter measurement, using Agilent E5071C 4-port network analyzer over the frequency range of interest. Chapter 6 concludes work and makes recommendation for further research.

Chapter 2. Literature Review

In the past decades, much effort has been devoted to the realization of single-band coupler circuits with reduced size and enlarged bandwidth. For further size miniaturization, dual-band designs have been proposed in recent years. These dual-band circuits are mainly based on the adoption of shunt stub, semi-lumped components, or coupled lines.

In 2004, a dual-band impedance transformer was proposed by the authors [8], which composes of a serial line and two shunt stubs. This transformer was applied to the design of branch-line coupler with dual-frequency property. Unfortunately, such transformer cannot be adopted in the design of dual-band rat-race coupler or Wilkinson power divider, due to the extreme high branch-line impedance involved.

In the following years, several new dual band devices, including branch-line couplers, rat-race couplers, power dividers and crossover have been developed by different research teams all over the world. In this chapter, the design theories, implementation procedures, as well as the electrical performances of these devices, are reviewed.

2.1 Dual-band microstrip rat-race coupler using step-impedance transformer

Conventional rat-race coupler is basically composed of four branch-lines (three of them are 90° long and the fourth one is 270° long) of equal characteristic impedance ($\sqrt{2}Z_o$). In [11], a step-impedance transformer and two shunt admittances were combined to form a basic cell (Figure 2-1), which exhibited an electrical length of 90° at two different frequencies, denoted as f_1 and f_2.

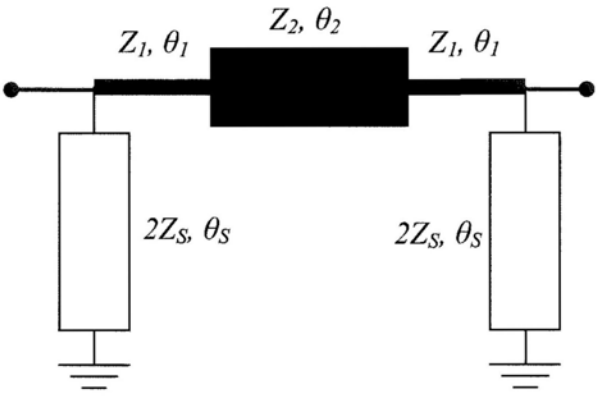

Figure 2-1: Proposed pi network for quarter wavelength transformer [11].

The proposed cell was used to replace branch-lines in a conventional rat-race coupler. The modified rat race coupler can offer dual frequency operation, but with a compact structure, as illustrated in Figure 2-2.

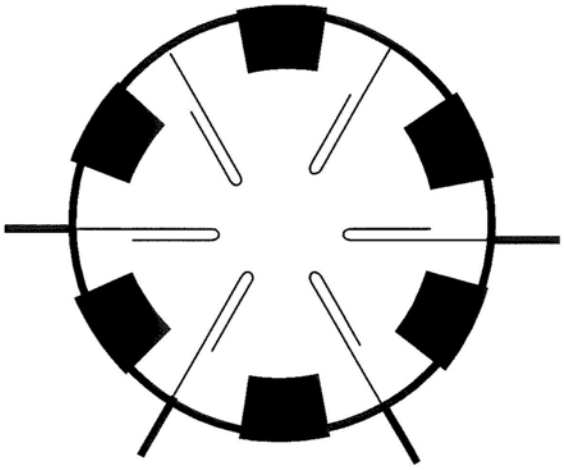

Figure 2-2: Dual band rat-race coupler using basic cells [11].

The design parameters of the basic cell include the impedance ratio (R) of the step impedance transformer, the electrical lengths of the transformer (θ_1 and θ_2) , the characteristic impedance (Z_S) and the electrical lengths (θ_S) of the shunt stubs. It was observed that a higher impedance ratio can lead to a shorter step-impedance transformer, and resulting in a compact design. For illustration, the circuit parameters of a dual-band rat-race coupler operating at 2.45 GHz and 5.2 GHz are listed in the following table:

R	θ_1(°)	Z_1 (Ω)	Z_2 (Ω)	θ_S(°)	Z_S (Ω)
1	23.8	83.7	83.7	57.7	104.4
4	15.3	143.5	35.9	64.5	111.8

Table 2-1: Design example: circuit parameters of the dual-band rat-race coupler [11].

For a dual-band coupler with R=1 and R=4, size reduction of 59% and 79% can be achieved, in compared to the conventional rat-race circuit operating at 2.45 GHz. This design features substantial size reduction, especially when R is large. However, a high value of R implies the need of extreme branch-line impedances (see Table 1-1), which imposes difficulty in fabrication. Furthermore, this structure involves several junction discontinuities and may further degrade the performance of the rat-race coupler, in particular, the upper frequency band.

2.2 Dual-band rat-race coupler using coupled microstrip line

In [12], a new basic cell based upon coupled-line structure was proposed for the implementation of dual-band couplers.

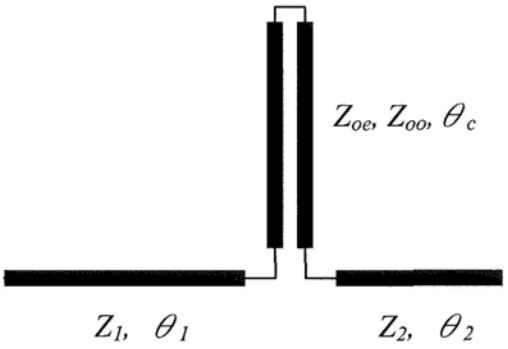

Figure 2-3: Coupled-line based quarter-wavelength impedance transformer [12].

Referring to

Figure 2-3, the basic unit consists of two serial sections of branch-line, and a microwave C-section. The C-section is actually a two-port network formed by a coupled line with connected ends. Due to its non-linear phase response with frequency, the proposed circuit can offer electrical length of 90° or 270°, by the proper selection of Z_{oo}, Z_{oe}, θ_c, θ_1 and θ_2. Hence, they can be employed to replace the quarter-wavelength branch-line in a conventional rat-race coupler, for the realization of dual-band couplers.

It was also shown that Z_1 and Z_2 can be expressed explicitly in terms of Z_{oo}, Z_{oe}, while

Z_{oo}, Z_{oe}, θ_c, θ_1 and θ_2 are interdependent variables. A small value of θ_c leads to an increased Z_{oe}, which imposes tight constraint on the gap size of the coupled line. On the other hand, a larger θ_c can reduce the value of θ. Therefore, this proposed design may offer dual-band operation as well as size reduction by the optimal choice of circuit parameters.

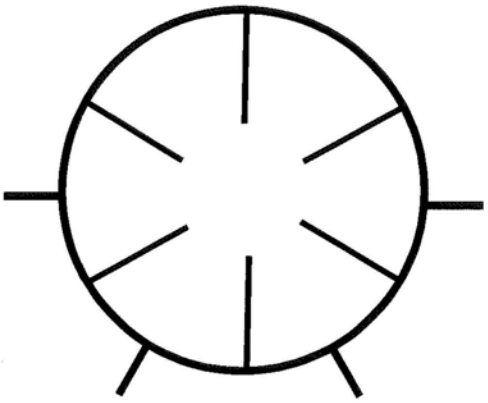

Figure 2-4: Dual band coupler design based upon microwave C-section [12].

The overall structure of the dual-band rat-race coupler design, with the adoption of the proposed unit, is illustrated in Figure 2-4. Two prototypes with frequency ratio of 2.2, were designed, fabricated and measured. The circuits were found to exhibit size reduction of 70%, in compared to the conventional designs operating at the lower frequency band. The return loss bandwidth (20dB requirement) of the upper and lower frequency bands were, respectively, 9% and 30%. The major drawback of this topology is the small gap size, in particular, when a thin substrate is being adopted.

2.3 Dual-band rat-race coupler using step-impedance stub-line

Figure 2-5 shows an alterative design of quarter-wavelength transformer based upon T-network and step-impedance shunt stub. This basic cell was employed for the realization of dual-band branch-line couplers as well as power dividers [35-37].

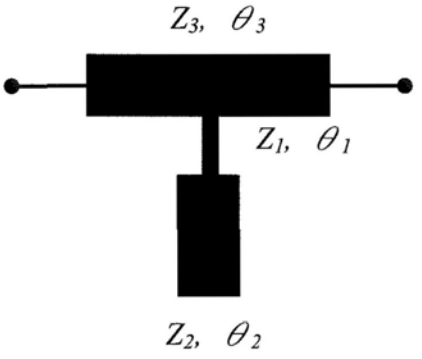

Figure 2-5: Dual-band quarter-wavelength impedance transformer using step impedance shunt stub.

In the basic cell design, there are a total of six circuit variables (Z_1, Z_2, Z_3, θ_1, θ_2 and θ_3) which allow increased flexibility in the design of dual-band coupler with size reduction, wide frequency band separation and more relaxed requirement on line impedance values.

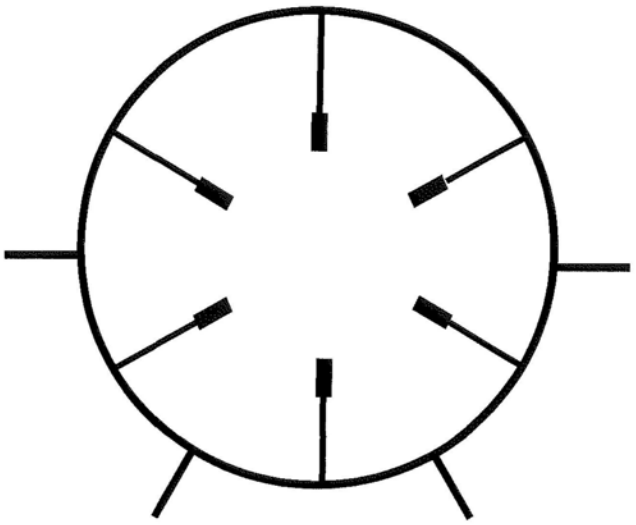

Figure 2-6: Dual-band rat-race coupler, based on step-impedance stub line [35].

Figure 2-6 shows the typical structure of a dual-band rat-race coupler implemented using step-impedance stub lines. Experimental circuits with centre frequencies of 2.4 GHz and 5.2 GHz were fabricated and characterized. The measurement results indicated that a low insertion loss (about 3.5dB), good return loss (about 20dB) and high port isolation (> 30dB) had been attained at both centre frequencies. Note that the large impedance ratio (Z_1 / Z_2) involved in the structure can introduce severe junction discontinuity effect and may further degrade its performance at higher operating frequencies.

2.4 Dual-band Wilkinson power divider with open/ short stubs

Dual band power dividers are capable of providing power division at the two designated frequency bands. The first dual-band power divider was constructed (Figure 2-7) by using a two-section dual-frequency impedance transformer [40]. Equal power division was realized but with degraded output return loss and port isolation.

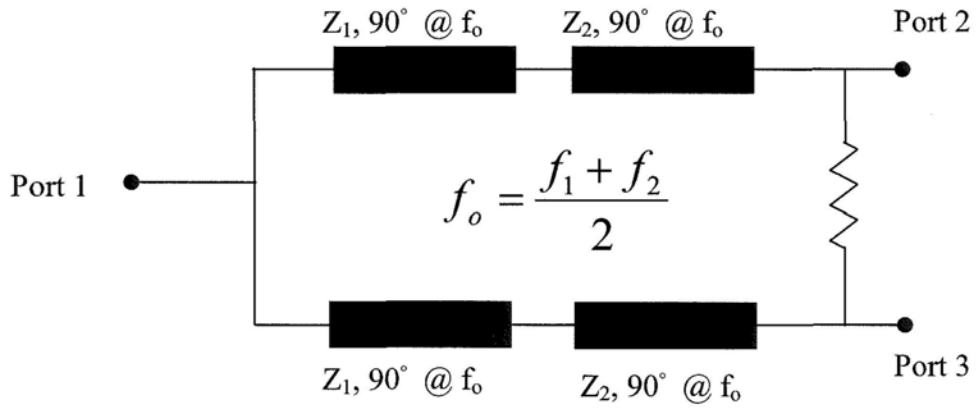

Figure 2-7: Dual-band power divider using impedance transformer proposed in [40].

In [38], a dual-band Wilkinson power divider was proposed, as given in Figure 2-8. The basic unit consists of two serial transmission lines and a shunt stub. It was used to replace the quarter-wavelength branch-line in a conventional Wilkinson power divider.

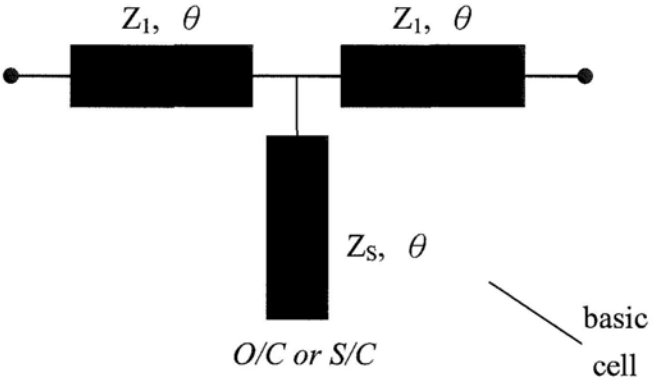

Figure 2-8: Dual-band quarter-wavelength transformer based on T-network [38].

The choices of θ and the types of stub (open / short) circuit are highly dependent on the intended frequency ratio (f_2/f_1) to be achieved, and the available range of line impedance. Transmission zeros are introduced by the shunt stubs but with entirely different frequency locations (short or open). The overall structure of the proposed dual-band power divider is shown in Figure 2-9.

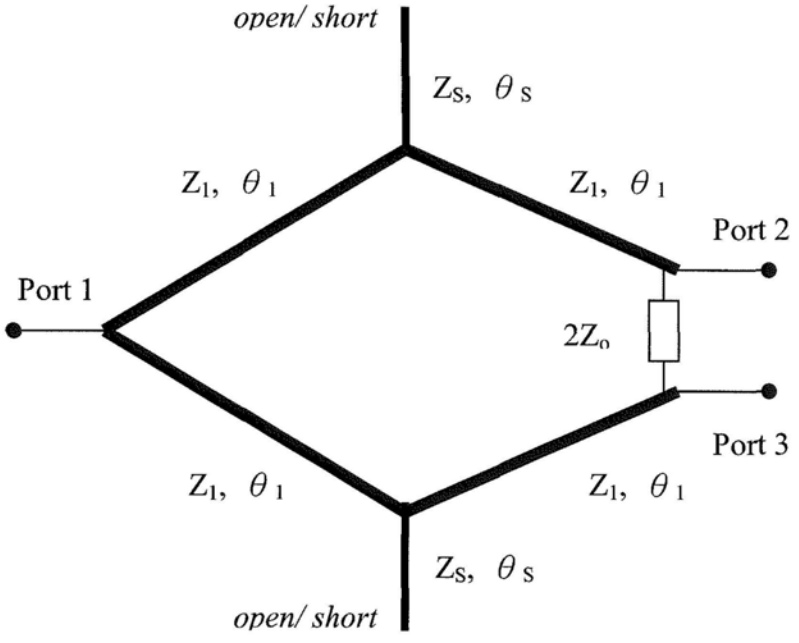

Figure 2-9: Proposed dual band power divider configuration [38].

Two prototypes, operating at the same frequency bands (1 GHz and 2 GHz), with open- and short-circuited stub were constructed. Theoretically, the transmission zero frequencies of the two designs were, 750 / 2250 MHz (open-circuited stub), and 330 / 3000 MHz (short-circuited stub). Low insertion loss (3.3dB), return loss of greater than 20dB, and port isolation of over 30dB were measured. Like the single-band approach, the output ports were connected to the isolation resistor ($2Z_o$) directly. Therefore, care must be taken in layout design, to avoid unnecessary coupling and discontinuity effect.

2.5 Dual-band power divider with extended branch-line

Figure 2-10 shows the design of a compact dual-band power divider [39].

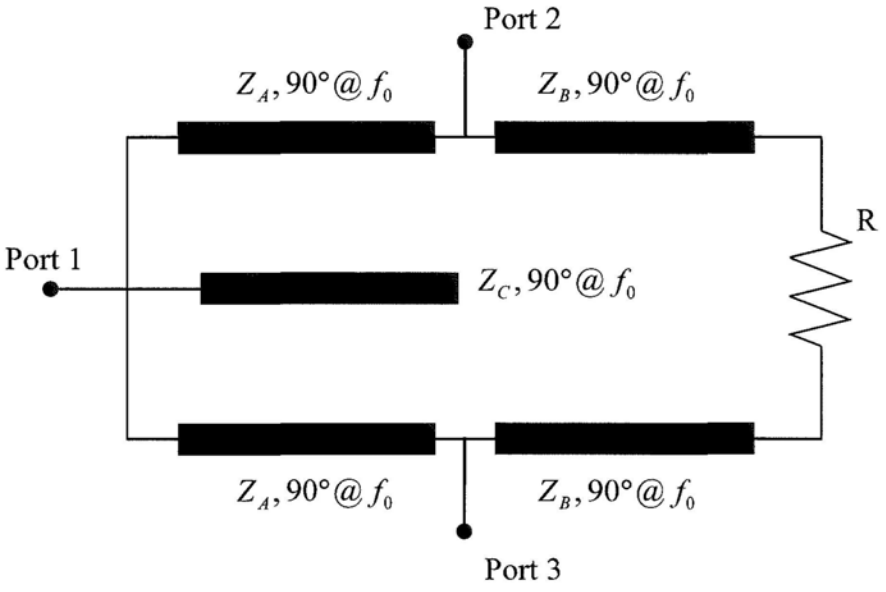

Figure 2-10: Dual band power divider with a simpler structure.

It basically consists of a shunt stub (open circuited), two extended branch-lines, and an isolation resistor. Dual-band operation is enforced by the proper selection of Z_A, Z_B, Z_C and R. This divider offers very low loss performance due to the absence of lumped reactive elements. In contrary to all previous designs [14-16], the output ports are widely separated from R by the extended branch-lines, with increased flexibility in layout design. The transmission zeros introduced by the shunt stub offers inter-band rejection. The proposed structure can easily be constructed over a wide range of frequency band ratio ($1.2 < f_2/f_1 < 3$), with practical values of line impedance (20 -

100Ω). The typical bandwidth of this power divider is roughly 5%, which is useful for narrow band applications. The performance of this divider was also found to be rather insensitive to the tolerances of circuit parameters (Z_A, Z_B and R).

2.6 Dual-band power divider using slow-wave structures

Slow-wave structures are widely used in microwave circuit designs for size miniaturization. Many slow-wave structures have been proposed [42-44] in recent years and applied to compact coupler designs. The slow-wave effect generally reduces the phase velocity of the propagating waves and hence engenders higher electrical lengths with smaller physical size. A common type of slow-wave structure, as given in Figure 2-11, is a transmission line loaded by open stubs. Those open stubs, serving as capacitive loading, alter the effective line capacitance per unit length and hence the phase velocity of the propagating signal. In other words, the same electrical length can be realized by an artificial transmission line of reduced physical length.

Figure 2-11: Slow-wave structure based upon capacitive loaded transmission line.

Note that the dispersive nature (amount of phase shift) and the cut-off frequency of the slow-wave structure are closely related to the number of cascaded cells and the stub length.

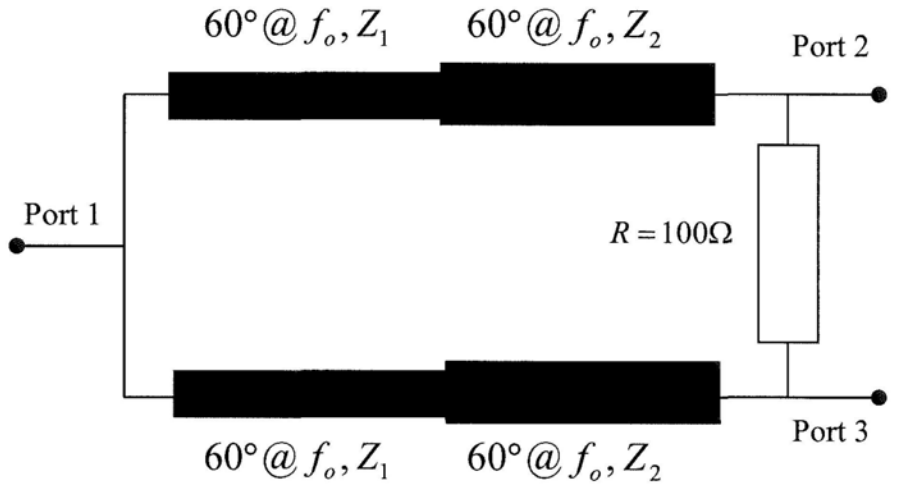

(a)

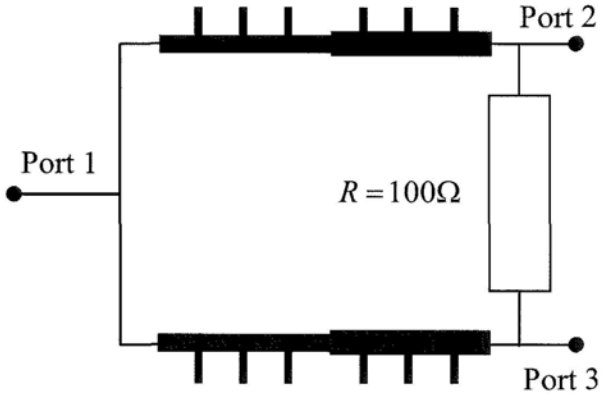

(b)

Figure 2-12: (a) Original dual-band Wilkinson power divider design, and, (b) Modified design with slow-wave structure.

Figure 2-12 illustrates the application of slow-wave structure to reduce the size of a conventional dual-band power divider. The modified power divider was prototyped and characterized [41]. It was found to operate at 850 MHz and 1960 MHz, with insertion loss of 3.3dB, return loss and port isolation of over 15dB, and size reduction of roughly 30%.

2.7 Single-band symmetrical compact crossover junction

Besides cascaded hybrid, several new crossover designs have been proposed in recent years with compact size or wider bandwidth. In [33], a symmetric crossover junction was proposed and analyzed (Figure 2-13).

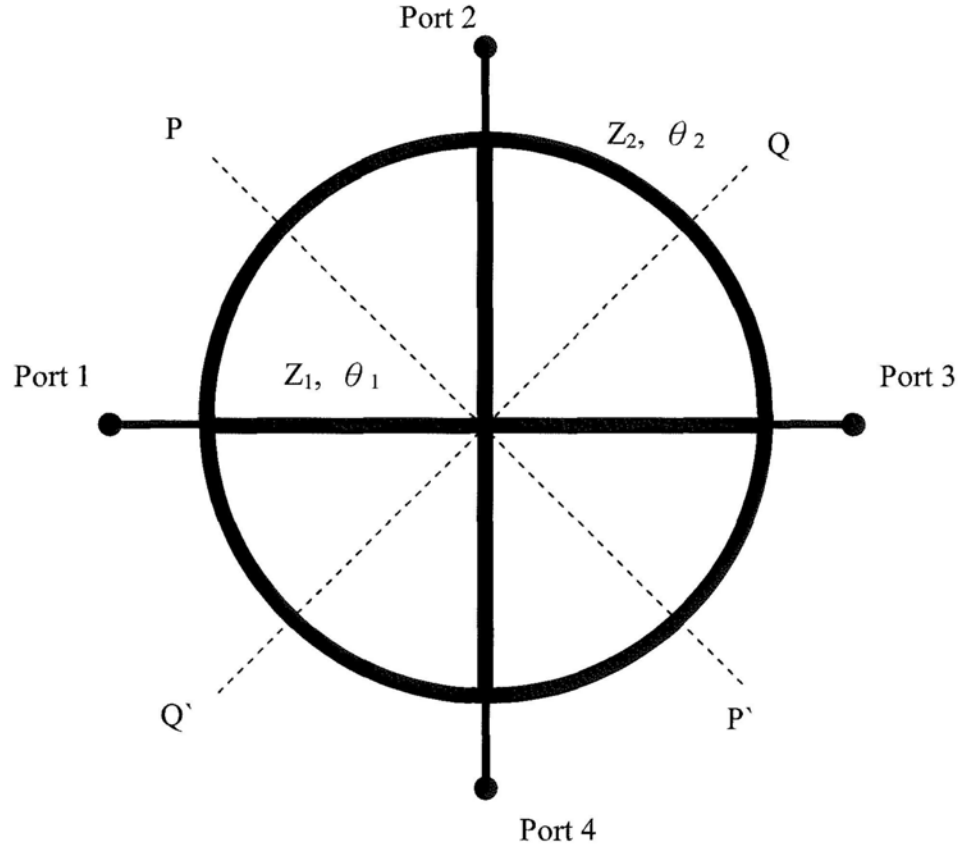

Figure 2-13: Symmetrical crossover junction design [33].

It basically consists of a ring with characteristic impedance of Z_2, and a cross junction with line impedance of Z_1. Since the circuit is bi-symmetric (along PP` and QQ`), it can be simplified and analyzed as a single port network. In Figure 2-14, the reduced network was derived, in which the individual branch-line is terminated by either open

or short, depending on the mode of excitation applied. And by the enforcement of the operating conditions of an ideal crossover ($S_{11}=S_{21}=S_{41}=0$ and $|S_{31}|=1$) at the centre frequency, multiple solutions can be revealed. Simulation results illustrated that the solution of θ_2 is ranged between 40° and 45°.

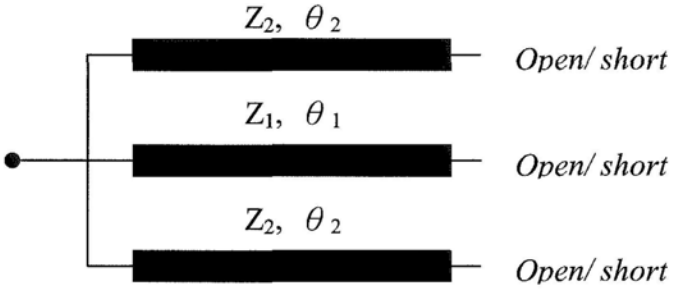

Figure 2-14: Reduced network of symmetrical crossover junction.

A prototype, with operating frequency of 1 GHz, was designed and characterized. Return loss and port isolation of better than 25dB were observed. Insertion loss (from port 1 to port 3) was found to be around 0.5dB, with an occupied area of approximately λ/3 by λ/3. This circuit offers only single-band operation with a fractional bandwidth of 10-15%.

2.8 Double ring crossover junction with arbitrary diagonal port impedances

Most crossover designs are assumed to operate with equal terminating impedance of 50Ω. In fact, there is a need for two transmission lines to crossover each other with different characteristic impedances. In this case, a crossover junction with different port impedances is preferred.

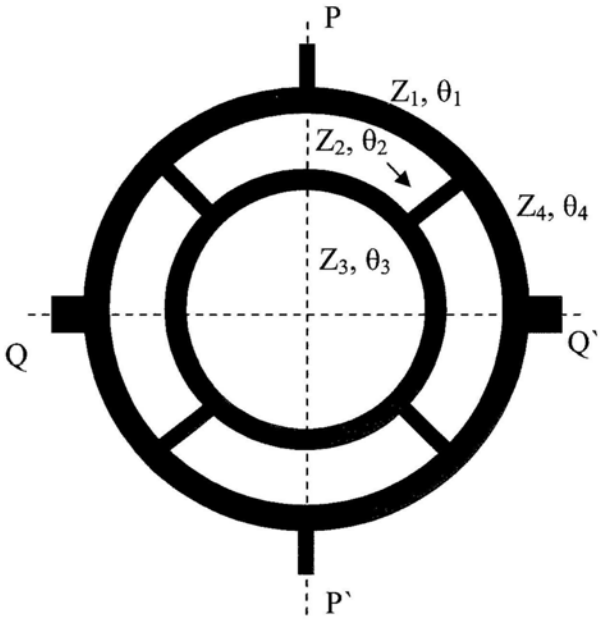

Figure 2-15: Topology of a double-ring crossover junction

In [45], a crossover junction with different port impedances was reported based on a double-ring structure (Figure 2-15). The circuit is bi-symmetric along PP` and QQ`. By applying even and odd mode analysis, implicit design equations were formulated as a function of branch-line and termination impedances. As infinite number of solutions are available, it is desirable to choose the one with small physical size and

reasonable line impedance values.

For experimental verification, a crossover junction operating at 2.45 GHz was realized, with port impedances of 50Ω and 100Ω. The branch-line impedances and electrical lengths of the crossover junction were found to be $Z_A = 90\ \Omega$, $Z_B = 126\ \Omega$, $Z_C = 140\ \Omega$, $Z_D = 108\ \Omega$, $\theta_1 = 55°$, $\theta_2 = 33°$, $\theta_3 = 40°$ and $\theta_4 = 70°$. The bandwidth of the design, based one a minimal return loss and port isolation of 15dB, was measured to be roughly 18%.

Chapter 3. Proposed Dual-Band Rat-race Coupler

In this chapter, several novel dual-band rat-race coupler topologies are introduced. Besides, mathematical analysis of these couplers is conducted to obtain closed-form expressions for the evaluation of circuit parameters. In addition, the applicable of f_2/f_1 with practical value of line impedance is examined. For verifications, simulated and measured results are presented and compared. For easy reference, the basic operating conditions of an ideal rat-race coupler are recalled and summarized as follows:

$$S_{11} = \frac{1}{2}(\Gamma_e + \Gamma_o) = 0 \tag{3.1}$$

$$S_{22} = \frac{1}{2}(\tau_e + \tau_o) = 0 \tag{3.2}$$

$$S_{31} = \frac{1}{2}(T_e - T_o) = 0 \tag{3.3}$$

$$|S_{41}| = \frac{1}{2}|\Gamma_e - \Gamma_o| = \frac{1}{\sqrt{2}} \tag{3.4}$$

$$|S_{21}| = \frac{1}{2}|T_e + T_o| = \frac{1}{\sqrt{2}} \tag{3.5}$$

$$|S_{23}| = \frac{1}{2}|\tau_e - \tau_o| = \frac{1}{\sqrt{2}} \tag{3.6}$$

$$\angle S_{21} - \angle S_{41} = 0^\circ \tag{3.7}$$

$$\angle S_{23} - \angle S_{43} = 180^\circ \tag{3.8}$$

Combining the above equations with ABCD parameters (refer to appendix I) and solving them, we have:

$$B_e = B_o = C_e = C_o \tag{3.9}$$

$$A_e = D_o = A_o + 2 = D_e + 2 \tag{3.10}$$

$$A_e A_o - B_e C_e = 1 \tag{3.11}$$

where $A_{e,o}$, $B_{e,o}$, $C_{e,o}$ and $D_{e,o}$ are the transmission coefficients of the corresponding even- and odd- mode circuits. These formulas are the necessary and sufficient conditions for the normal operation of the coupler, and they must be satisfied at both frequency bands of interest.

3.1 Rat-race coupler design I

Figure 3-1 shows the basic configuration of the proposed dual-band rat race coupler [17], where f_1 & f_2 are the centre frequencies of the lower and upper bands respectively.

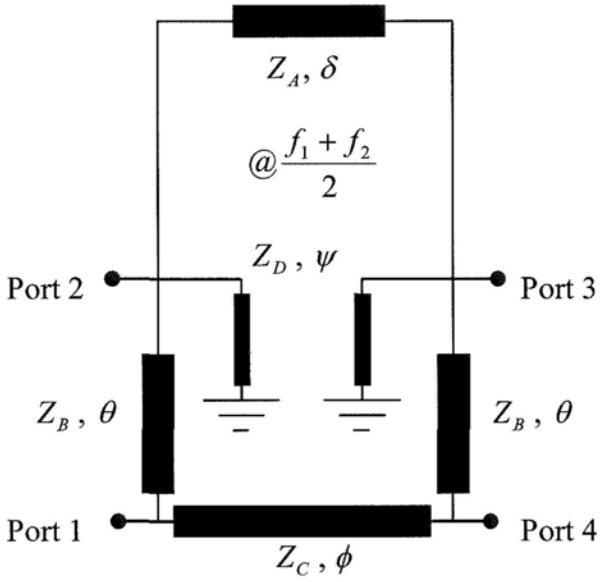

Figure 3-1: Proposed dual band rat race coupler I

3.1.1 Design and Analysis

Unlike the single-band design, the proposed dual-band coupler consists of branch-lines of unequal electrical length (θ , φ and δ) as well as a pair of shunt stubs (ψ). Besides, the branch line impedances (Z_A, Z_B, Z_C and Z_D) are unequal and yet to be determined. Figure 3-2 shows the even-odd mode circuits of the proposed structure.

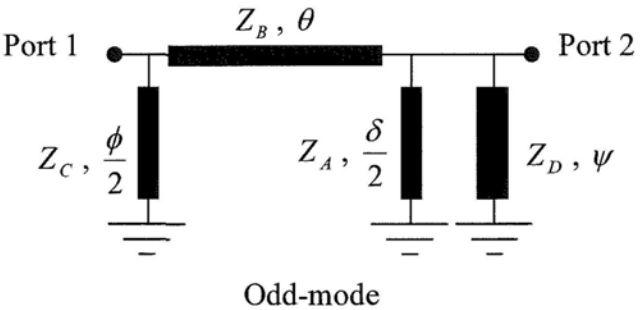

Odd-mode

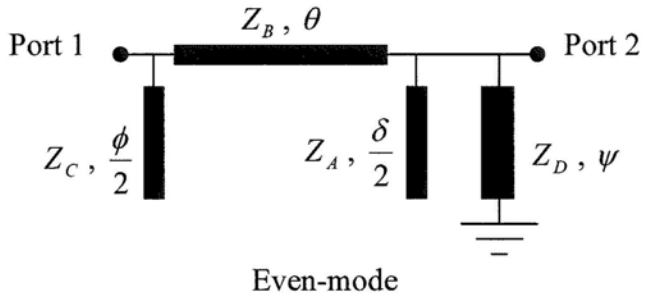

Figure 3-2: Rat-race coupler I: Even-odd mode analysis

The ABCD parameters of the even- and odd-mode circuits can simply be found by matrix multiplication (appendix II) as follows:

$$\begin{bmatrix} A & B \\ C & D \end{bmatrix}_e = \begin{bmatrix} 1 & 0 \\ jB_{1e} & 1 \end{bmatrix} \begin{bmatrix} \cos\theta & jZ_B \sin\theta \\ j\dfrac{\sin\theta}{Z_B} & \cos\theta \end{bmatrix} \begin{bmatrix} 1 & 0 \\ jB_{3e} & 1 \end{bmatrix}$$

$$\begin{bmatrix} A & B \\ C & D \end{bmatrix}_e = \begin{bmatrix} \cos\theta - Z_B B_{3e} \sin\theta & jZ_B \sin\theta \\ j\left\{(B_{1e} + B_{3e})\cos\theta + \left(\dfrac{1}{Z_B} - Z_B B_{1e} B_{3e}\right)\sin\theta\right\} & \cos\theta - Z_B B_{1e} \sin\theta \end{bmatrix} \quad (3.12)$$

$$\begin{bmatrix} A & B \\ C & D \end{bmatrix}_o = \begin{bmatrix} 1 & 0 \\ jB_{1o} & 1 \end{bmatrix} \begin{bmatrix} \cos\theta & jZ_B \sin\theta \\ j\dfrac{\sin\theta}{Z_B} & \cos\theta \end{bmatrix} \begin{bmatrix} 1 & 0 \\ jB_{3o} & 1 \end{bmatrix}$$

$$\begin{bmatrix} A & B \\ C & D \end{bmatrix}_o = \begin{bmatrix} \cos\theta - Z_B B_{3o} \sin\theta & jZ_B \sin\theta \\ j\left\{(B_{1o} + B_{3o})\cos\theta + \left(\dfrac{1}{Z_B} - Z_B B_{1o} B_{3o}\right)\sin\theta\right\} & \cos\theta - Z_B B_{1o} \sin\theta \end{bmatrix} \quad (3.13)$$

where

$$
\begin{aligned}
B_{1e} &= Y_C \tan \phi/2 \\
B_{1o} &= \frac{-Y_C}{\tan \phi/2} \\
B_{3e} &= Y_A \tan \delta/2 - \frac{Y_D}{\tan \psi} \\
B_{3o} &= -\left(\frac{Y_A}{\tan \delta/2} + \frac{Y_D}{\tan \psi} \right)
\end{aligned}
\tag{3.14}
$$

Substituting the above equations into (3.9) – (3.11) and solving, we obtain,

$$\frac{Z_C}{Z_B} = \frac{\sin \theta_{1,2}}{\sin 2\phi_{1,2}} \tag{3.15}$$

$$\frac{Z_A}{Z_B} = -\frac{\sin \theta_{1,2}}{\sin 2\delta_{1,2}} \tag{3.16}$$

$$\frac{Z_B}{Z_D} = t\tan \psi_{1,2} \frac{\cos 2\phi_{1,2} + \cos 2\delta_{1,2}}{\sin \theta_{1,2}} \tag{3.17}$$

$$\frac{Z_B}{Z_0} = \frac{2 - \left(\cos \theta_{1,2} + \cos 2\phi_{1,2}\right)^2}{\sin^2 \theta_{1,2}} \tag{3.18}$$

where $\theta_{1,2}$, $\phi_{1,2}$, $\delta_{1,2}$ and $\psi_{1,2}$ are the electrical lengths of the branch-lines evaluated at f_1 & f_2. However, these variables are interrelated via the following expressions:

$$\frac{\theta_2}{\theta_1} = \frac{\delta_2}{\delta_1} = \frac{\phi_2}{\phi_1} = \frac{\psi_2}{\psi_1} = \frac{f_2}{f_1} \tag{3.19}$$

As a result, one can deduce that the solution (shortest line lengths) is simply given by:

$$\theta(f_0)=\phi(f_0)=\psi(f_0)=\frac{\pi}{2} \tag{3.20}$$

$$\delta(f_0)=\frac{5\pi}{2} \tag{3.21}$$

where $f_0=\frac{f_2+f_1}{2}$.

Finally, the unknown characteristic impedances can be computed by:

$$Z_B=Z_C=\frac{Z_0}{\cos\varepsilon}\sqrt{2\cos 2\varepsilon} \tag{3.22}$$

$$Z_A=-Z_B\frac{\cos\varepsilon}{\cos 5\varepsilon} \tag{3.23}$$

$$Z_D=\frac{Z_B\sin\varepsilon}{\sin\varepsilon+\sin 5\varepsilon} \tag{3.24}$$

where $\varepsilon=\frac{f_2-f_1}{f_2+f_1}\cdot\frac{\pi}{2}$.

The realization of branch-line imposes lower and upper limits to the usable range of f_2/f_1 for proposed coupler design. In practice, the possible range of line impedance is between 30 Ω and 100 Ω. Figure 3-3 shows the computed branch line impedance (normalized) values as a function of f_2/f_1. It can be observed that the usable frequency range of the coupler is roughly equal to $2 < f_2/f_1 < 2.7$.

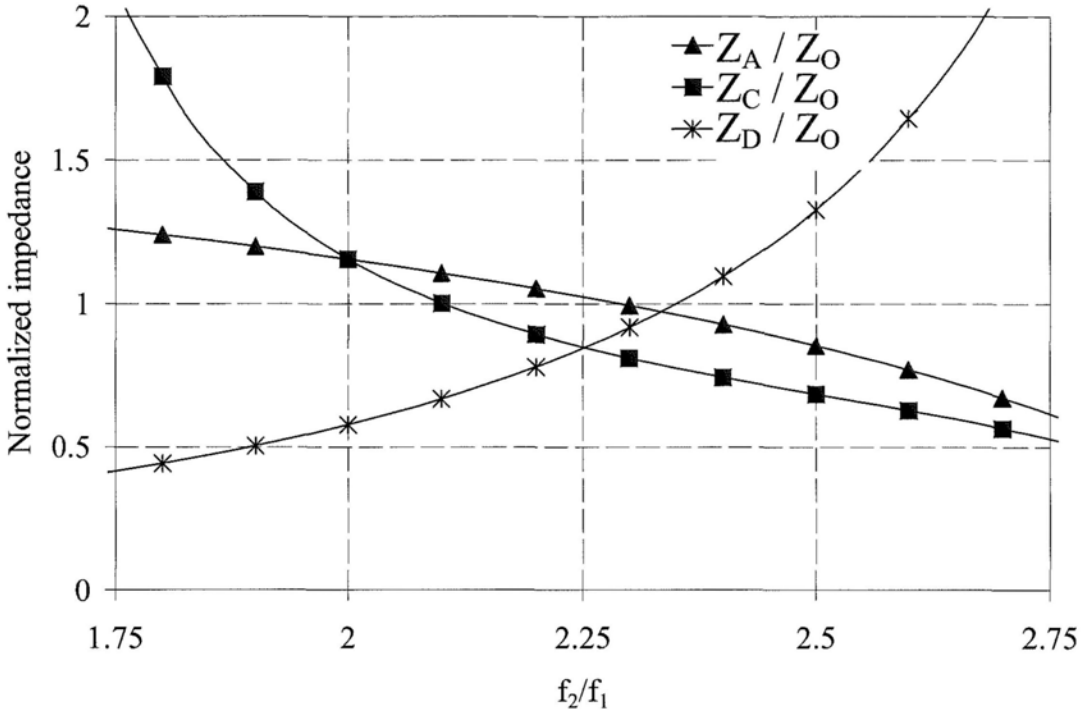

Figure 3-3: Computed line impedance versus f_2/f_1

3.1.2 Simulation results

Dual-band rat race coupler with f_1 = 1GHz and f_2 = 2 GHz was chosen for verification. According to the equations derived, the corresponding branch-line impedances are: Z_A=57.7Ω, Z_B=57.7Ω, Z_C=57.7Ω and Z_D=28.9Ω. According to the simulation results (Figure 3-4 to Figure 3-6), ideal coupler performances were attained (return los, insertion loss, port isolation, etc) at both f_1 and f_2. Operating bandwidth is mainly limited by the output return loss. Excellent amplitude and phase balances are achieved at f_1 & f_2 for both in-phase and anti-phase output ports. According to Figure 3-6, an operating bandwidth of about 30 MHz, was observed with phase mismatch requirement of ± 5°.

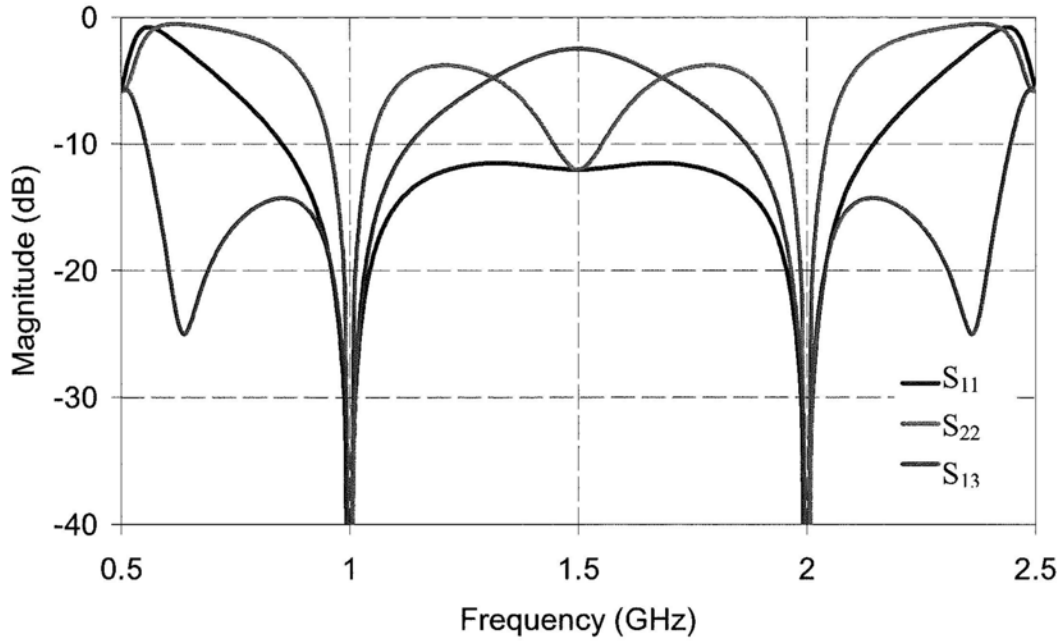

Figure 3-4: Simulated return loss and port isolation.

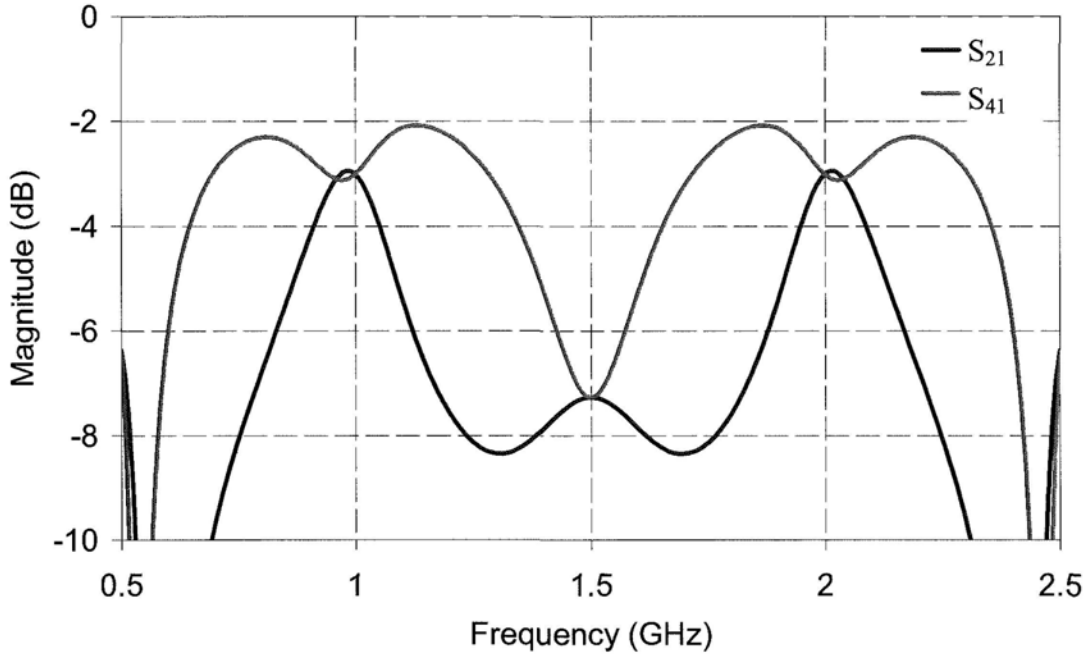

Figure 3-5: Simulated insertion loss (In-phase).

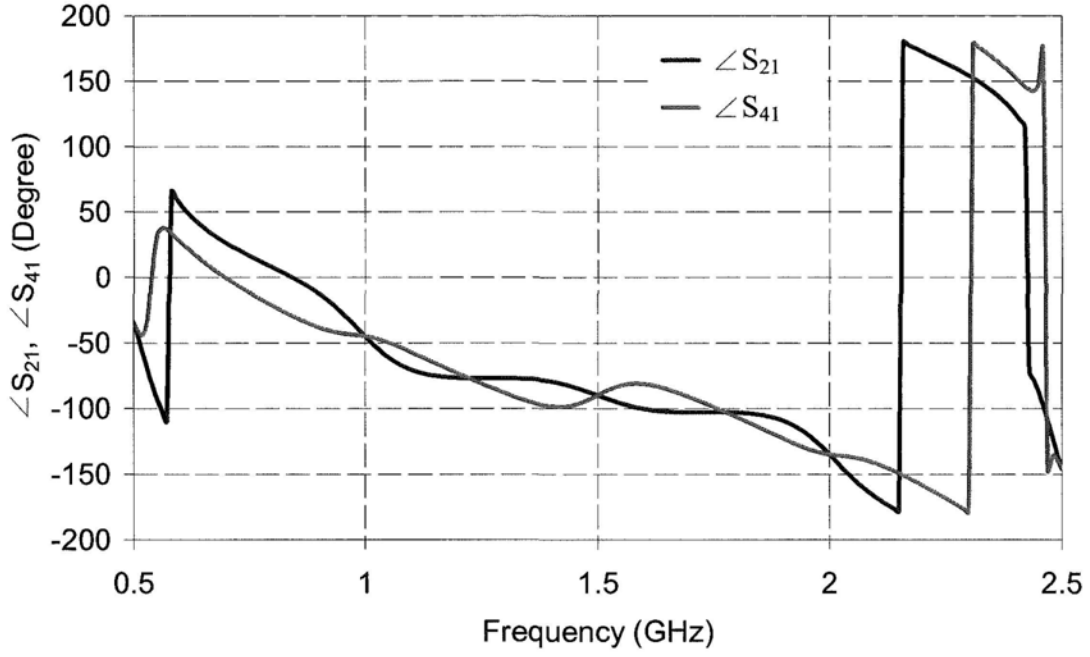

Figure 3-6: Simulated phase response (In-phase).

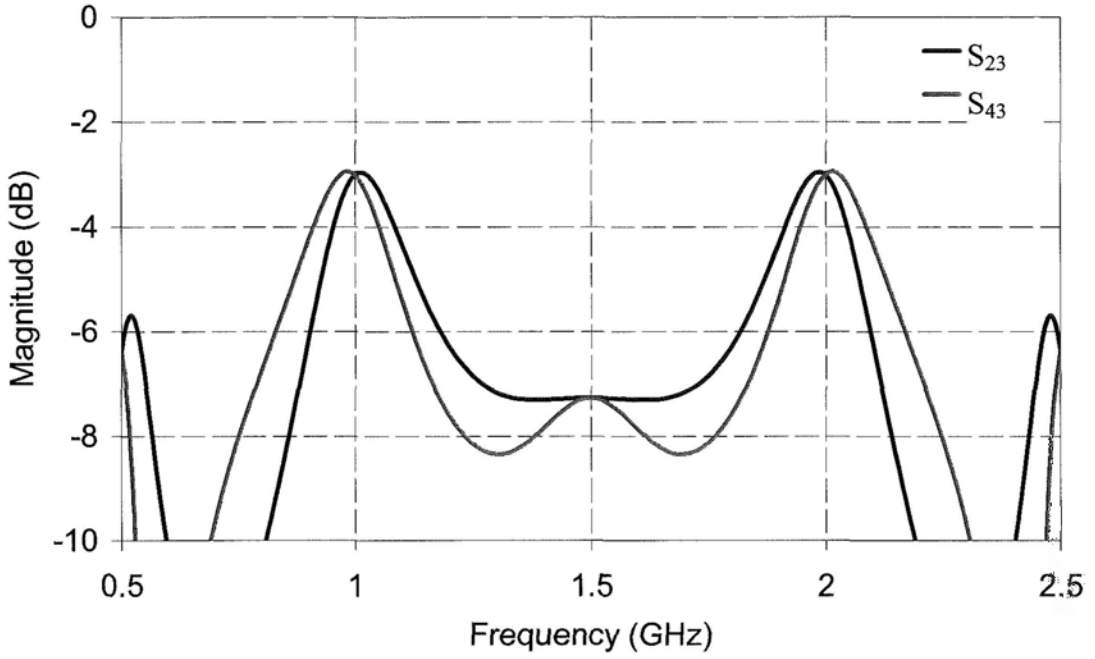

Figure 3-7: Simulated insertion loss (anti-phase).

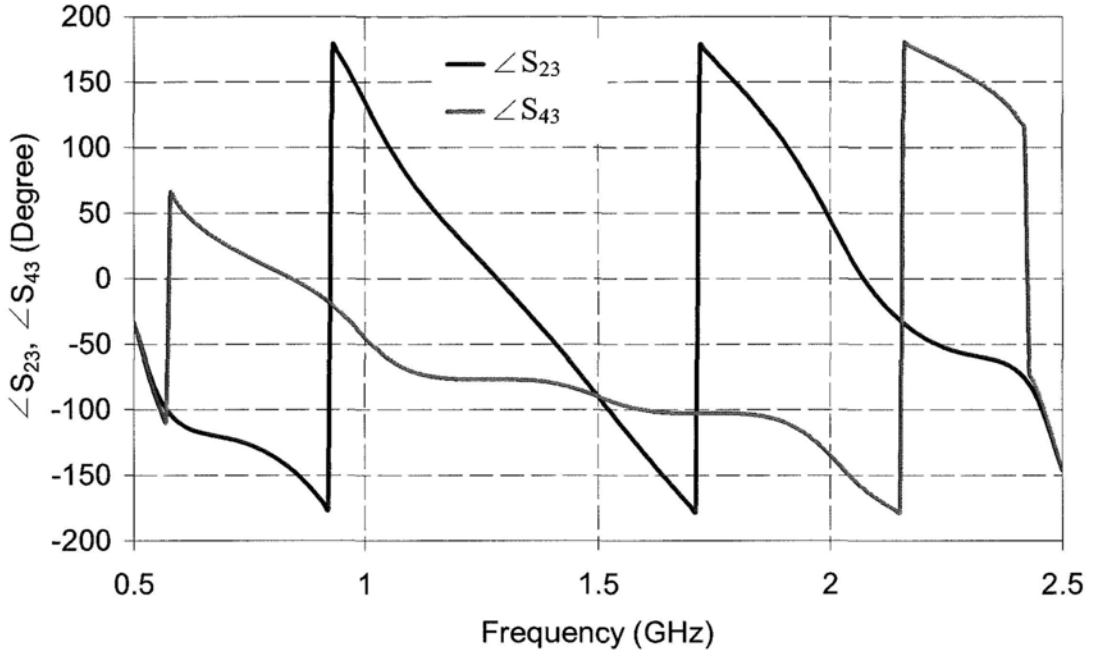

Figure 3-8: Simulated phase response (Anti-phase).

3.1.3 Experimental results

Prototype of design I was constructed to operate at 900MHz and 2GHz using microstrip. The optimized values of circuit parameters were $Z_A = 44\Omega$, $Z_B = 52\Omega$, $Z_C = 52\Omega$ and $Z_D = 40\Omega$. Figure 3-9 shows the top view of the fabricated circuit.

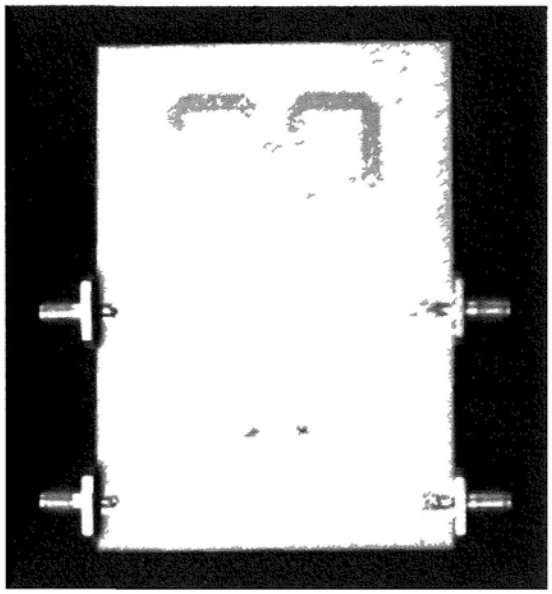

Figure 3-9: Photograph of the fabricated coupler (design I).

Figure 3-10 to 3-14 show the measured frequency response of coupler I over the frequency ranged from 0.6 to 2.4 GHz. The center frequencies of the two operating bands were found to be slightly shifted to 880 MHz and 1980 MHz.

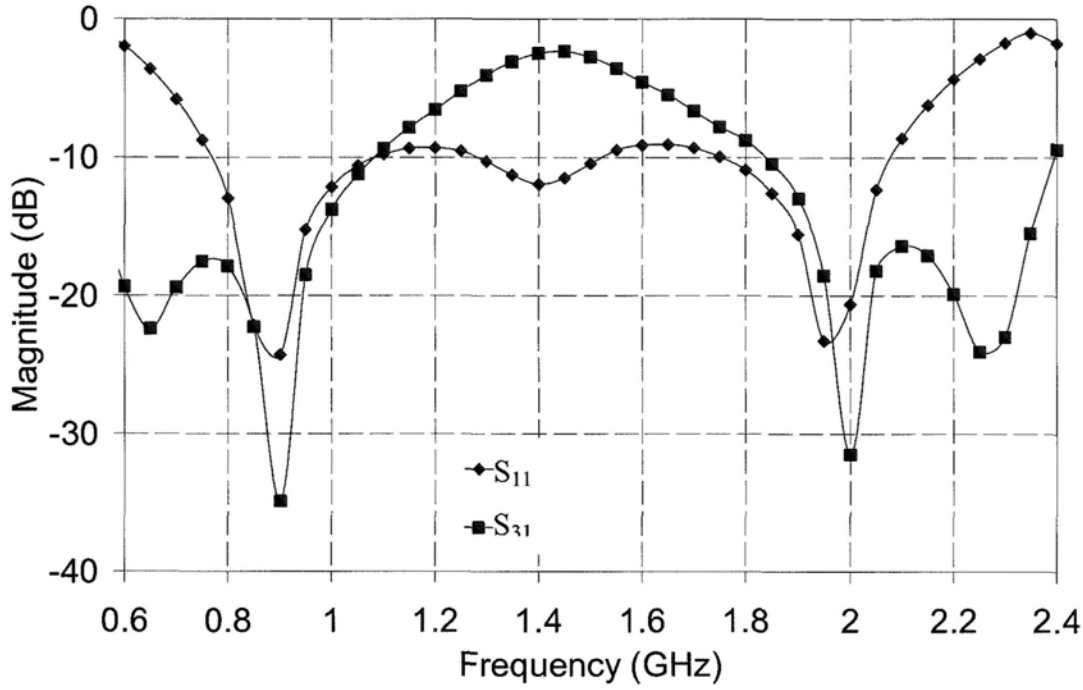

Figure 3-10: Measured return loss and port isolation (design I).

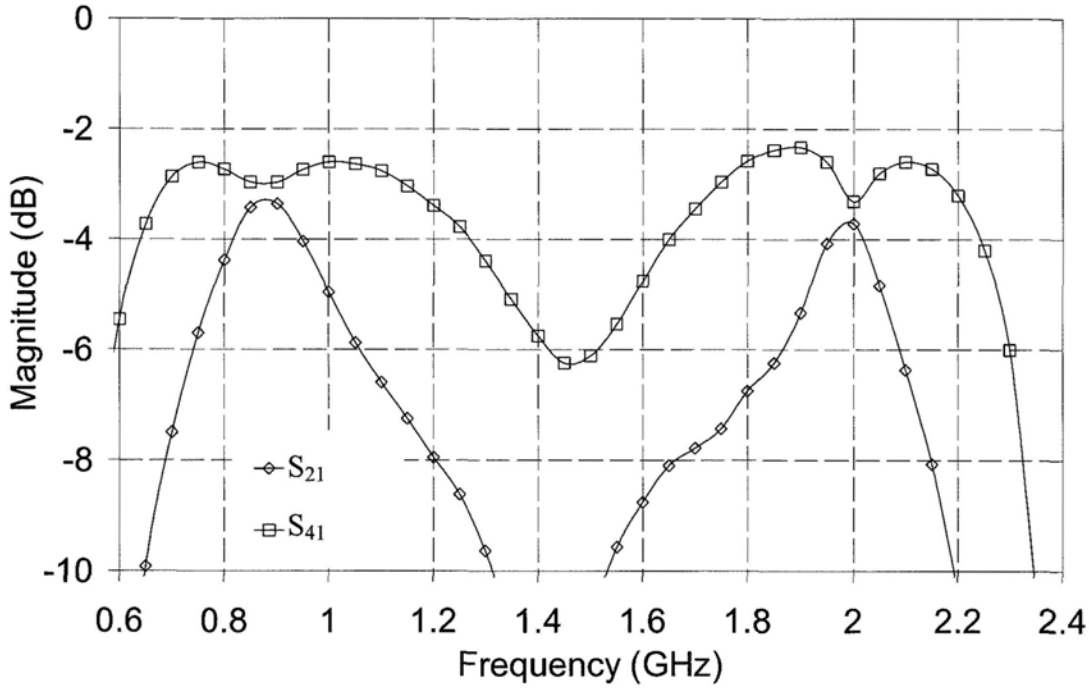

Figure 3-11: Measured insertion loss of in-phase outputs (design I).

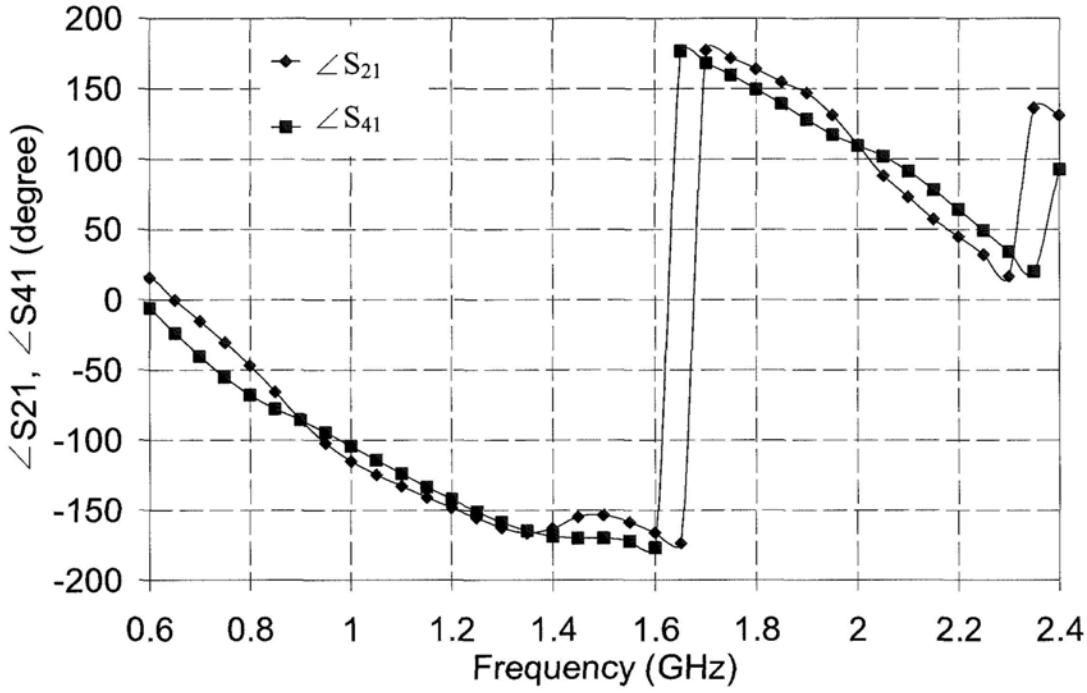

Figure 3-12: Measured phase response of in-phase outputs (design I).

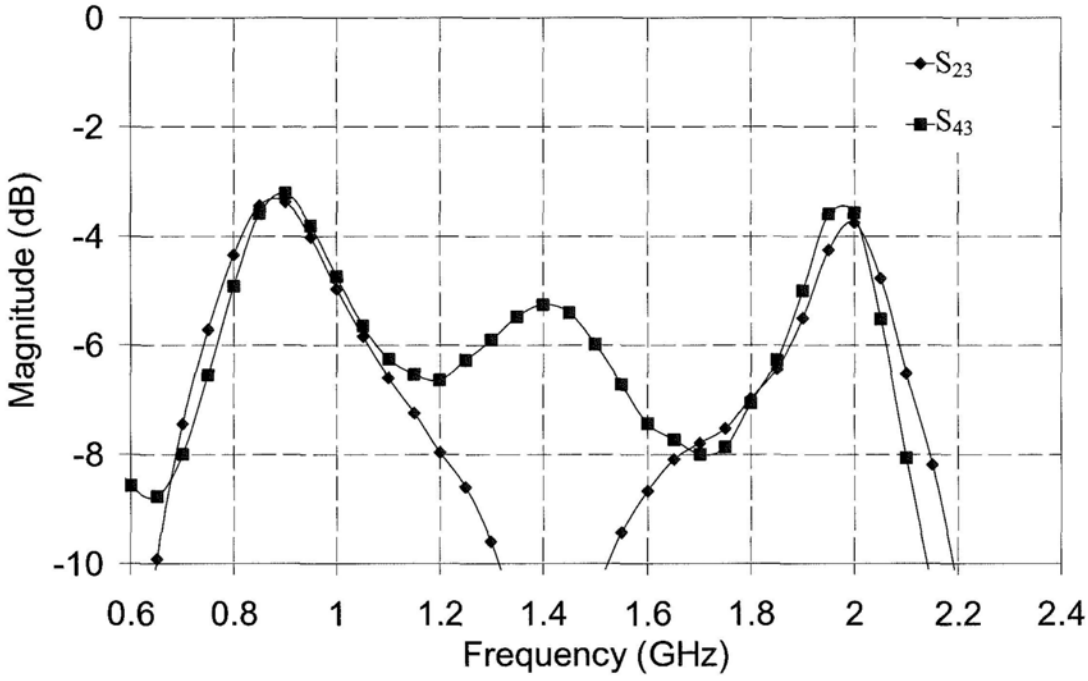

Figure 3-13: Measured insertion loss of anti-phase outputs (design I).

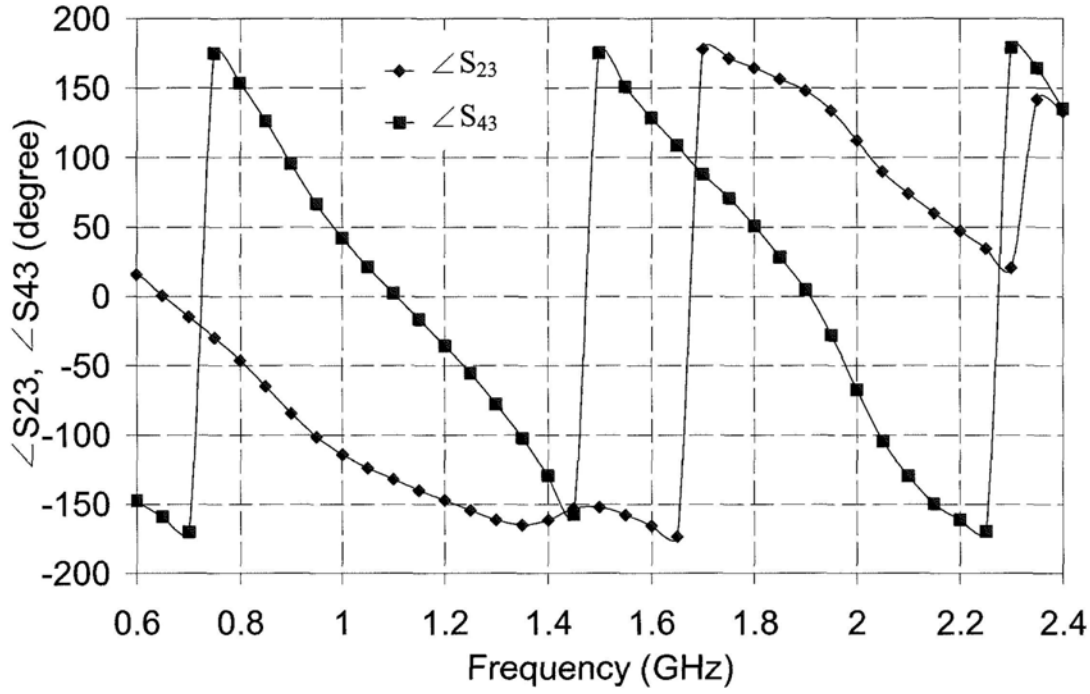

Figure 3-14: Measured phase response of anti-phase outputs (design I)

According to the measurement results, return loss and port isolation of better than 28dB and 29dB, respectively, were observed. Moreover, the insertion loss was found to be approximately 3.7dB (3dB in ideal case). Referring to the insertion loss frequency responses (both in-phase and anti-phase), attenuation of over 30dB was achieved at around 1.4GHz (both S_{21} and S_{23}). The operating bandwidth of the coupler is mainly limited by the amplitude and phase mismatch to approximately 50 MHz.

3.2 Rat-race coupler design II

Figure 3-15 shows the topology of the another design of rat-race coupler [18]. All electrical lengths are evaluated at f_0 (average value of f_1 and f_2). In compared to the previous configuration, this circuit requires a shorter branch-line (270° instead of 450°), and a different locations of shunt stubs. Furthermore, it occupies a smaller area due to the reduced length of the longer arm.

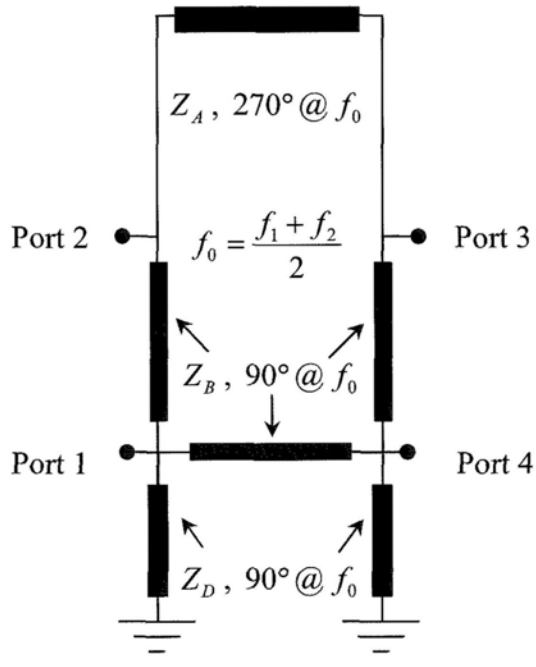

Figure 3-15: Proposed dual band rat race coupler II.

3.2.1 Design and Analysis

As before, the characteristic impedances of all branch-lines, are unknowns to be determined. For the purpose of analysis, even-odd mode formulation is applied to

design II as depicted in Figure 3-16.

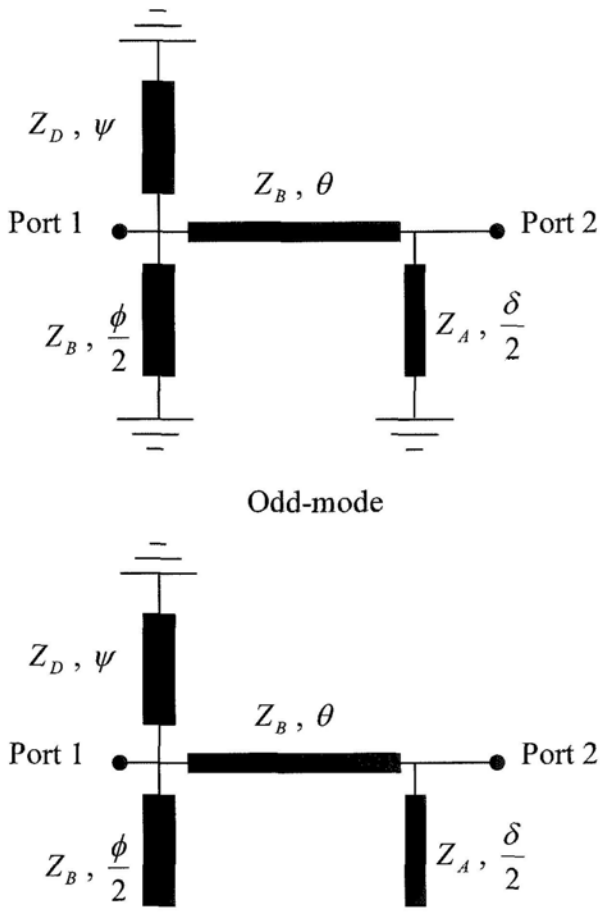

Figure 3-16: Design II: Even-odd mode networks.

Accordingly, the overall ABCD parameters of even- and odd-mode circuits can be thus derived as:

$$\begin{bmatrix} A & B \\ C & D \end{bmatrix}_e = \begin{bmatrix} 1 & 0 \\ jB_{1e} & 1 \end{bmatrix} \begin{bmatrix} \cos\theta & jZ_B \sin\theta \\ j\dfrac{\sin\theta}{Z_B} & \cos\theta \end{bmatrix} \begin{bmatrix} 1 & 0 \\ jB_{3e} & 1 \end{bmatrix}$$

$$\begin{bmatrix} A & B \\ C & D \end{bmatrix}_e = \begin{bmatrix} \cos\theta - Z_B B_{3e} \sin\theta & jZ_B \sin\theta \\ j\left\{ (B_{1e} + B_{3e})\cos\theta + \left(\dfrac{1}{Z_B} - Z_B B_{1e} B_{3e} \right) \sin\theta \right\} & \cos\theta - Z_B B_{1e} \sin\theta \end{bmatrix} \quad (3.17)$$

$$\begin{bmatrix} A & B \\ C & D \end{bmatrix}_o = \begin{bmatrix} 1 & 0 \\ jB_{1o} & 1 \end{bmatrix} \begin{bmatrix} \cos\theta & jZ_B \sin\theta \\ j\dfrac{\sin\theta}{Z_B} & \cos\theta \end{bmatrix} \begin{bmatrix} 1 & 0 \\ jB_{3o} & 1 \end{bmatrix}$$

$$\begin{bmatrix} A & B \\ C & D \end{bmatrix}_o = \begin{bmatrix} \cos\theta - Z_B B_{3o} \sin\theta & jZ_B \sin\theta \\ j\left\{(B_{1o} + B_{3o})\cos\theta + \left(\dfrac{1}{Z_B} - Z_B B_{1o} B_{3o}\right)\sin\theta\right\} & \cos\theta - Z_B B_{1o} \sin\theta \end{bmatrix} \quad (3.18)$$

where

$$\begin{aligned} B_{1e} &= Y_B \tan \phi/2 - \frac{Y_D}{\tan\psi} \\ B_{1o} &= \frac{-Y_B}{\tan \phi/2} + \frac{-Y_D}{\tan\psi} \\ B_{3e} &= Y_A \tan \delta/2 \\ B_{3o} &= -\frac{Y_A}{\tan \delta/2} \end{aligned} \quad (3.19)$$

Under the assumption of dual-band operation, the required branch-line impedances can simply be solved and expressed by the following expressions:

$$Z_B = \frac{Z_0}{\cos\varepsilon}\sqrt{2 - 16\sin^2\varepsilon\ \cos^4\varepsilon} \quad (3.20)$$

$$Z_A = Z_B \frac{\cos\varepsilon}{\cos 3\varepsilon} \quad (3.21)$$

$$Z_D = \frac{Z_B}{2\cos 2\varepsilon} \quad (3.22)$$

where $\varepsilon = \dfrac{f_2 - f_1}{f_2 + f_1} \cdot \dfrac{\pi}{2}$.

The variation of the branch-line impedance (normalized) as a function of f_2/f_1 are

computed and plotted in Figure 3-17. By inspection, the usable range of f_2/f_1 for design II is lying between 1 and 1.75 with line impedance values ranged from 30 Ω to 100 Ω.

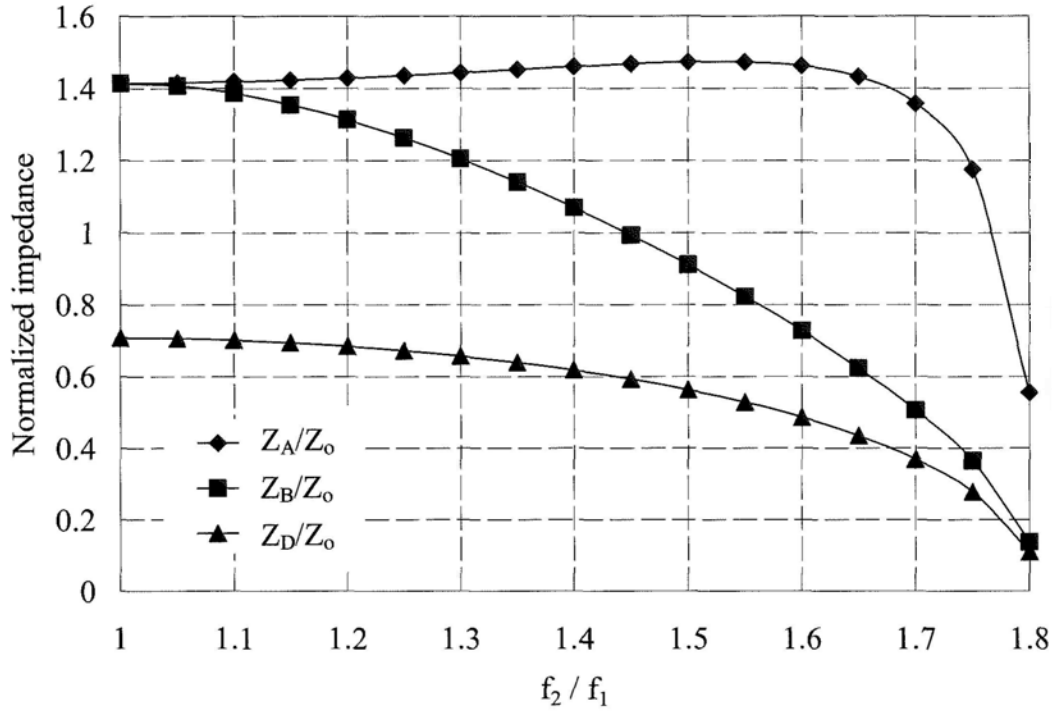

Figure 3-17: Computed line impedance versus f_2/f_1.

3.2.2 Simulation results

Dual-band rat-race coupler II is smaller in size, in compared to design I. For illustration, f_2/f_1 of 1.5 is selected with branch-line impedances of $Z_A = 73.7\Omega$, $Z_B = 45.5\Omega$ and $Z_D = 28.1\Omega$. Simulated return loss, insertion loss and phase response are shown in Figure 3-18 to 3-20. According to these results, ideal return loss and insertion loss were observed at both centre frequencies. The achievable operating bandwidth seems to be limited by the phase mismatch performance (tolerances of ±5°) to around 30MHz (Figure 3-20).

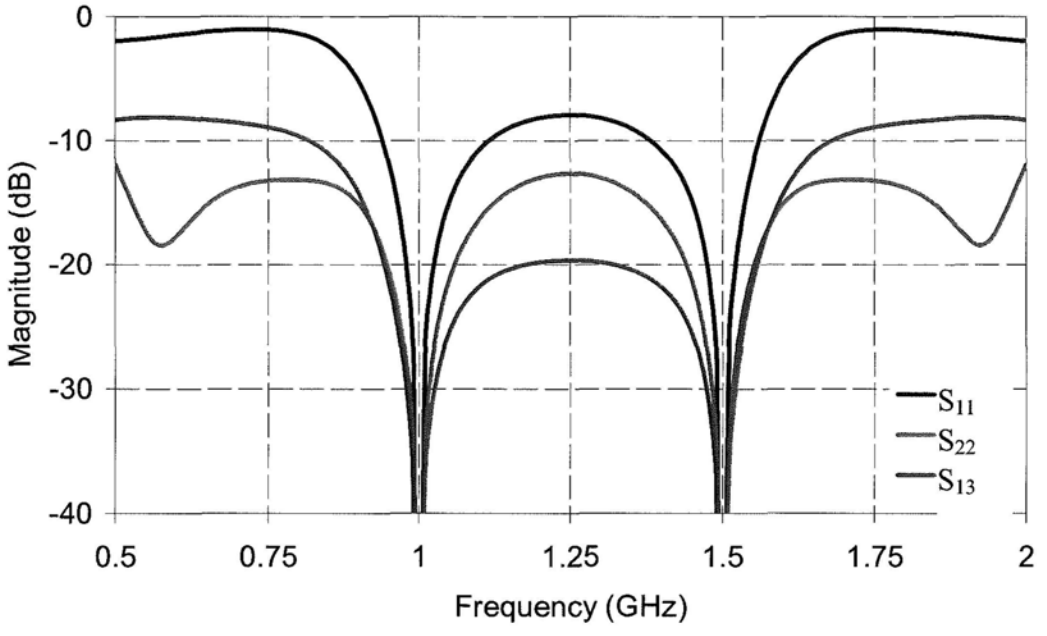

Figure 3-18: Simulated return loss and port isolation.

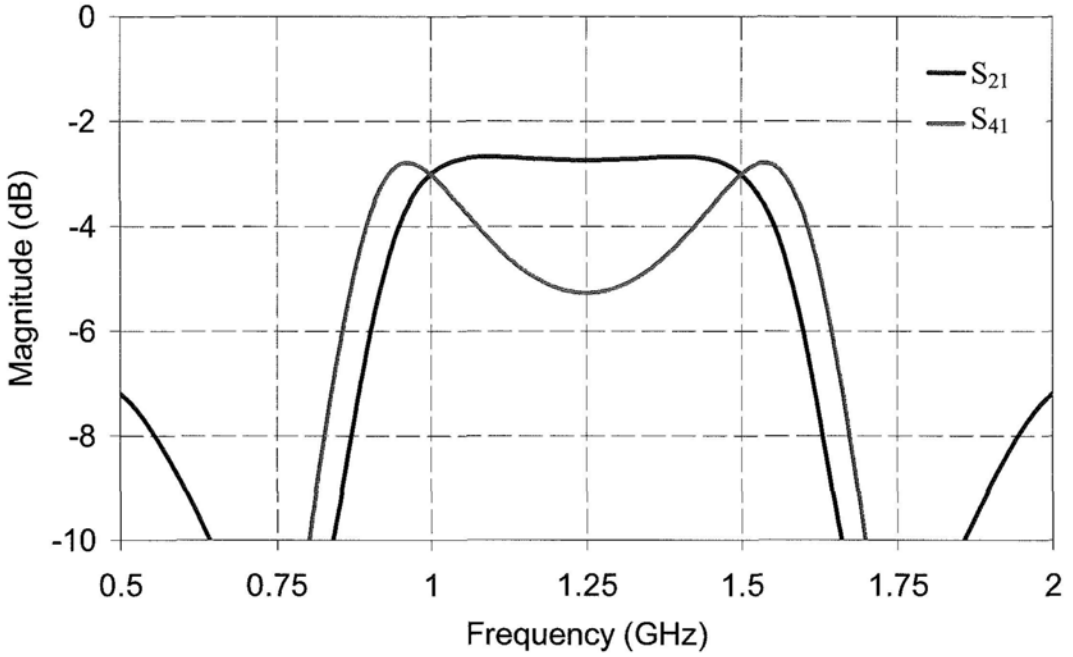

Figure 3-19: Simulated insertion loss (In-phase outputs).

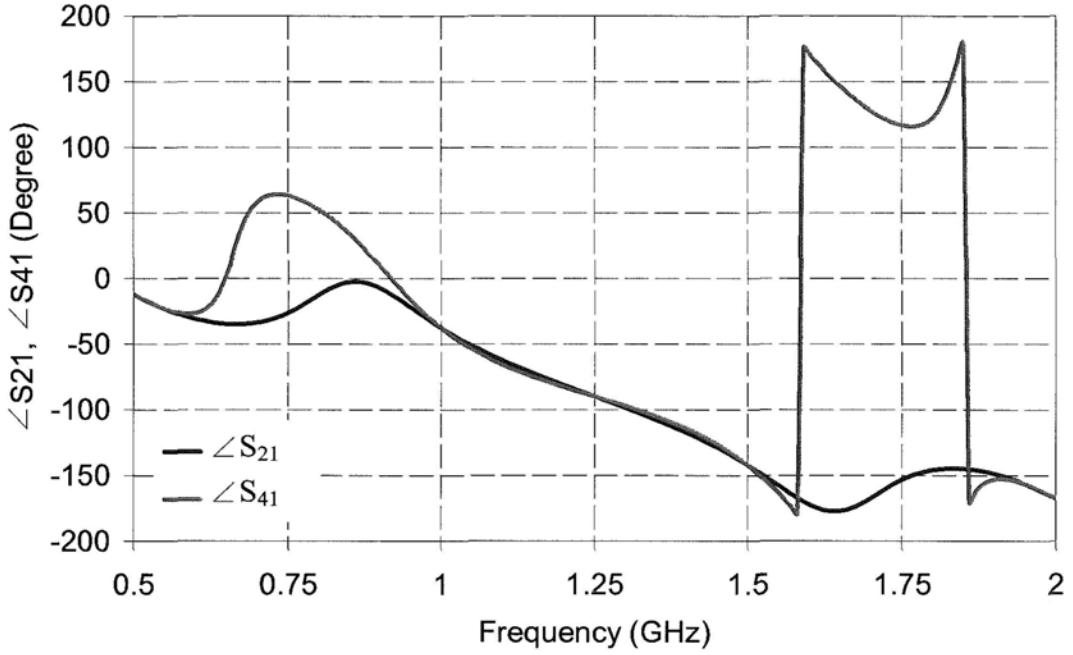

Figure 3-20: Simulated phase response (In-phase outputs).

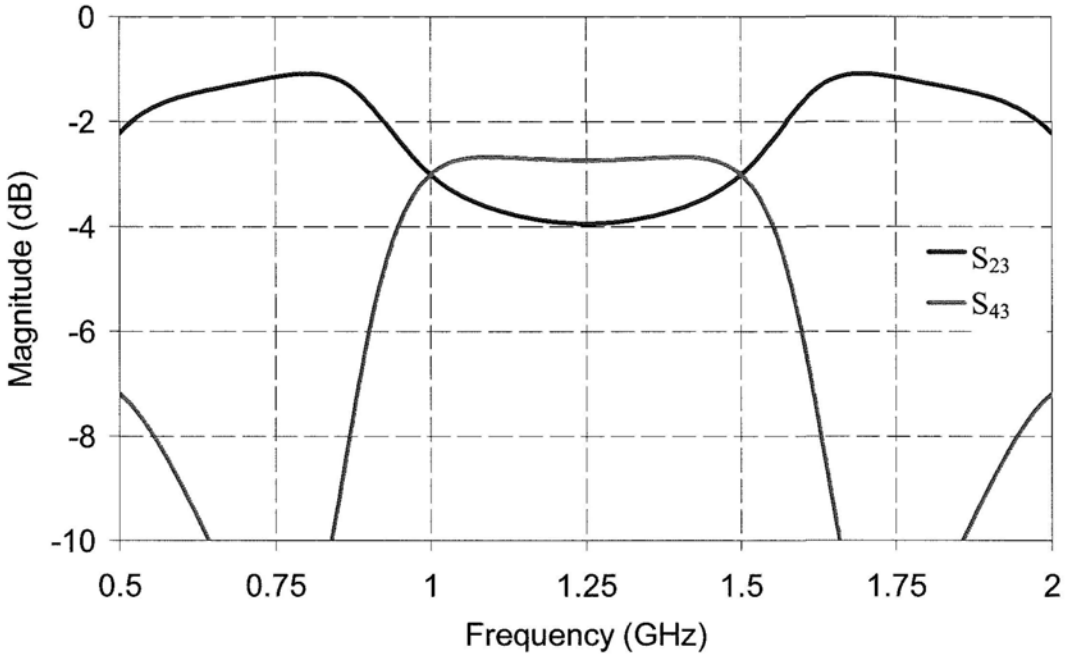

Figure 3-21: Simulated insertion loss (Anti-phase outputs).

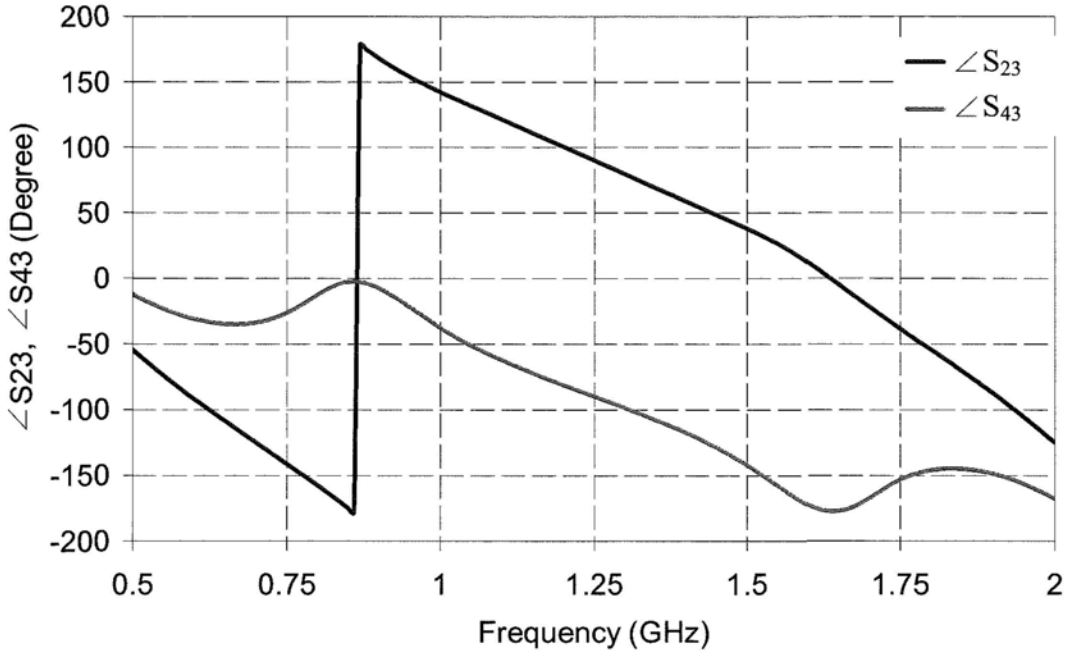

Figure 3-22: Simulated phase response (Anti-phase outputs).

3.2.3 Experimental results

For experimental verifications, prototype of design II with operating frequencies of 900 MHz and 1.5 GHz ($f_2/f_1 = 1.67$) was fabricated. Accordingly, the corresponding values of Z_A, Z_B and Z_D, were found to be 70.7 Ω, 29.3 Ω and 20.7 Ω, respectively. Figure 3-23 shows the physical layout of coupler II implemented on Duroid substrate. For further size reduction, the two shunt stubs may be placed inside the square loop, whereas the layer area may be shortened by line meandering.

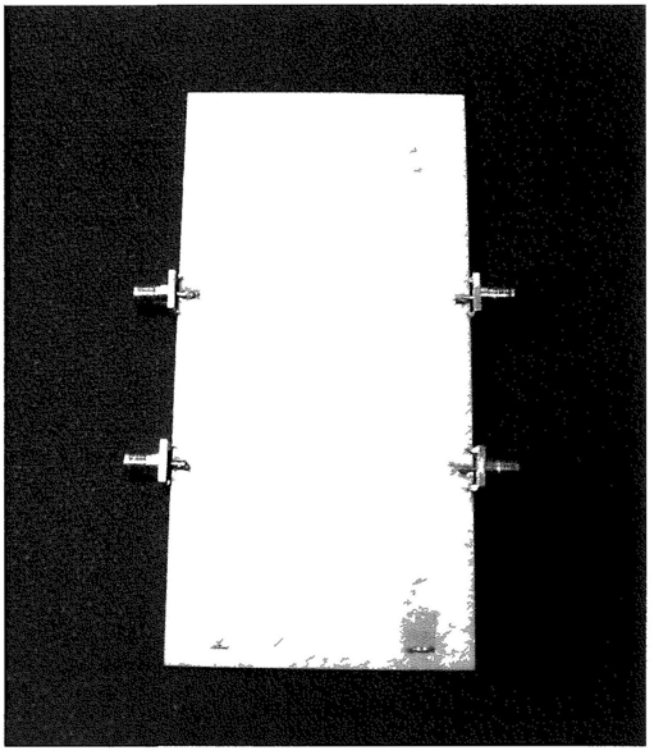

Figure 3-23: Photograph of the fabricated coupler (design II).

Figure 3-24 to 3-28 show the measured responses of the coupler in which the center frequencies of the two operating bands were found to be 860 MHz and 1.45 GHz. The

frequency shift is mainly due to the junction effect and tolerances of the fabrication process. Referring to Figure 3-24, measured return loss and port isolation of greater than 15dB and 18dB, respectively, were found at the two centre frequencies. Figure 3-26 and Figure 3-28 indicate that the amount of phase mismatch is small for both in-phase and anti-phase outputs. The measured insertion losses of the in-phase (S_{21} and S_{41}) and anti-phase (S_{23} and S_{43}) outputs were approximately 3.8dB and 3.7dB, respectively (3dB in ideal case).

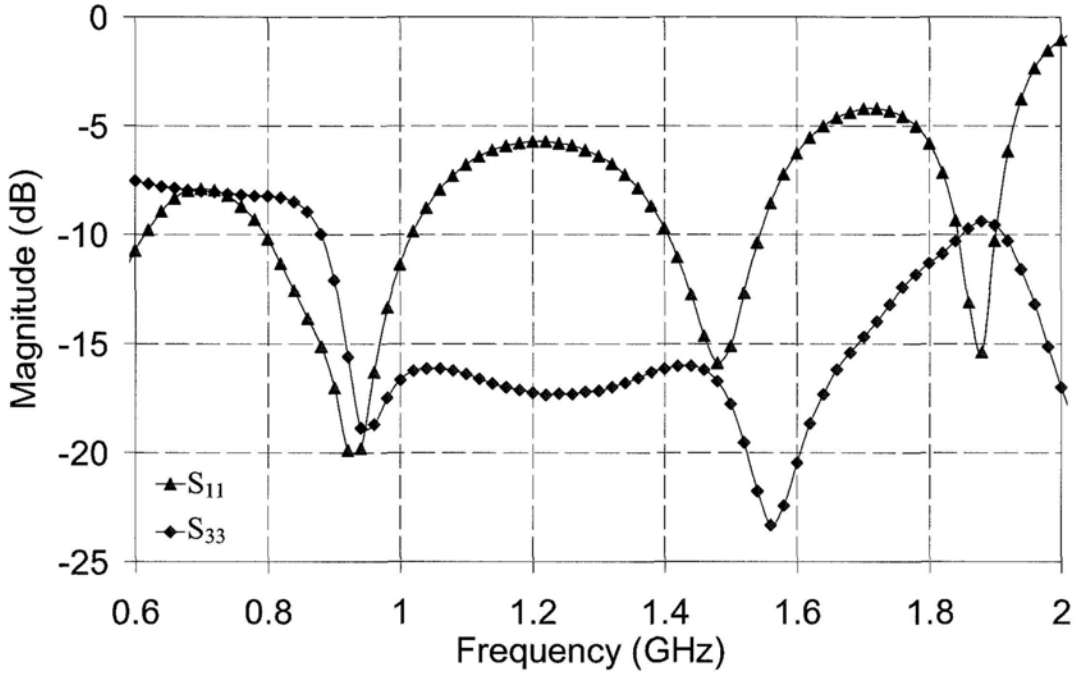

Figure 3-24: Measured return loss and port isolation (design II).

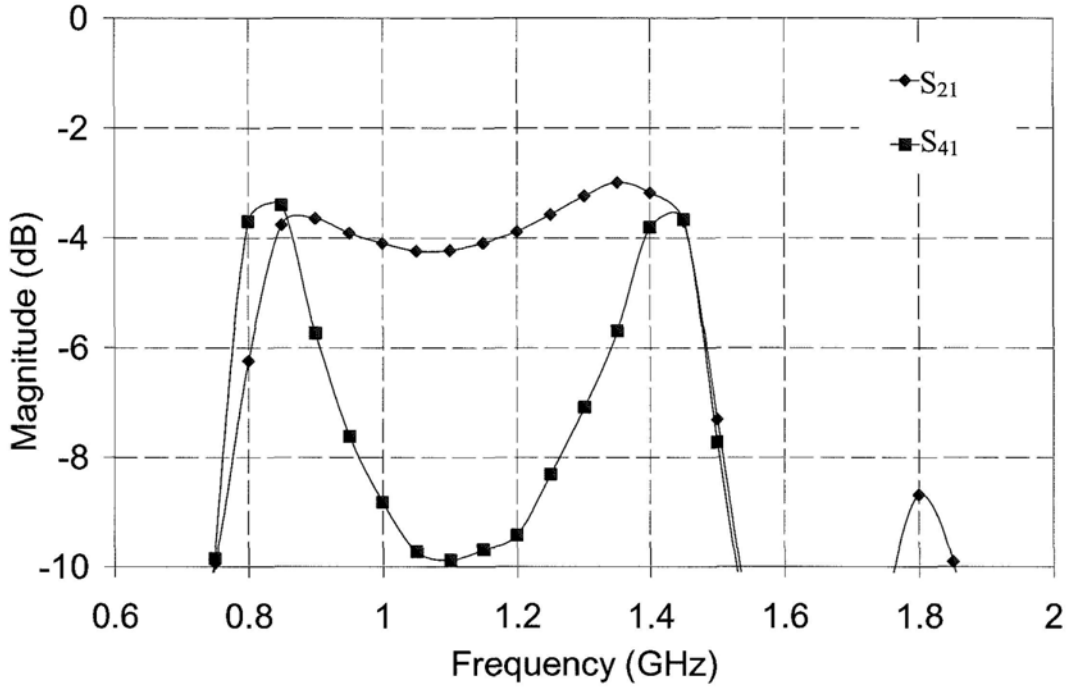

Figure 3-25: Measured insertion loss of in-phase outputs (design II).

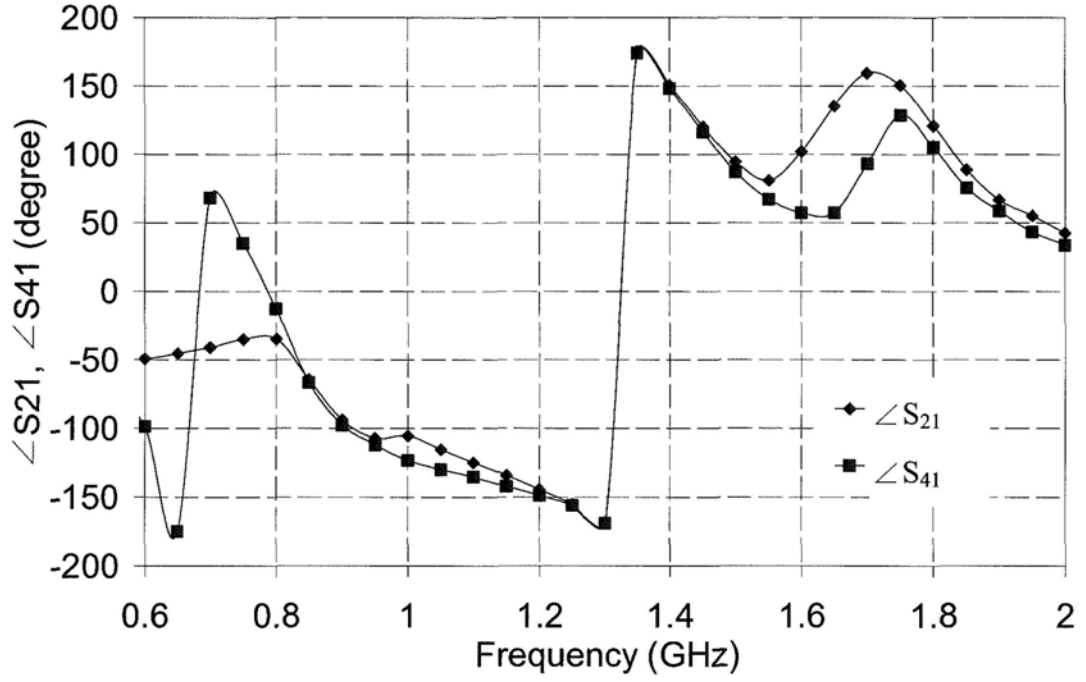

Figure 3-26: Measured phase response of in-phase outputs (design II).

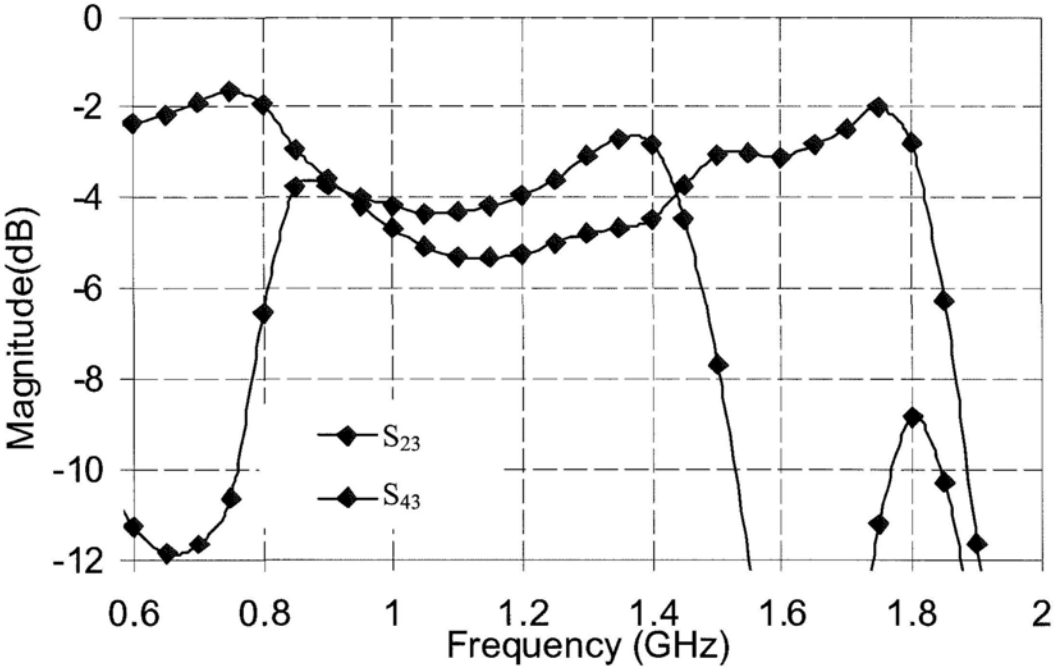

Figure 3-27: Measured insertion loss of anti-phase outputs (design II).

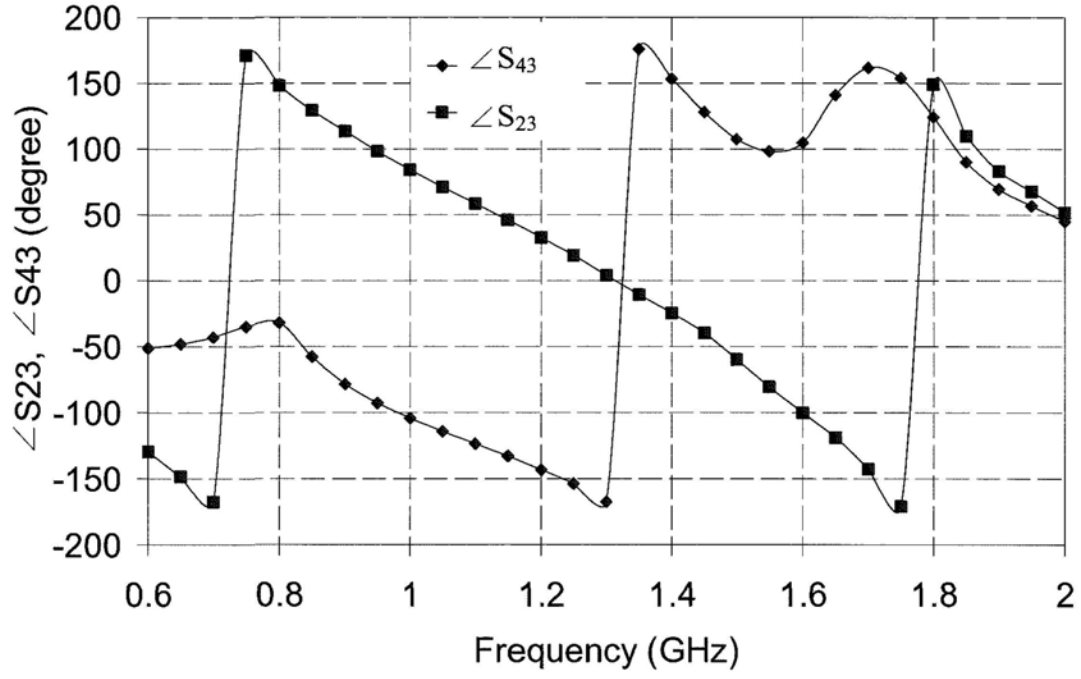

Figure 3-28: Measured phase response of anti-phase outputs (design II).

3.3 Rat-race coupler design III

This design is basically consisted of 6 sections of branch-line (90°, evaluated at f_0) and two shunt stubs. In compared to design I, the new structure offers less occupied area due to the absence of extended branch-line. In addition, only open stubs are needed without ground vias. The usable range (f_2/f_1) of the present design is also extended.

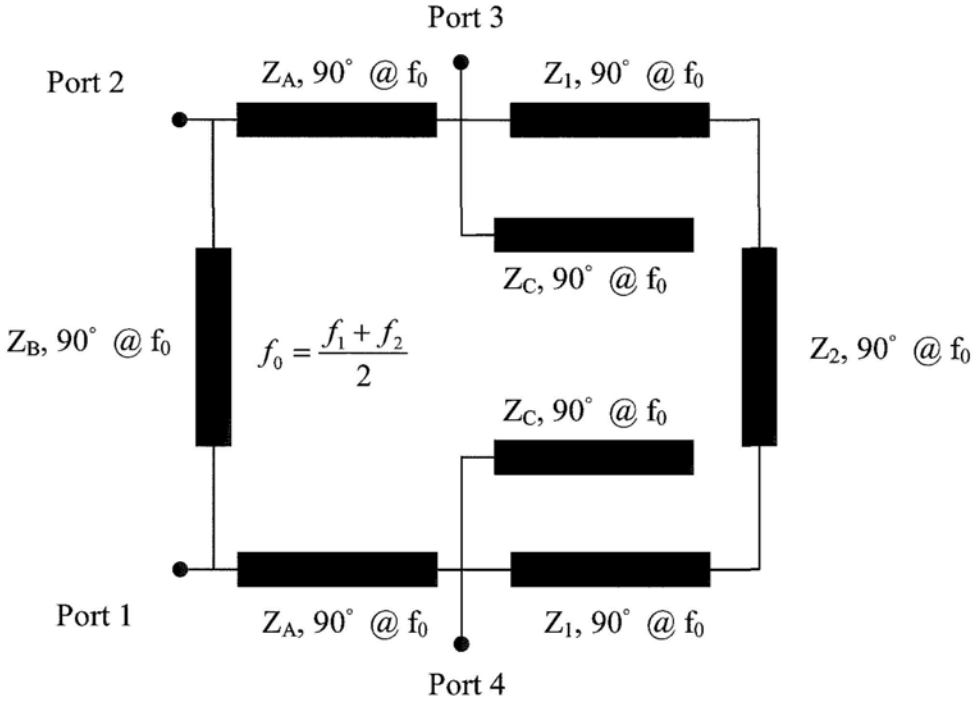

Figure 3-29: The third proposed dual band rat race coupler

3.3.1 Design and Analysis

By applying even- and odd-mode formulation to the reduced networks of the coupler (Figure 3-30), it is possible to derive and express the operation conditions as:

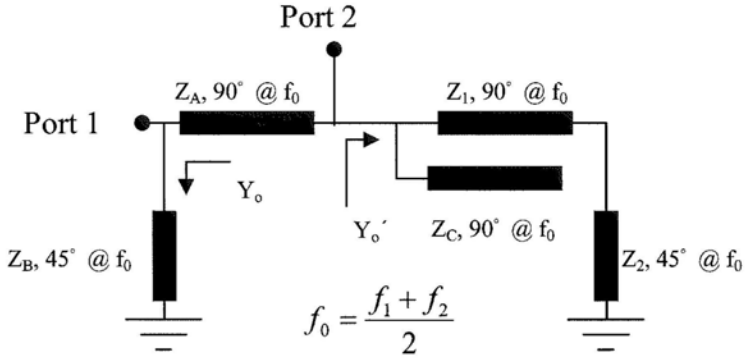

Odd mode

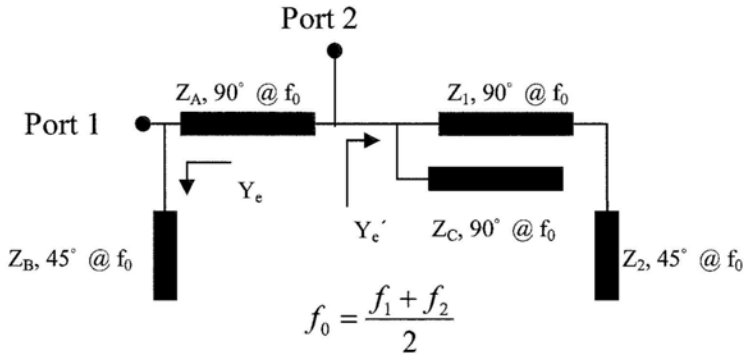

Even mode

Figure 3-30: Rat-race coupler III: even-odd mode circuit.

$$Y_A = Y_B = -Y_1 P \cos\frac{\pi}{2}\varepsilon \tag{3.23}$$

$$\frac{-\sin\frac{\pi}{2}\varepsilon + \sqrt{2 - \frac{Z_A^2}{Z_0^2}\cos^2\frac{\pi}{2}\varepsilon}}{Z_A \cos\frac{\pi}{2}\varepsilon} = Y_1 Q \tag{3.24}$$

$$Y_B \tan\frac{\pi}{2}\varepsilon - Y_C \cot\frac{\pi}{2}\varepsilon = Y_1 Q \tag{3.25}$$

where

$$P = \frac{1}{2}[F(\varepsilon) + F(-\varepsilon)]$$

$$Q = \frac{1}{2}[F(\varepsilon) - F(-\varepsilon)]$$

$$F = \frac{k \tan\frac{\pi}{4}(1+\varepsilon) + \tan\frac{\pi}{2}(1+\varepsilon)}{1 - k \tan\frac{\pi}{4}(1+\varepsilon)\cdot\tan\frac{\pi}{2}(1+\varepsilon)}$$

$$k = \frac{Z_2}{Z_1}$$

$$\varepsilon = \frac{f_2 - f_1}{f_2 + f_1}$$

Finally, by solving the above expressions, the impedance values of the branch-lines can thus be obtained as:

$$Z_A = Z_B = \frac{\sqrt{2\cos\pi\varepsilon}}{\cos\frac{\pi}{2}\varepsilon} Z_0 \tag{3.26}$$

$$Z_1 = -Z_A P \cos\frac{\pi}{2}\varepsilon \tag{3.27}$$

$$Z_2 = \frac{Z_1}{k} \tag{3.28}$$

$$Z_C = \frac{-Z_A}{\frac{Q}{P}\cos ec\frac{\pi}{2}\varepsilon + 1} \cot^2\frac{\pi}{2}\varepsilon \tag{3.29}$$

According to (3.26) - (3.29), Z_A and Z_B are uniquely set by f_2/f_1. As a result, the values of Z_A and Z_B simply lie between 25 Ω to 80 Ω for $1 < f_2/f_1 < 3$. However, Z_C, Z_1 and Z_2, are dependent on the choice of k for a given f_2/f_1. In other words, k may be considered as a free parameter for further tuning of impedances for extended operating range. Figure 3-31 shows the calculated line impedances (Z_C, Z_1 and Z_2) as a function of f_2/f_1 for different value of k. Z_C sets the lower bound of f_2/f_1 to

approximately 1.9. It can be seen that, for a given value of f_2/f_1, there exists some flexibility in the selection of line impedance. For example, for f_2/f_1 = 2.7, a smaller range of impedance (30 Ω -90 Ω) may be attained with k = 2.8. Hence, by the proper choice of k, design III is usable for $1.9 < f_2/f_1 < 2.9$. The variation of line impedance as a function of f_2/f_1 (from 1.7 to 2.9) is evaluated and shown in Figure 3-32 for k = 2.2, 2.5 and 2.8.

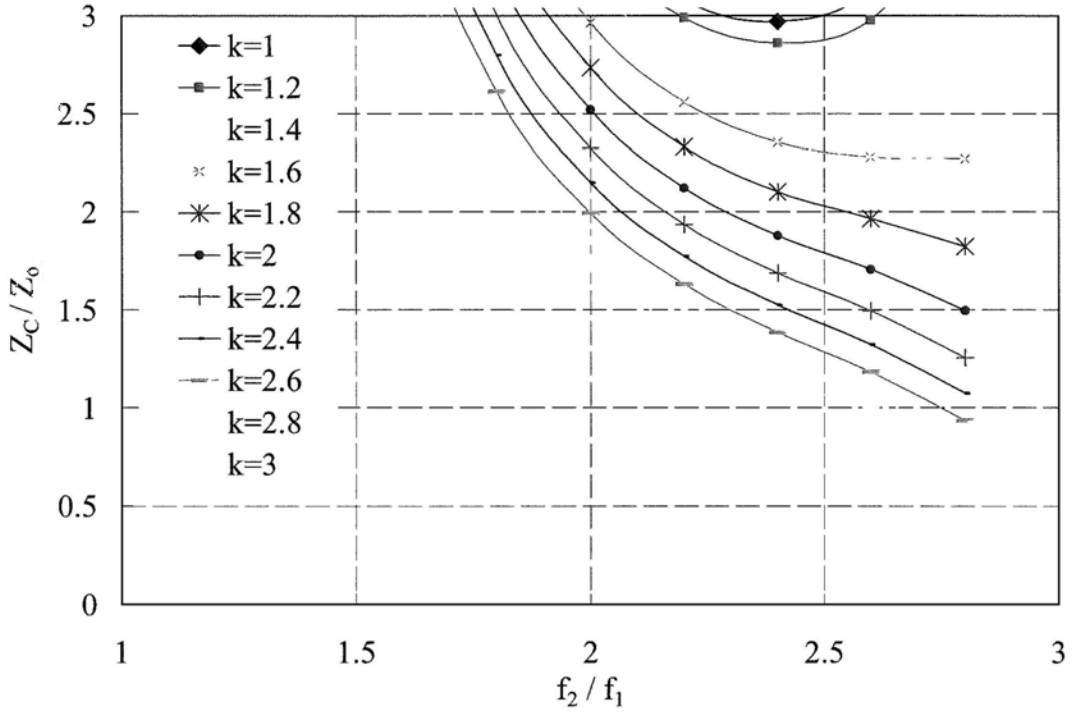

(a)

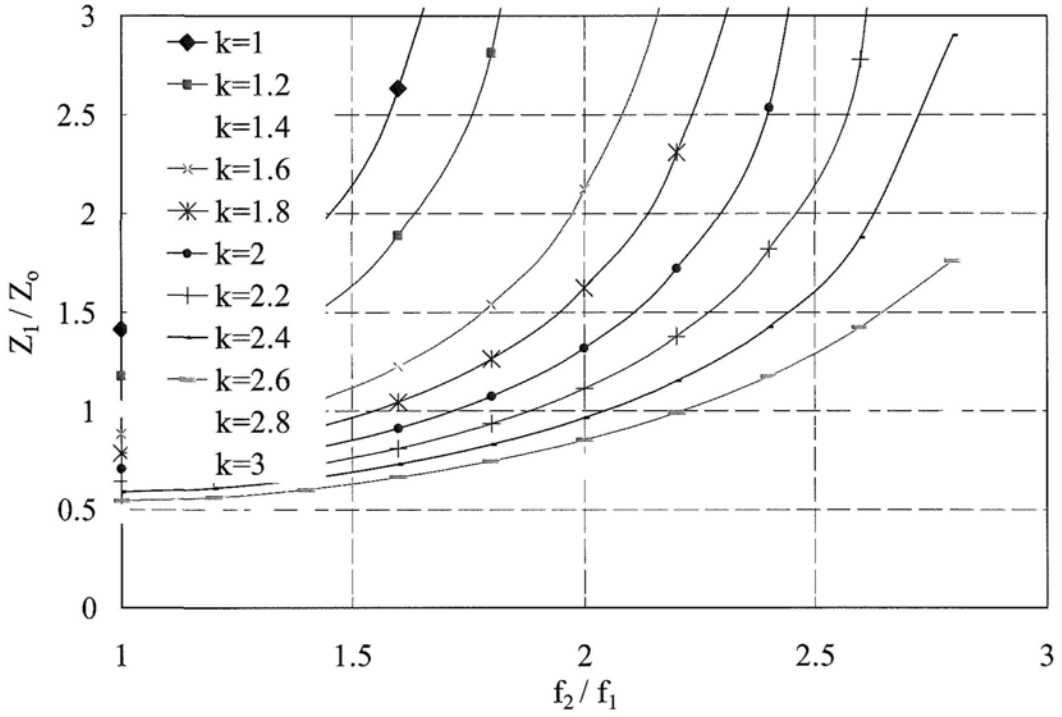

(b)

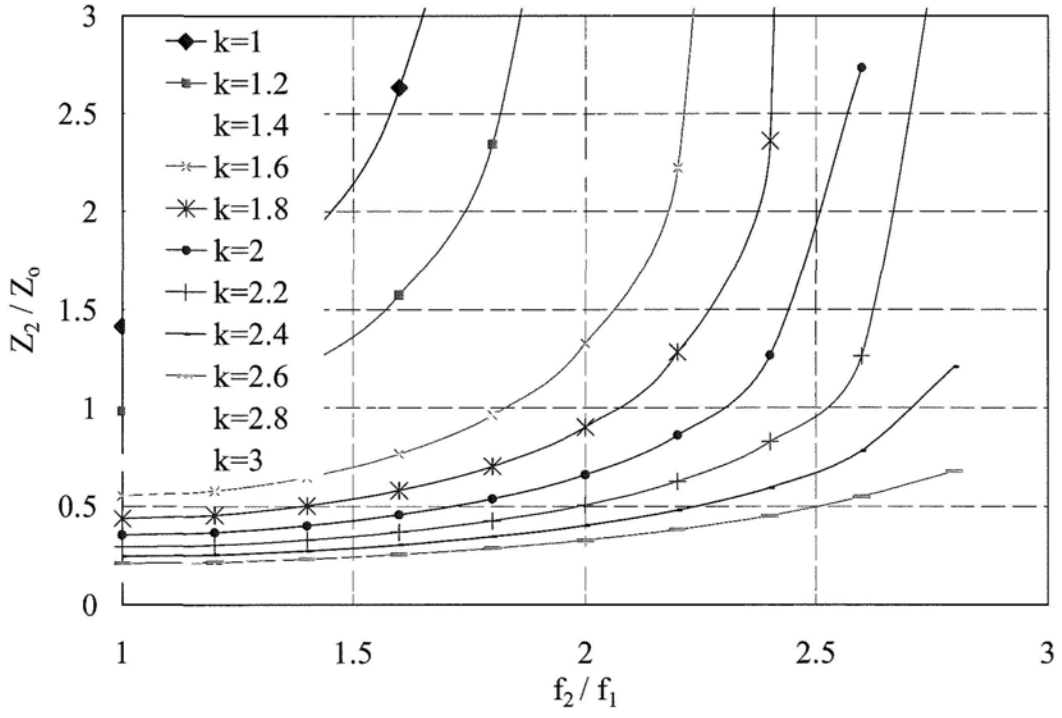

(c)

Figure 3-31: Normalized impedance of (a) Z_C, (b) Z_1 and (c) Z_2, versus frequency ratio, with different *k*.

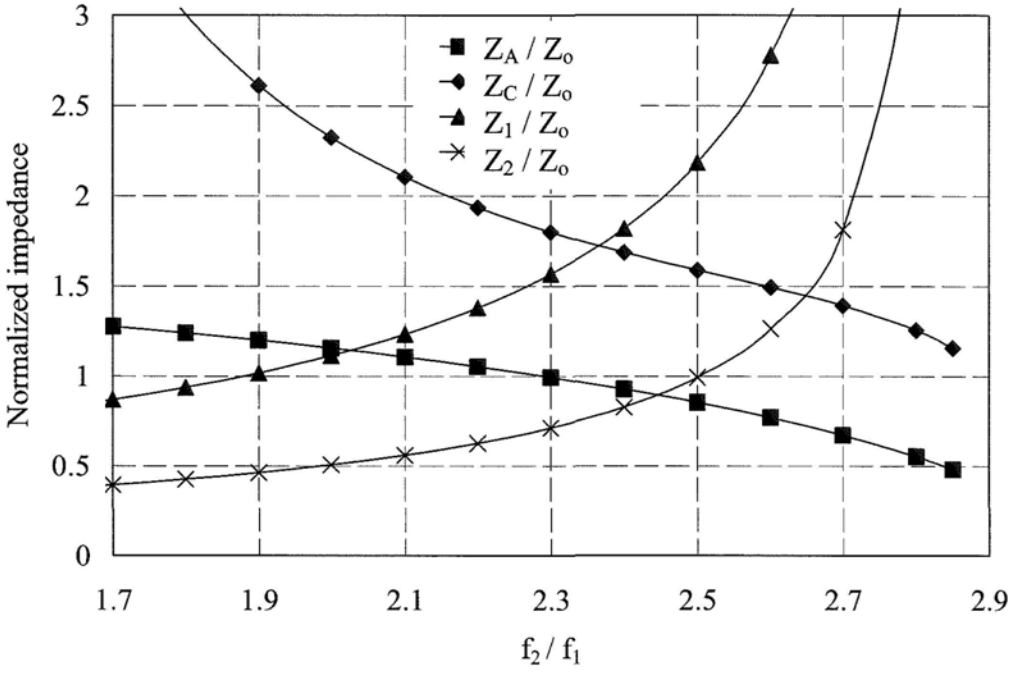
Normalized impedance
3
2.5
2
1.5
1
0.5
0
1.7
1.9
2.1
2.3
2.5
2.7
2.9
f_2 / f_1
Z_A / Z_o
Z_C / Z_o
Z_1 / Z_o
Z_2 / Z_o

(a) k=2.2

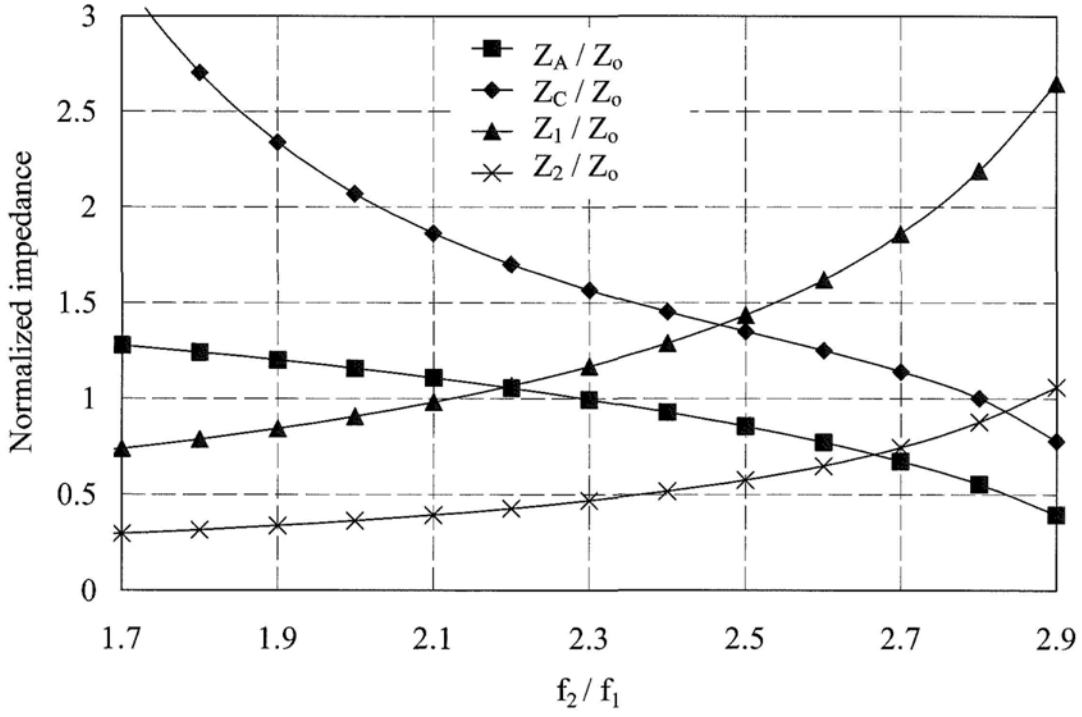
Normalized impedance
3
2.5
2
1.5
1
0.5
0
1.7
1.9
2.1
2.3
2.5
2.7
2.9
f_2 / f_1
Z_A / Z_o
Z_C / Z_o
Z_1 / Z_o
Z_2 / Z_o

(b) k=2.5

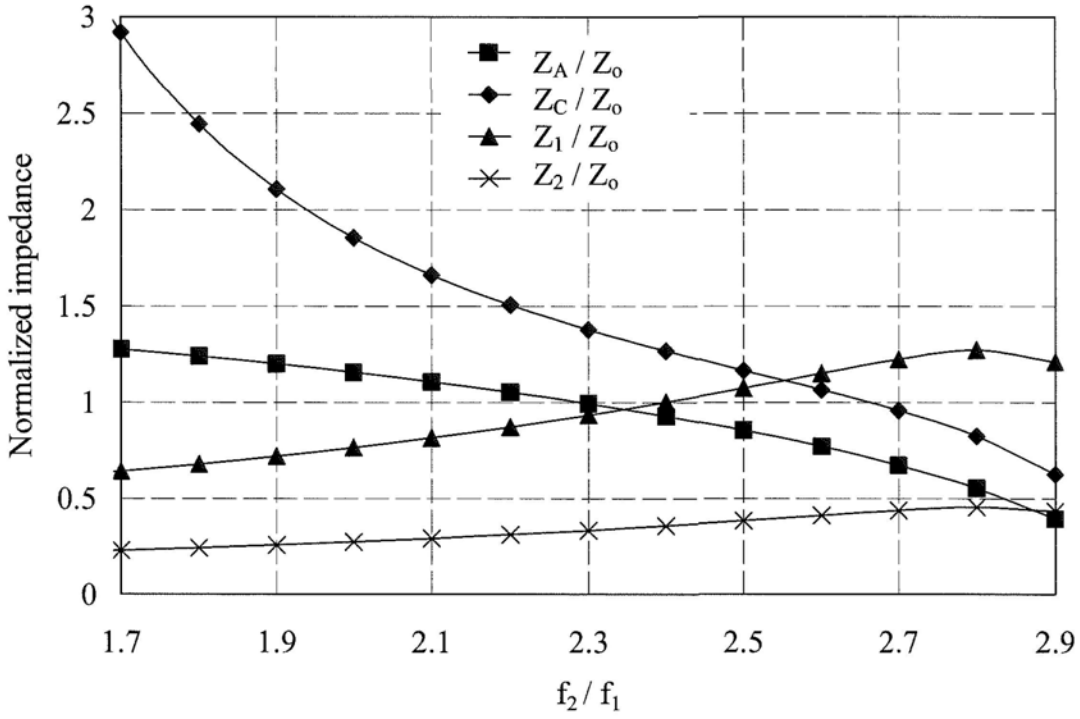

(c) k=2.8

Figure 3-32: Line impedances versus frequency ratio, when k equals (a) 2.2, (b) 2.5 and (c) 2.8.

3.3.2 Simulation results

Dual band rat-race coupler II and III are similar in structure but the latter design can operate with $f_2/f_1 > 2$. For demonstration, a frequency ratio of 2.5 is selected for design III. According to the design formulas, the branch-line impedances were found to be $Z_A = 42.7\ \Omega$, $Z_B = 42.7\ \Omega$, $Z_C = 67.4\ \Omega$, $Z_1 = 71.7\ \Omega$, and $Z_2 = 28.7\ \Omega$ ($k = 2.5$). Simulated return loss, insertion loss and phase response are given in Figure 3-33, 3-34 and 3-35. Its operating bandwidth is mainly limited by the input return loss performance (~ 30 MHz based on a minimal return loss of 20dB). Interestingly, the

phase mismatch (S_{21} and S_{41}) of the coupler was found to be fairly small over a wide bandwidth (~ 200MHz with tolerance of ±5°).

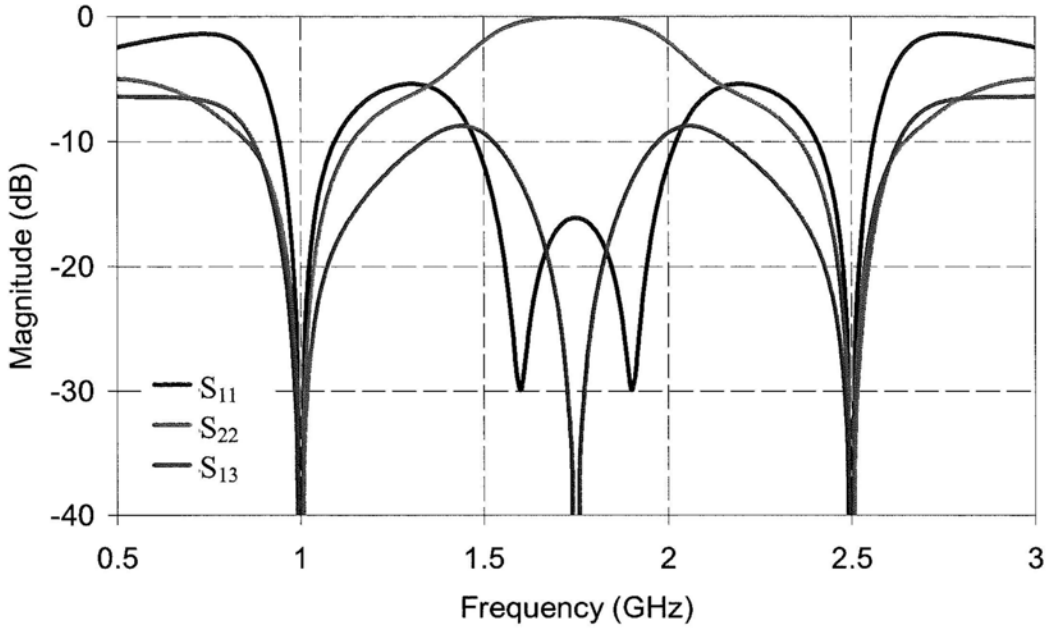

Figure 3-33: Simulated return loss and port isolation.

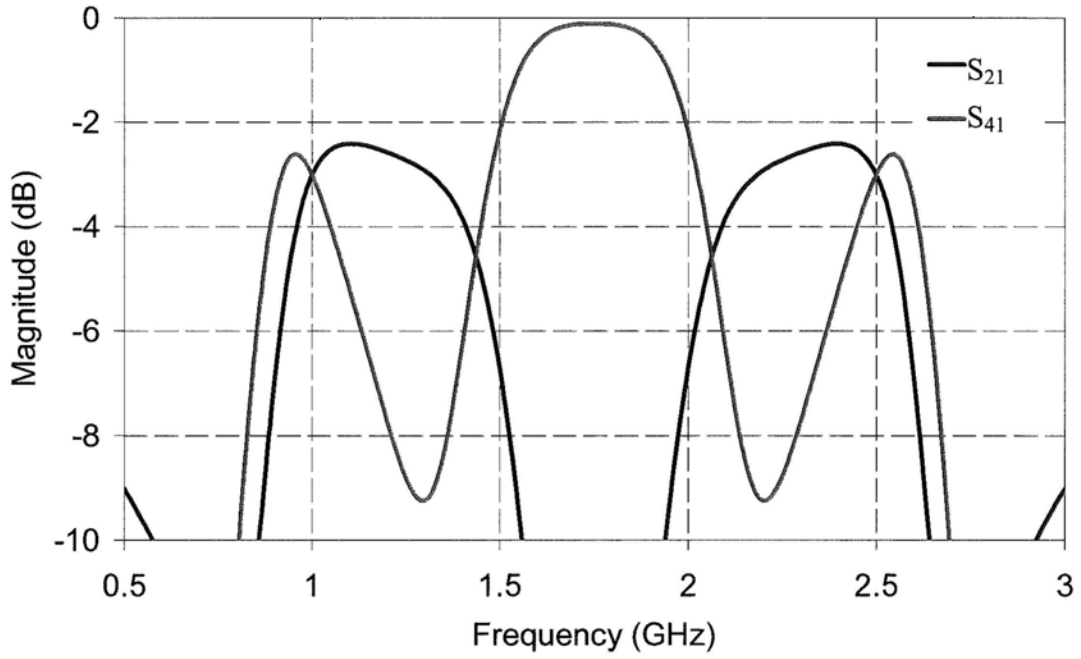

Figure 3-34: Simulated insertion loss (In-phase output).

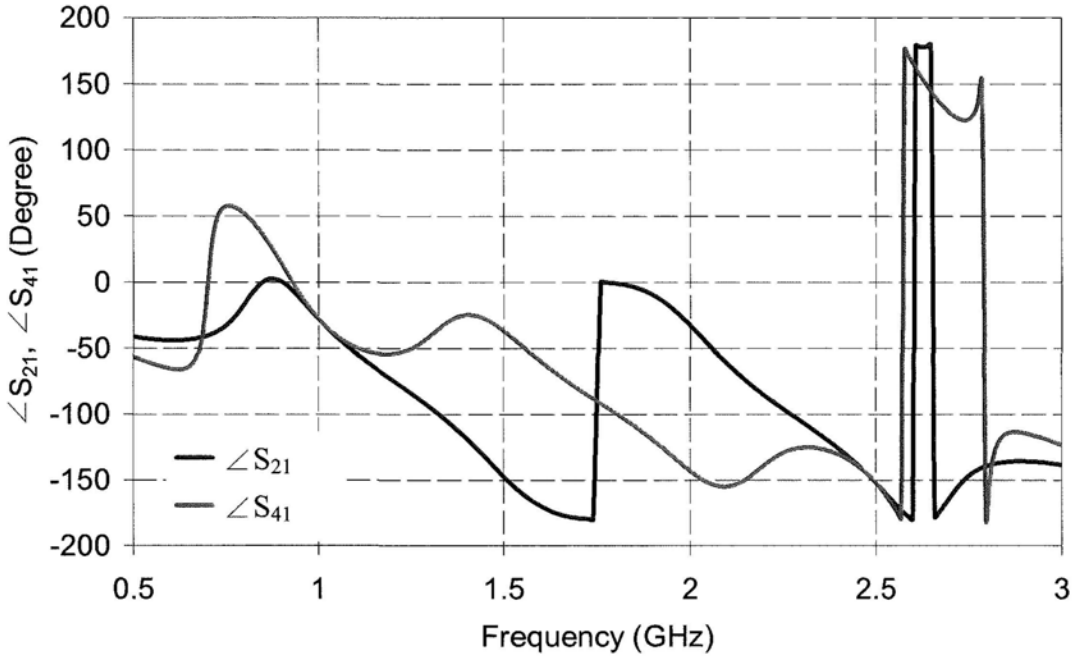

Figure 3-35: Simulated phase response (In-phase output).

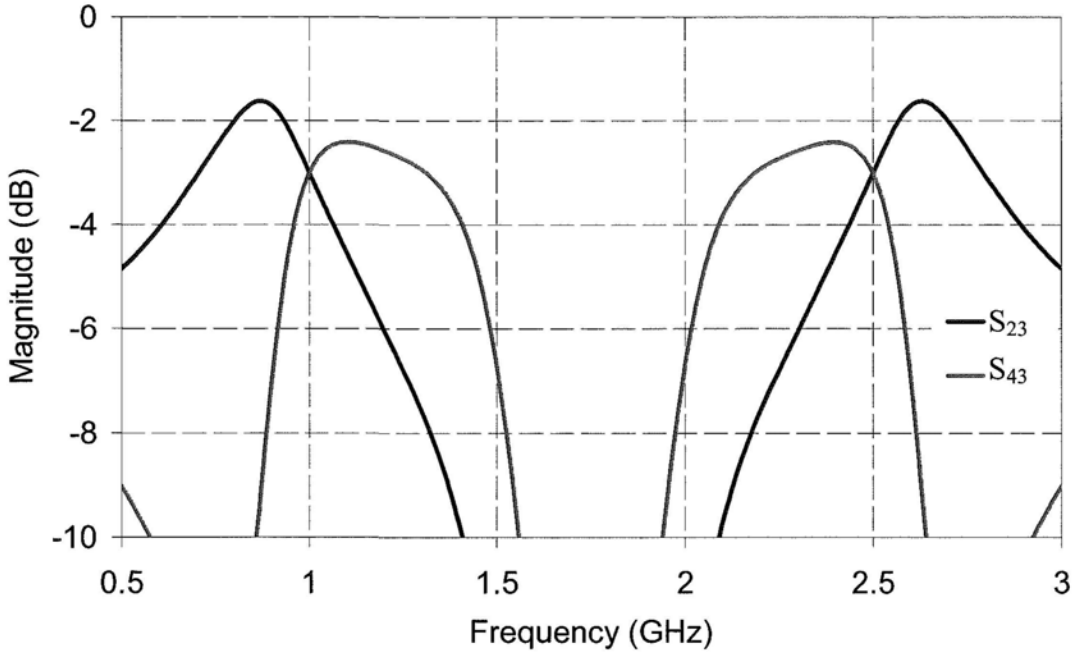

Figure 3-36: Simulated insertion loss (Anti-phase output).

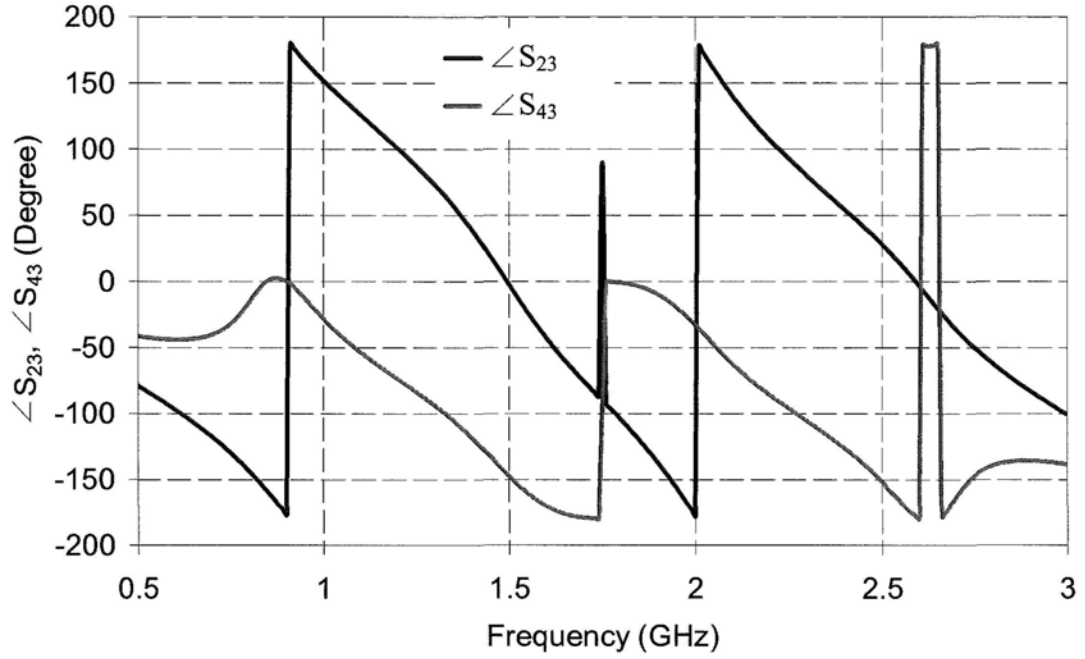

Figure 3-37: Simulated phase response (Anti-phase output).

3.3.3 Experimental results

Among the three proposed designs, this one occupies the smallest area and without the need of via holes. For illustration, a prototype, with operating frequencies of 2.45 GHz and 5.8 GHz was built and characterized. The selected values of Z_A, Z_C, Z_1 and Z_2 are, respectively, 47.5 Ω, 86.1 Ω, 86.4 Ω and 39.3 Ω. Figure 3-38 shows the final layout of the fabricated circuit. The physical size of the dual-band coupler is almost reduced by 40%, in compared to the conventional single-band rat-race hybrid that operates at 2.45GHz.

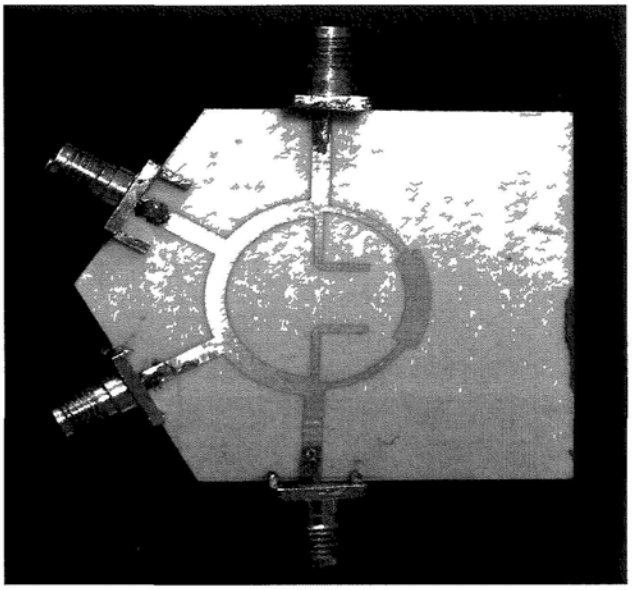

Figure 3-38: Photograph of the fabricated coupler (design III).

Figure 3-39 to Figure 3-43 give the measured results of the prototype in which the center frequencies of the two operating bands were found to be slightly shifted to 2.40 GHz and 5.60 GHz. Return loss and port isolation of more than 20dB were attained at both center frequencies. In addition, the measured insertion losses (S_{21}, S_{41}, S_{23} and S_{43}) were all closet 3.6dB. It is believed that the discrepancies between the simulated and measured performance were mainly caused by the junction effect and the tolerances of the fabrication process. These results also indicate that the phase mismatches are small (±5°) over bandwidth of almost 200MHz. However, the bandwidth of the coupler is limited by its amplitude imbalance to approximately 60MHz.

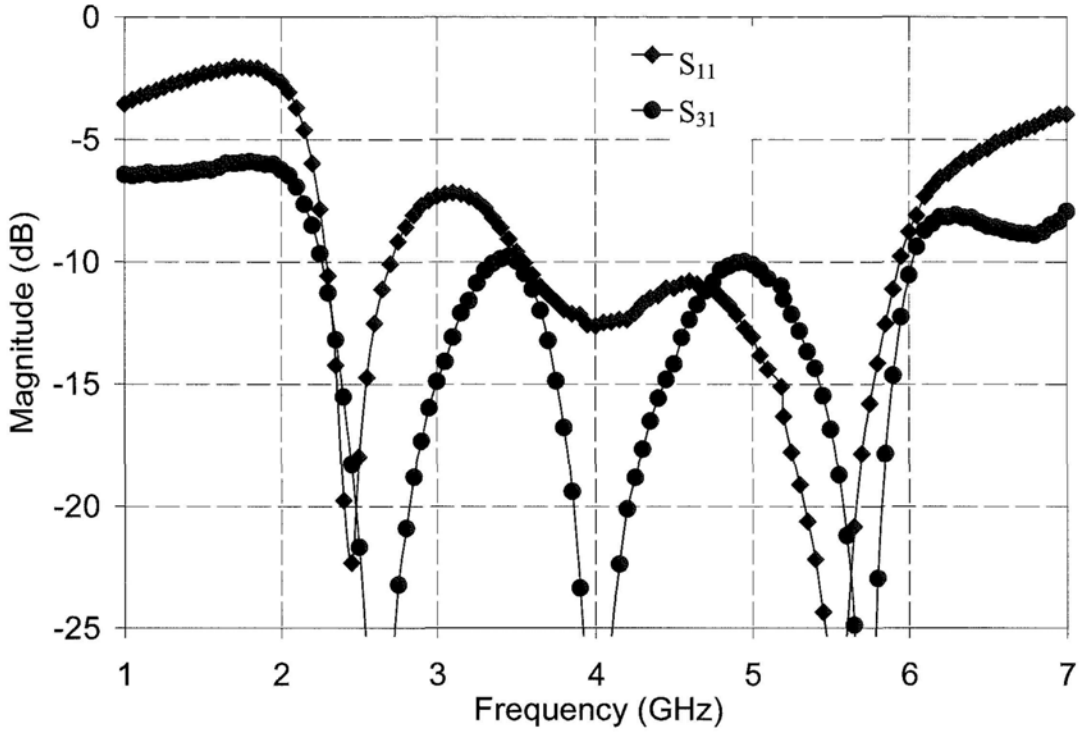

Figure 3-39: Measured return loss and port isolation (design III).

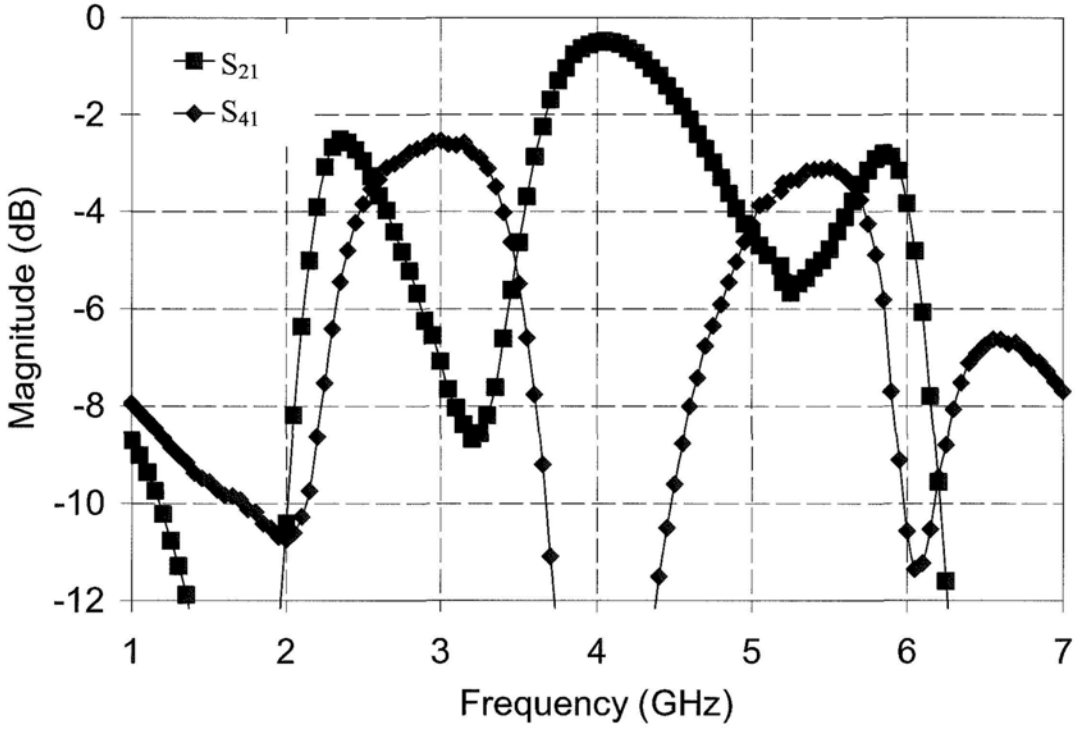

Figure 3-40: Measured insertion loss of in-phase outputs (design III).

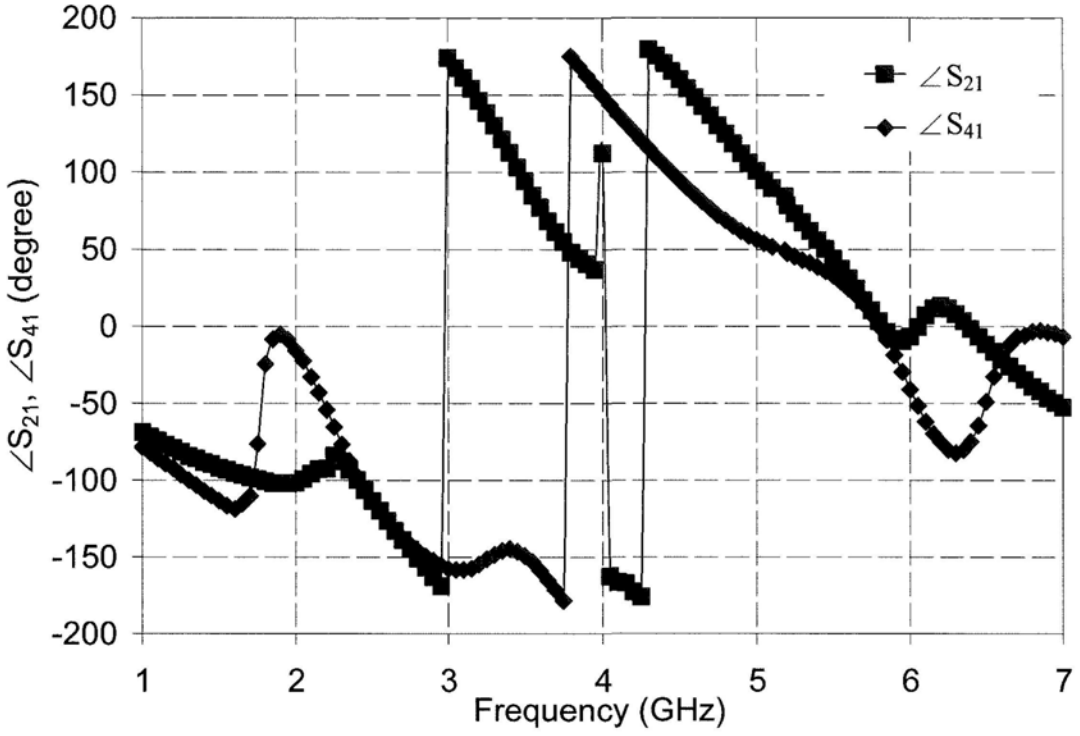

Figure 3-41: Measured phase response of in-phase outputs (design III).

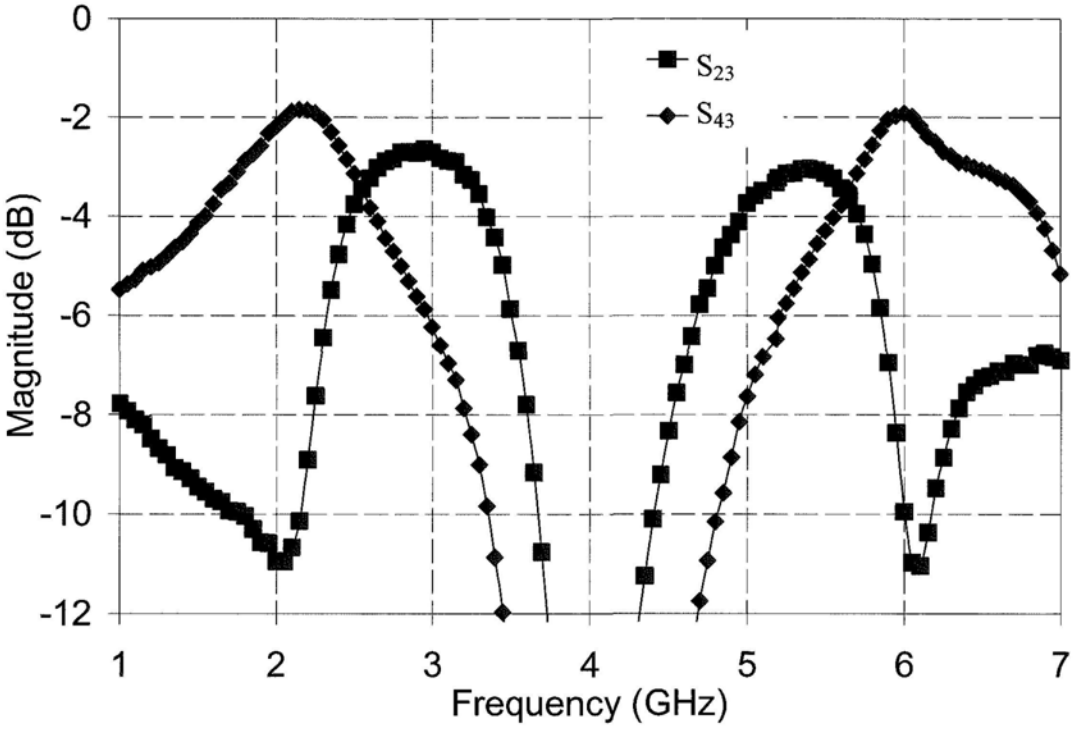

Figure 3-42: Measured insertion loss of anti-phase outputs (design III).

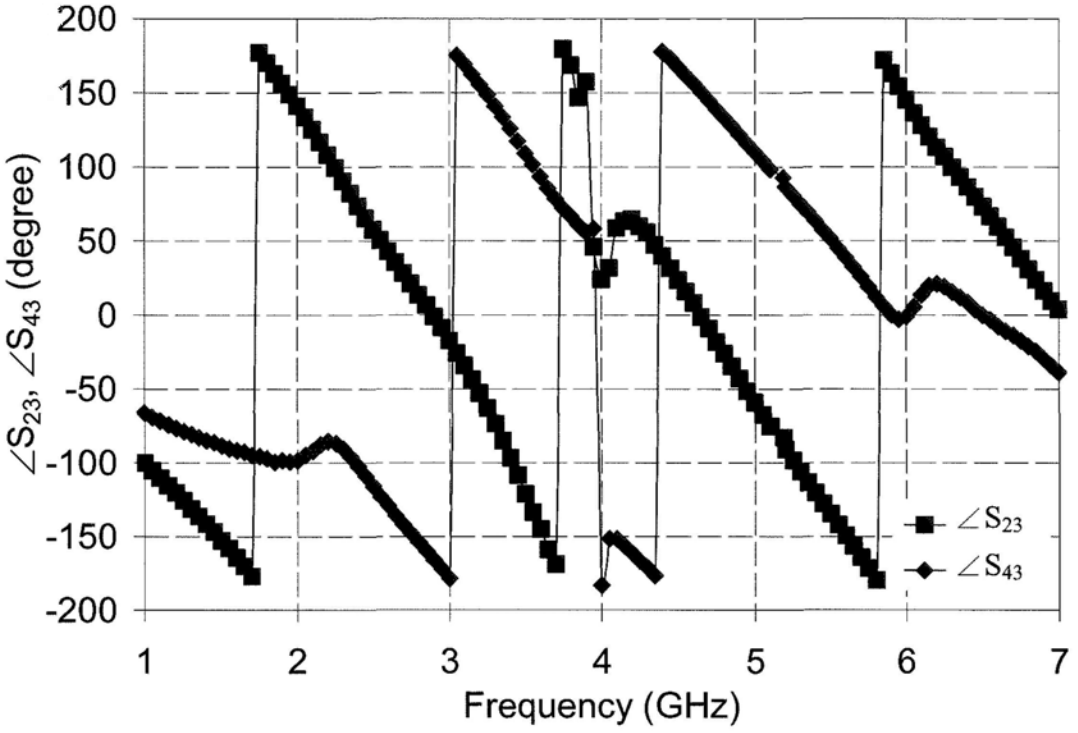

Figure 3-43: Measured phase response of anti-phase outputs (design III).

3.4 Summary

Three similar structures of dual-band rat-race couplers have been proposed. They are similar in structure but with slightly different sizes and respectively usable f_2/f_1 thus it affects the design choice. Table 3-1 summarizes all key design parameters of these designs for sake of comparison.

Parameters	Design I	Design II	Design III
Circumference (λ @ f_0)	1.75	1.25	1.25
Range of f_2/f_1	2 – 2.7	1 – 1.75	1.9 – 2.9
Necessity of ground vias	YES	YES	NO

Table 3-1: Key parameter comparison among three proposed dual-band rat-race circuits.

Chapter 4. Proposed Dual-Band Power Divider

A conventional Wilkinson power divider exhibits a relatively wide bandwidth (about 38%). The early designs of dual-band power dividers were reported in [14-16], but they were found to suffer from either finite output return loss and port isolation or the requirement of lumped reactive elements.

4.1. Dual band power divider

The proposed dual band power divider [20] is based on a new dual-band quarter-wavelength impedance transformer, as depicted in Figure 4-1.

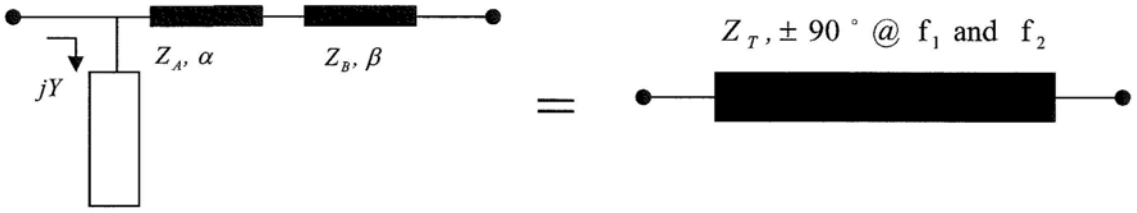

Figure 4-1: New dual-band impedance transformer and its equivalent.

The new transformer is composed of a two-section branch-line and a shunt element (Y). For dual-band operation, this transformer should exhibit an electrical length of ±90° and line impedance of Z_T, evaluated at f_1 and f_2. The ABCD parameterse of the transformer can be derived as follows:

$$\begin{bmatrix} 1 & 0 \\ jY & 1 \end{bmatrix} \begin{bmatrix} \cos\alpha & jZ_A \sin\alpha \\ j\dfrac{\sin\alpha}{Z_A} & \cos\alpha \end{bmatrix} \begin{bmatrix} \cos\beta & jZ_B \sin\beta \\ j\dfrac{\sin\beta}{Z_B} & \cos\beta \end{bmatrix} = \begin{bmatrix} 0 & \pm jZ_T \\ \pm j\dfrac{1}{Z_T} & 0 \end{bmatrix} \tag{4.1}$$

By equaling coefficients, the following expressions are obtained:

$$\cos\alpha\cos\beta - k\sin\alpha\sin\beta = 0 \tag{4.2}$$

$$\cos\alpha\cos\beta - \frac{1}{k}\sin\alpha\sin\beta = \pm Z_T\, Y \tag{4.3}$$

$$Z_B\left(\sin\beta\cos\alpha + k\sin\alpha\cos\beta\right) = \pm Z_T \tag{4.4}$$

$$k = \frac{Z_A}{Z_B} \tag{4.5}$$

After simplifying, we get:

$$Z_B = \pm Z_T \frac{\sin\beta}{\cos\alpha} \tag{4.6}$$

$$k = \frac{1}{\tan\alpha\tan\beta} \tag{4.7}$$

$$Y = \frac{\cos(\alpha+\beta)\cos(\alpha-\beta)}{\pm Z_T \cos\alpha\cos\beta} \tag{4.8}$$

Furthermore, the values of α and β, evaluated at the centre frequencies of the upper and lower bands (f_2 and f_1), may be expressed as:

$$\alpha(f_2) = \beta(f_2) = \frac{\pi}{2}\cdot\frac{f_2}{f_0} = \frac{\pi}{2} + \varepsilon \tag{4.9}$$

$$\alpha(f_1) = \beta(f_1) = \frac{\pi}{2}\cdot\frac{f_1}{f_0} = \frac{\pi}{2} - \varepsilon \tag{4.10}$$

where

$$\varepsilon = \frac{f_2 - f_1}{f_2 + f_1} \cdot \frac{\pi}{2}$$

$$f_0 = \frac{f_2 + f_1}{2}$$

Subsequently, by combining equation (4.7) – (4.10), we obtain:

$$Z_B = Z_T \cot\varepsilon \tag{4.11}$$

$$k = \tan^2\varepsilon \tag{4.12}$$

$$Y(f_2) = -Y(f_1) = \frac{\cos(2\varepsilon)}{Z_T \sin^2\varepsilon} \tag{4.13}$$

$$\alpha(f_0) = \beta(f_0) = \frac{\pi}{2} \tag{4.14}$$

The shunt element Y, as defined by equation (4.13), can be realized by either a short-circuit stub (90° at f_0) or an open-circuited stub (180° at f_0). As illustrated in Figure 4-1, a dual-band power divider can be constructed by using the proposed transformer with line impedance given by:

$$Z_A = \sqrt{2} Z_0 \tan\varepsilon \tag{4.15}$$

$$Z_B = \sqrt{2} Z_0 \cot\varepsilon \tag{4.16}$$

$$Z_{SC} = \frac{Z_0}{2} \frac{\tan 2\varepsilon}{\sqrt{2}} \tan^2\varepsilon \tag{4.17}$$

$$Z_{OC} = \frac{Z_0}{2} \frac{\tan^2 2\varepsilon}{\sqrt{2}} \tan\varepsilon \tag{4.18}$$

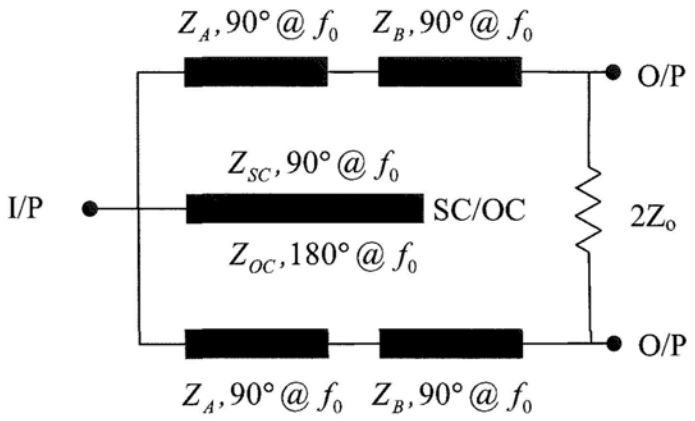

Figure 4-2: Proposed dual-band power divider

To examine the usable range of the power divider, line impedances are computed (Z_A, Z_B, Z_{SC} and Z_{OC}) as a function of f_2 / f_1 and are plotted in Figure 4-3. For practical circuit realization, the right type of shunt stub should be chosen for reasonable impedance range (20 Ω to 100 Ω). For example, a power divider with open-circuited stub should be used for $2 < f_2/f_1 < 2.3$; whereas a short-circuited stub should be chosen for $2.3 < f_2/f_1 < 2.75$.

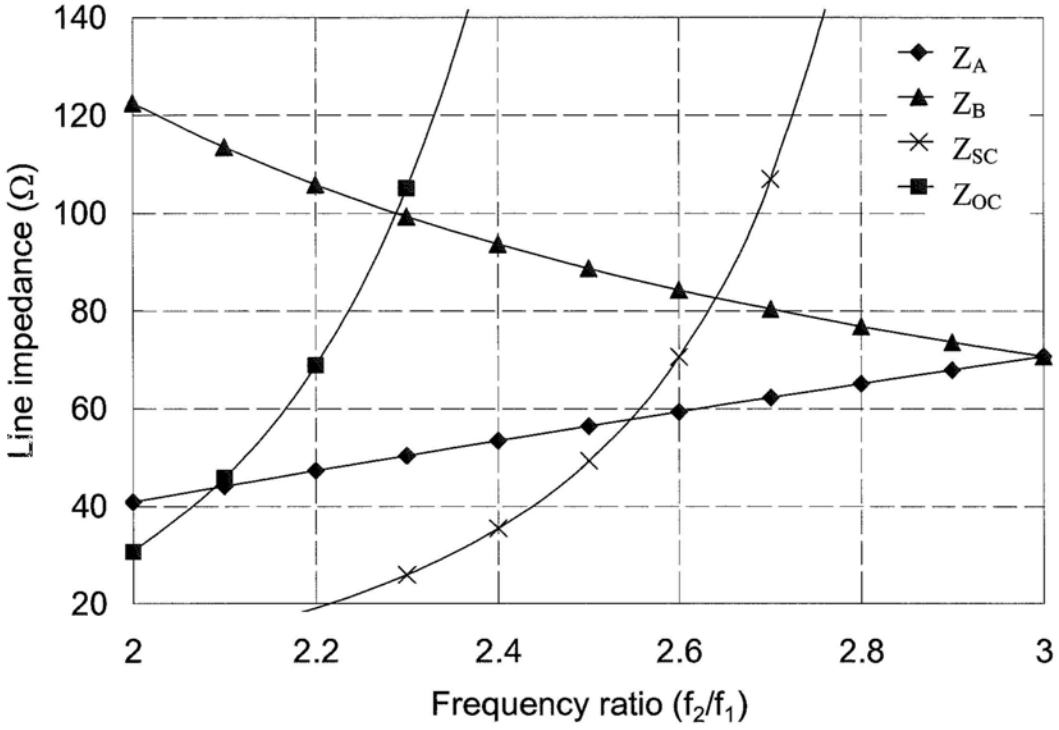

Figure 4-3: Line impedance variation versus frequency ratio (f_2/f_1)

4.2. Simulation results

The proposed dual-band power divider is usable for f_2/f_1 ranging from 2 to 2.8. For verification purposes, a design with f_1 = 1 GHz and f_2 = 2.5 GHz was chosen. As a result, a short-circuited stub was adopted for ease of construction. Accordingly, the corresponding line impedances were calculated: Z_A = 56.4 Ω, Z_B = 88.7 Ω and Z_{SC} = 49.3 Ω. To examine the performance of the power divider, return loss, port isolation and insertion loss were simulated and plotted in Figure 4-4 and 4-5.

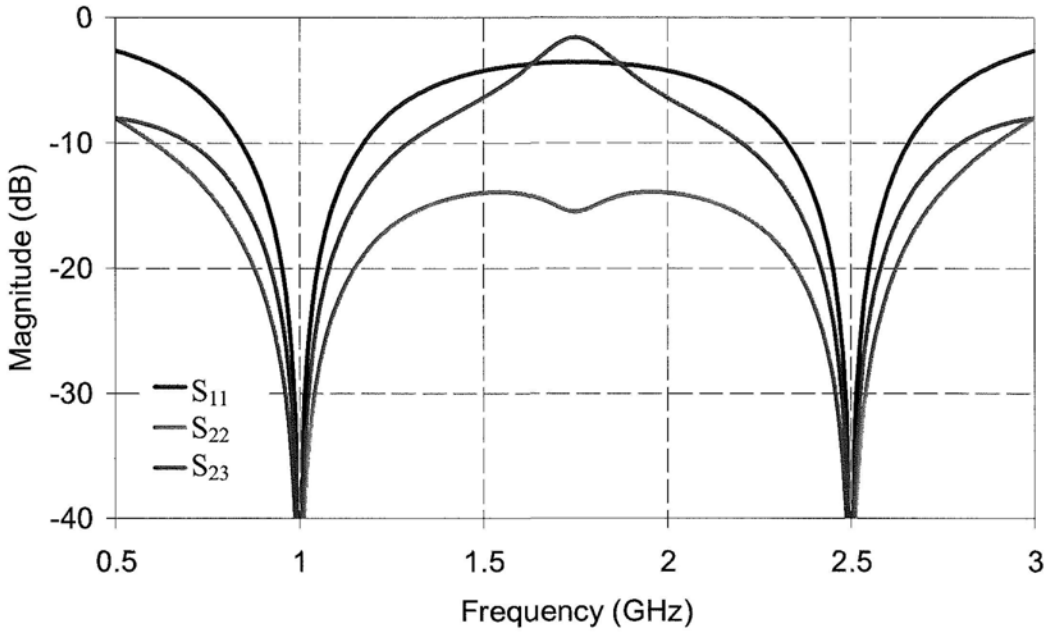

Figure 4-4: Simulated return loss and port isolation.

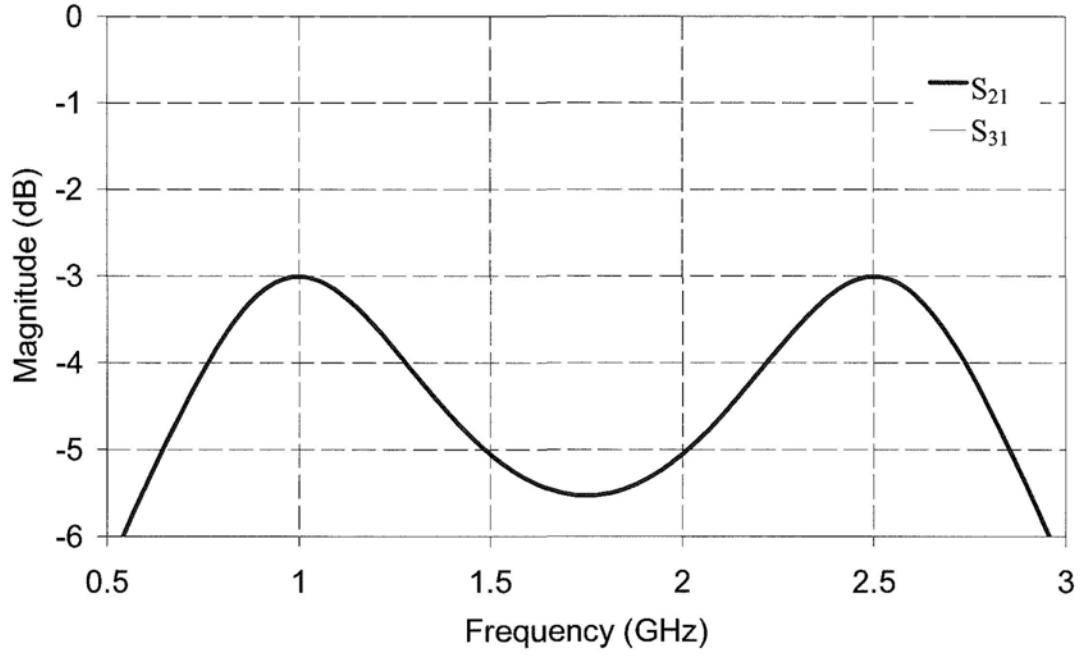

Figure 4-5: Simulated insertion loss.

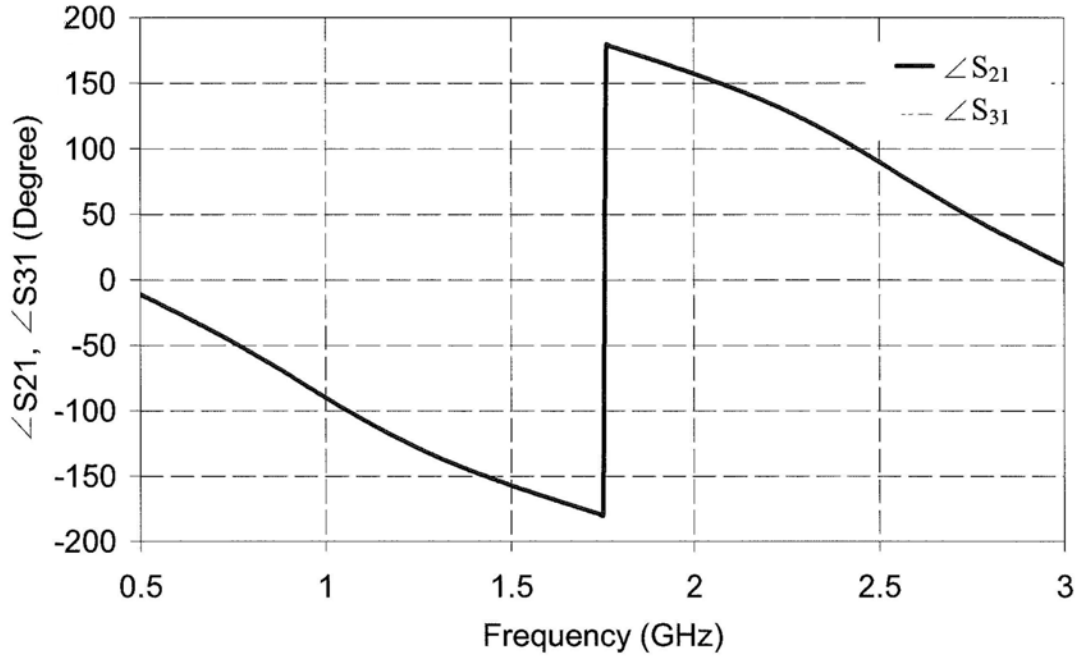

Figure 4-6: Simulated phase response.

It can be observed that ideal port isolation and return loss were achieved at both f_1 and f_2. The operating bandwidth is mainly limited by the input return loss performance. No amplitude or phase imbalance is found due to the symmetry in structure.

4.3. Experimental Results

For experimental verification, a dual-band power divider operating at 1 GHz and 2.65 GHz was implemented using microstrip. As $f_2/f_1 = 2.65$, a short-circuited stub was chosen for circuit realization. Based on the derived formulas, the values of Z_A, Z_B and Z_{SC}, were found to be 60.8 Ω, 82.3 Ω and 86.1 Ω, respectively.

Figure 4-7 shows the top view of the fabricated divider circuit.

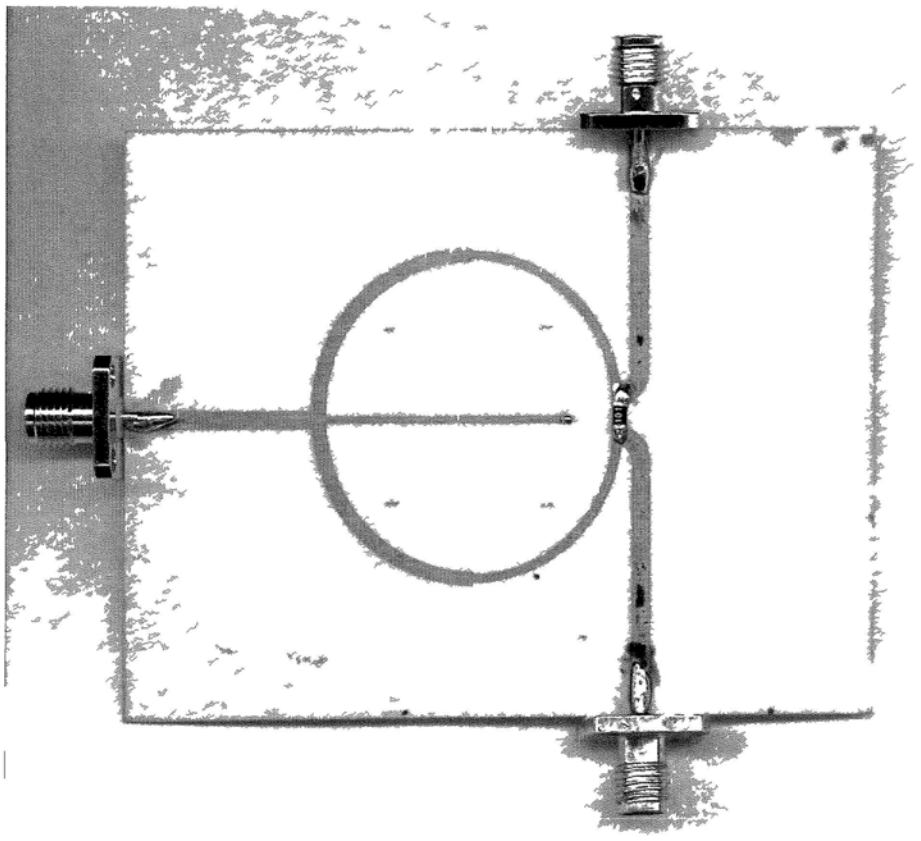

Figure 4-7: Photograph of the fabricated power divider

Figure 4-8 and Figure 4-10 show the measured performance of the divider in which the center frequencies of the two operating bands were found to be slightly shifted to 950 MHz and 2.55 GHz respectively. Minimal input / output return losses of 22dB and port isolation of 25dB were observed at both center frequencies. Almost zero amplitude or phase mismatches between the two output ports were attained, as expected. Low insertion loss (about 3.3dB) was achieved over a bandwidth of about 250MHz (both lower and upper bands). The operating bandwidth of the divider is mainly determined by the input return loss performance (approximately 100MHz) based on 20dB requirement.

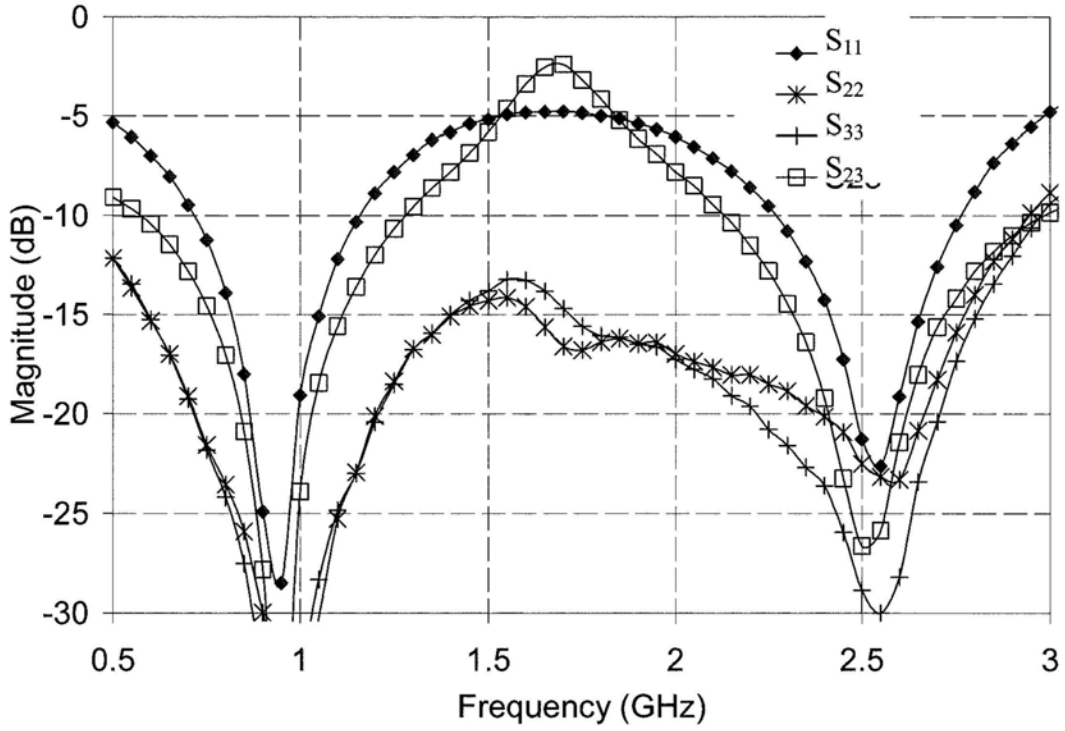

Figure 4-8: Measured return loss and port isolation of proposed power divider.

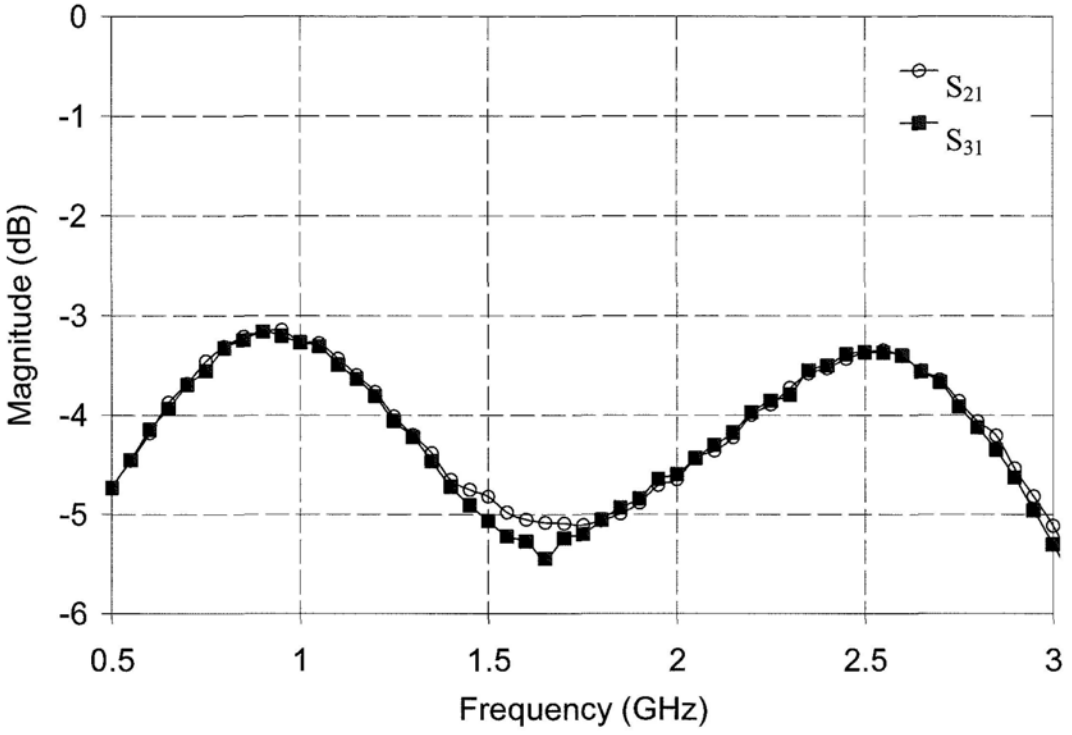

Figure 4-9: Measured insertion loss of proposed power divider.

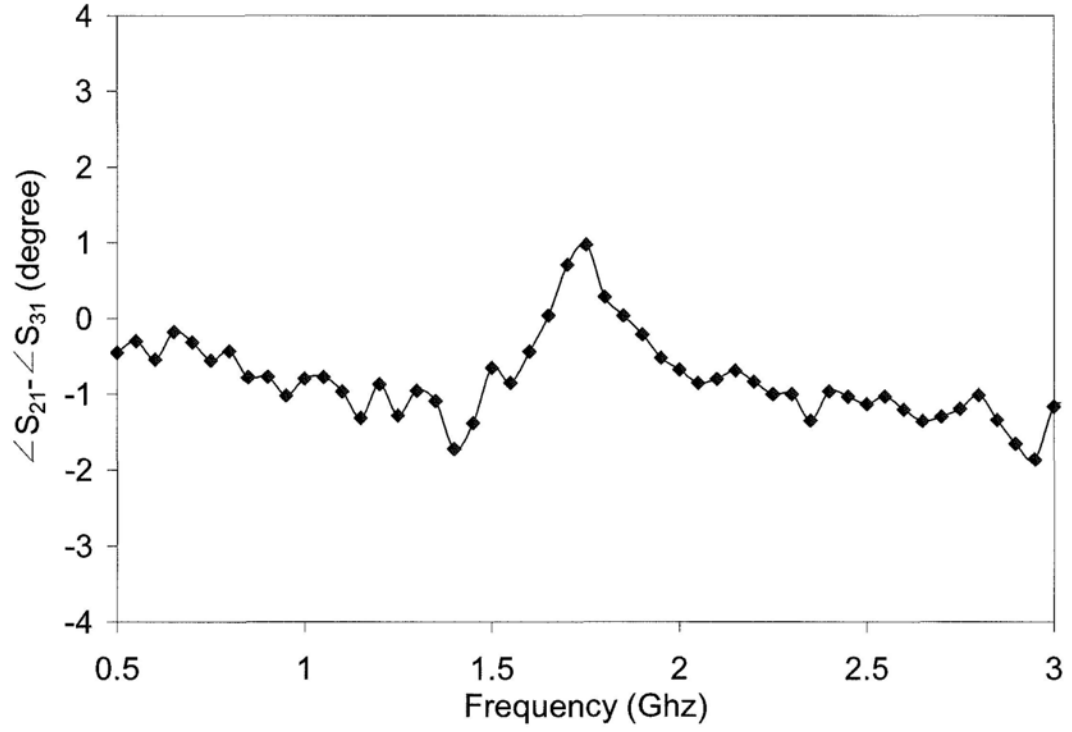

Figure 4-10: Measured phase response of proposed power divider.

4.4. Summary

A fully distributed dual band power divider is illustrated in this section, offering ideal

port isolation and equal power division at both centre frequencies. It is composed by newly designed dual-band quarter-wavelength impedance transformers. Regarding the topology, this design is highly similar as the conventional one, with the insertion of a shunt stub at the input port. Short or open circuited stub is chosen according to the range of f_2/f_1. The range of operating frequency ratio is from 2 to 2.7 and it is the practical limit of the design, allowing easy fabrication of branch line required.

Chapter 5. Proposed Dual-Band Crossover Junction

In modern communication systems, dual-band or multi-band operations are almost a necessity, and the adoption of dual-band microwave devices [10]-[13] has become an attractive solution to reduce size and cost. Unfortunately, previously published crossover circuits only offer an operating bandwidth of no more than 20% (based on a minimal return loss and port isolation requirement of 20 dB). Although, in theory, a wideband crossover may be realized by a multi-section branch-line coupler, its major drawbacks are the enlarged circuit size as well as the extremely high (and low) line impedances involved. In this section, a new dual-band crossover junction realized by microstrip is proposed. Closed-form design equations are formulated based upon even-odd mode analysis.

5.1 Dual-band cross-over junction design

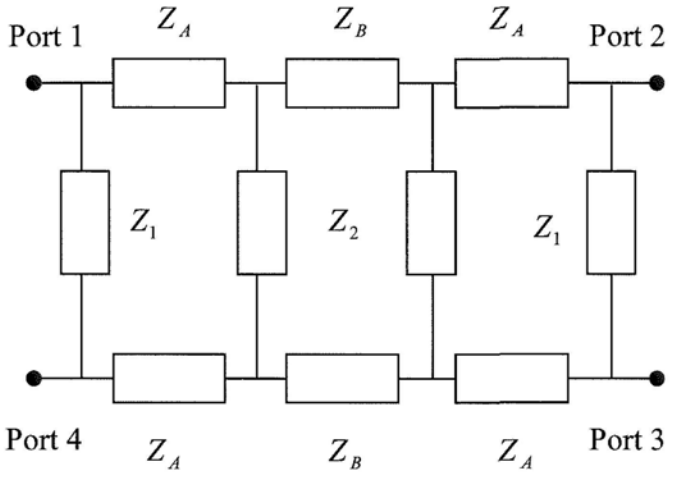

Figure 5-1: Proposed dual-band crossover junction.

Figure 5-1 shows the schematic diagram of the proposed circuit under analysis. Structurally speaking, it is based on a tri-section branch-line coupler but with its line impedances (Z_A, Z_B, Z_1 and Z_2) being enforced for dual-band operation. Moreover, all branch-lines are chosen to be quarter-wavelength long evaluated at the mid frequency (f_0) defined by: $f_0 = \frac{f_2 + f_1}{2}$.

Since the proposed circuit possesses vertical and horizontal bisymmetry, either electric wall (short-circuit) or magnetic wall (open-circuit) may be inserted for easy analysis. Figure 5-2 shows the four combination of reduced networks with purely reactive input admittances (Y_{ee}, Y_{eo}, Y_{oe} and Y_{oo}).

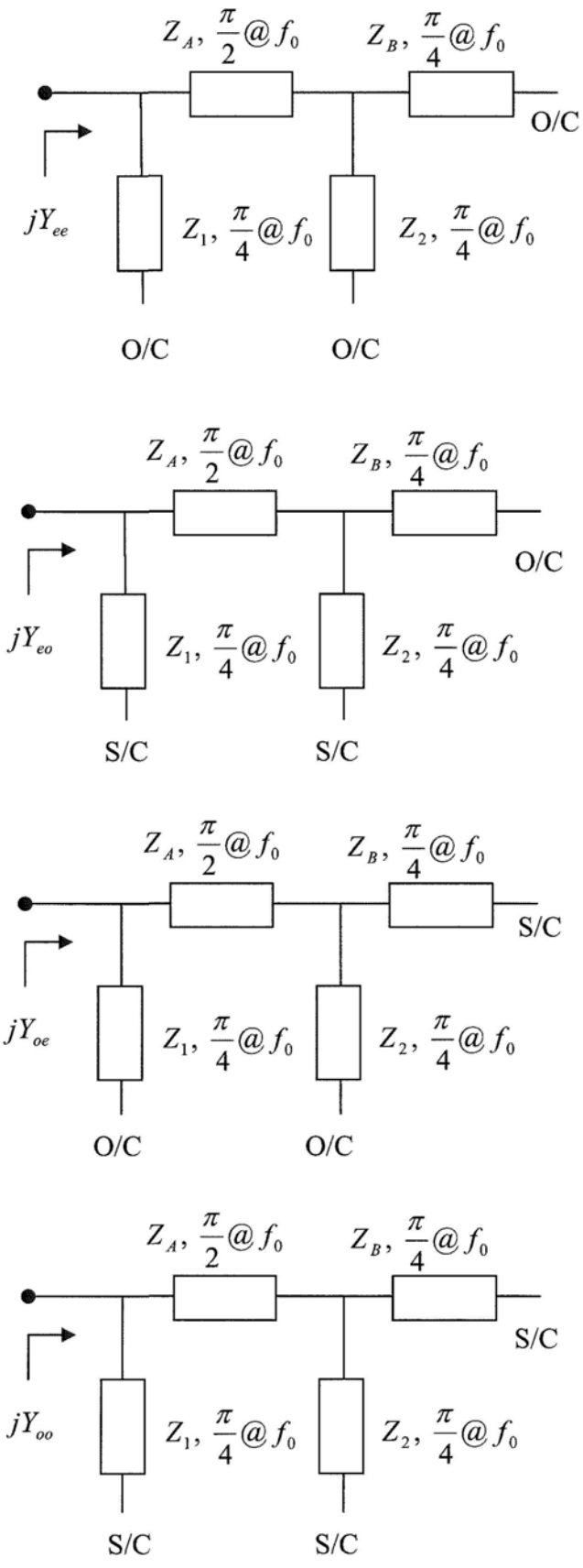

Figure 5-2: Reduced networks for analysis

According to [34], the scattering parameters of the crossover can simply be expressed as:

$$S_{11} = \frac{\Gamma_{ee} + \Gamma_{eo} + \Gamma_{oe} + \Gamma_{oo}}{4} \tag{5.1}$$

$$S_{21} = \frac{\Gamma_{ee} + \Gamma_{eo} - \Gamma_{oe} - \Gamma_{oo}}{4} \tag{5.2}$$

$$S_{31} = \frac{\Gamma_{ee} - \Gamma_{eo} - \Gamma_{oe} + \Gamma_{oo}}{4} \tag{5.3}$$

$$S_{41} = \frac{\Gamma_{ee} - \Gamma_{eo} + \Gamma_{oe} - \Gamma_{oo}}{4} \tag{5.4}$$

where Γ_{ee}, Γ_{eo}, Γ_{oe} and Γ_{oo} are input reflection coefficients defined by:

$$\Gamma_{ee,eo,oe,oo} = \frac{1 - jY_{ee,eo,oe,oo}Z_0}{1 + jY_{ee,eo,oe,oo}Z_0} \tag{5.5a}$$

$$Y_{ee} = Y_1 \cdot t + Y_A \frac{(Y_B + Y_2)\cdot t + Y_A \cdot T}{Y_A - (Y_B + Y_2)\cdot t \cdot T} \tag{5.5b}$$

$$Y_{eo} = -\frac{Y_1}{t} + Y_A \frac{Y_B \cdot t - \frac{Y_2}{t} + Y_A \cdot T}{Y_A - \left(Y_B \cdot t - \frac{Y_2}{t}\right)\cdot T} \tag{5.5c}$$

$$Y_{oe} = Y_1 \cdot t + Y_A \frac{Y_2 \cdot t - \frac{Y_B}{t} + Y_A \cdot T}{Y_A - \left(Y_2 \cdot t - \frac{Y_B}{t}\right)\cdot T} \tag{5.5d}$$

$$Y_{oo} = -\frac{Y_1}{t}\cdot + Y_A \frac{-\frac{Y_B + Y_2}{t} + Y_A \cdot T}{Y_A + \frac{Y_B + Y_2}{t}\cdot T} \tag{5.5e}$$

$$t = \tan\left(\frac{\pi}{4} \cdot \frac{f}{f_0}\right) \tag{5.5f}$$

$$T = \tan\left(\frac{\pi}{2} \cdot \frac{f}{f_0}\right) \tag{5.5g}$$

Based on the assumption of an ideal crossover, i.e. $S_{11} = S_{21} = S_{41} = 0$, a mathematical relationship between the various coefficients can be established as follows:

$$\Gamma_{ee} = \Gamma_{oo} = -\Gamma_{eo} = -\Gamma_{oe} \tag{5.6}$$

Subsequently, by adopting the input admittances of the reduced networks, the above expression can thus be reduced to:

$$Y_{ee} = Y_{oo} \tag{5.7}$$

$$Y_{eo} = Y_{oe} \tag{5.8}$$

$$Y_{ee}\, Y_{eo}\, Z_0^{\,2} = -1 \tag{5.9}$$

Meanwhile, the two frequency-dependent functions (t and T), evaluated at f_2 and f_1, are found to be interrelated via (5.10) and (5.11).

$$K = \tan\left(\pi \frac{f_2}{2f_0}\right) = -\tan\left(\pi \frac{f_1}{2f_0}\right) = \tan(\pi\alpha) \tag{5.10}$$

$$k = \tan\left(\pi \frac{f_2}{4f_0}\right) = \frac{1}{\tan\left(\pi \frac{f_1}{4f_0}\right)} = \tan\left(\frac{\pi\alpha}{2}\right) \tag{5.11}$$

where $\alpha = \dfrac{f_2/f_1}{f_2/f_1 + 1}$

By further inspection, the following relations are obtained.

$$Y_{ee}(f_1) = -Y_{oo}(f_2) \tag{5.12}$$

$$Y_{eo}(f_1) = -Y_{oe}(f_2) \tag{5.13}$$

$$Y_{oe}(f_1) = -Y_{eo}(f_2) \tag{5.14}$$

$$Y_{oo}(f_1) = -Y_{ee}(f_2) \tag{5.15}$$

The above results reveal that the design equations of the crossover, as dictated by (5.7) - (5.9), are concurrently satisfied at the two center frequencies. In other words, it is only necessary to have these equations solved at either f_2 or f_1. Hence, by putting (5.5b)-(5.5e), (5.10)-(5.11) into (5.7) and (5.8), one obtains:

$$y_1 = \frac{Y_1}{Y_A} = \frac{k}{1+k^2}\cdot\left\{\frac{K-\frac{y_B+y_2}{k}}{1+\frac{y_B+y_2}{k}\cdot K} - \frac{K+(y_B+y_2)\cdot k}{1-(y_B+y_2)\cdot k\cdot K}\right\} \tag{5.16}$$

$$y_1 = \frac{k}{1+k^2}\cdot\left\{\frac{K+y_B\cdot k-\frac{y_2}{k}}{1-\left(y_B\cdot k-\frac{y_2}{k}\right)\cdot K} - \frac{K+y_2\cdot k-\frac{y_B}{k}}{1-\left(y_2\cdot k-\frac{y_B}{k}\right)\cdot K}\right\} \tag{5.17}$$

And by combining the above expressions, y_1 and y_B (= Y_B/Y_A) can then be written in terms of y_2 (= Y_2/Y_A) and K as given by (5.18) and (5.19)

.

$$y_1 = \frac{1}{2y_2} \tag{5.18}$$

$$y_B = \frac{1 + y_2 + \sqrt{(1+K^2)\cdot\left[(1+y_2)^2 + (y_2 K)^2\right]}}{K^2} \tag{5.19}$$

Similarly, by inserting equations (5.5b)-(5.5c), (5.10)-(5.11) into (5.9), we get

$$Z_A = Z_0 \cdot \sqrt{A \cdot B} \tag{5.20}$$

where

$$A = \frac{Y_{ee}(f_2)}{Y_A} = ky_1 + \frac{K + (y_B + y_2)\cdot k}{1 - (y_B + y_2)\cdot k \cdot K} \tag{5.21}$$

$$B = \frac{-Y_{eo}(f_2)}{Y_A} = \frac{y_1}{k} - \frac{K + y_B \cdot k - \frac{y_2}{k}}{1 - \left(y_B \cdot k - \frac{y_2}{k}\right)\cdot K} \tag{5.22}$$

Consequently, the remaining unknowns can thus be evaluated by the following formulas:

$$Z_B = \frac{Z_A}{y_B} \tag{5.23}$$

$$Z_1 = \frac{Z_A}{y_1} \tag{5.24}$$

$$Z_2 = \frac{Z_A}{y_2} \tag{5.25}$$

Furthermore, the transmission phase of the crossover (S_{31}) may be determined from (5.26).

$$\angle S_{31}(f_2) = -\angle S_{31}(f_1) = -2\tan^{-1}\sqrt{\frac{A}{B}} \tag{5.26}$$

Accordingly, for a given value of f2/f1, the required line impedances can be found using (5.10) - (5.11) and (5.18) - (5.25), where y_2 is a free parameter to be varied for ease of circuit construction.

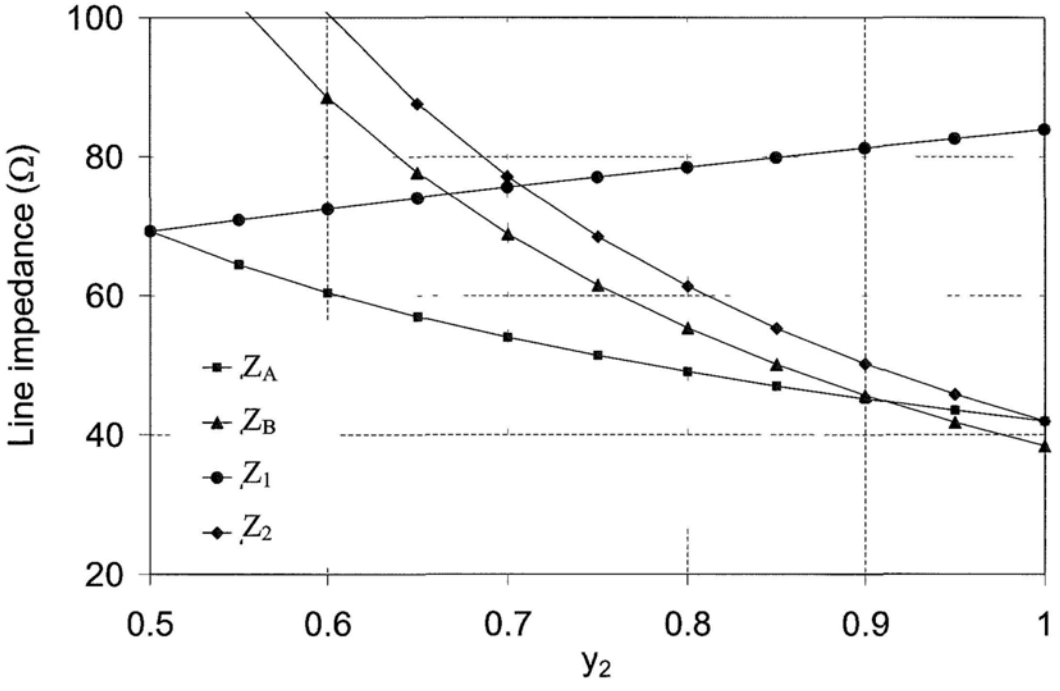

(a)

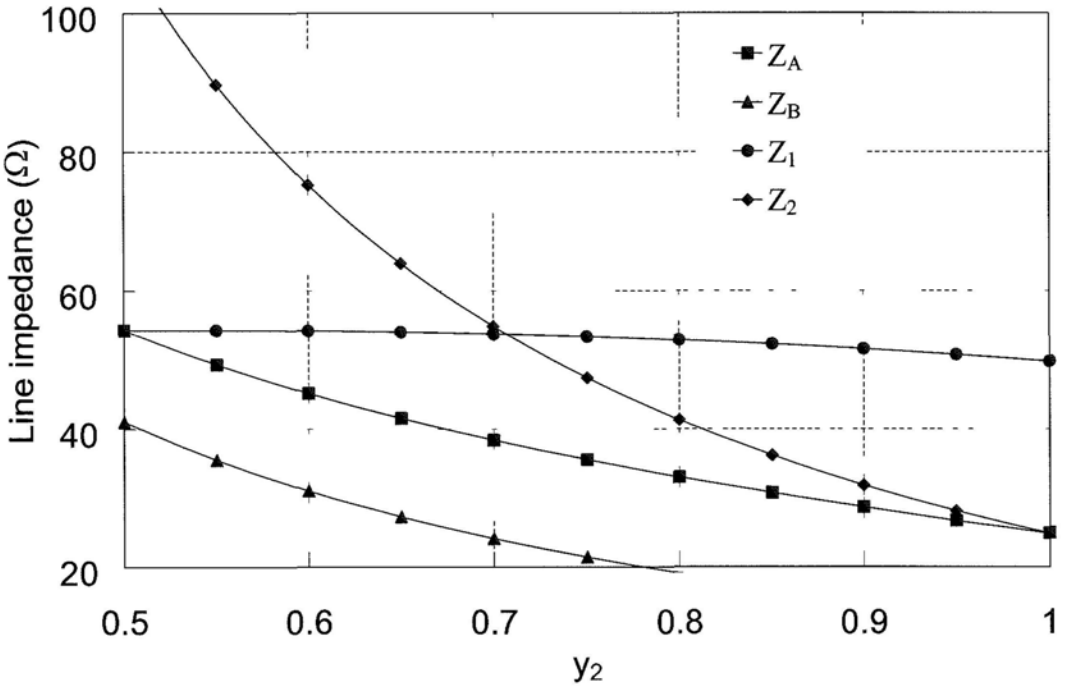

(b)

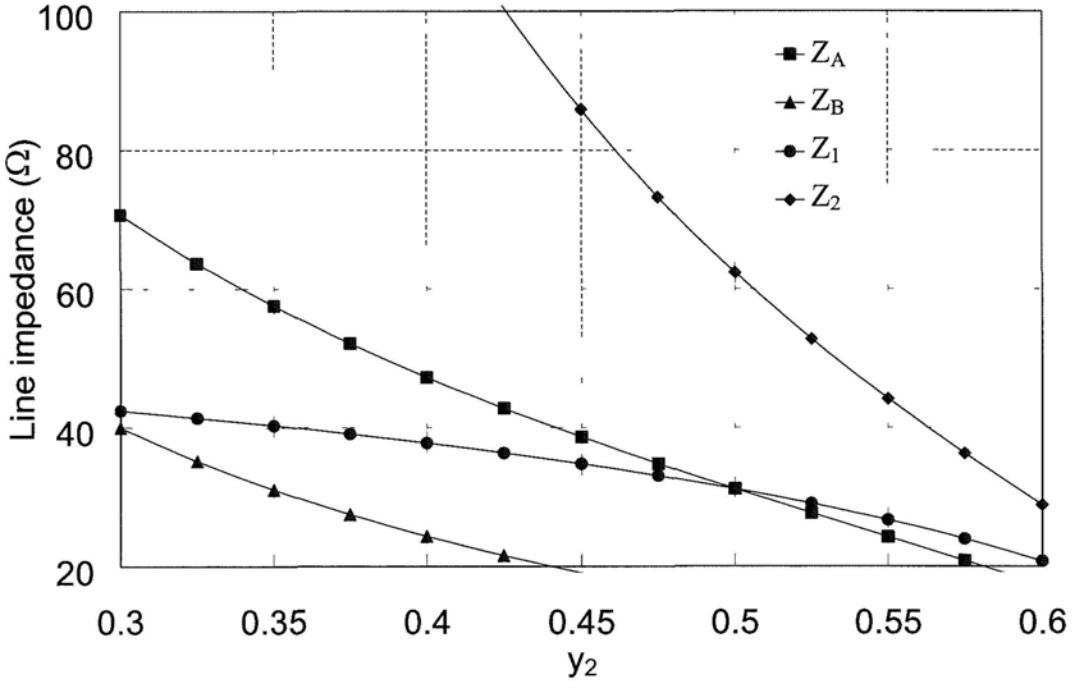

(c)

Figure 5-3: Line impedance versus y_2, with f_2/f_1 equals (a) 1.2, (b) 1.8 and (c) 2.25.

For illustration, Figure 5-3 shows the variations of the computed line impedances versus y_2, for $f_2/f_1 = 1.2$, 1.8 and 2.25. These graphs indicate that the preferred range of y_2 is from 0.6 to 1.0 when $f_2/f_1 = 1.2$, based on impedance value lying between 20 Ω and 100 Ω. When $f_2/f_1 = 1.8$, a lower value of y_2 (< 0.7) should be chosen.

5.2 Simulation results

The proposed dual-band crossover is usable for $1 < f_2/f_1 < 2$. For verification, $f_2/f_1 = 1.5$ (f_1 = 1 GHz, f_2 = 1.5 GHz) and y_2 = 0.65 were chosen. Subsequently, the corresponding line impedances were found to be: $Z_A = 51.1\ \Omega$, $Z_B = 48.2\ \Omega$, $Z_1 = 66.5\ \Omega$ and $Z_2 = 78.7\ \Omega$.

For performance evaluation, the return loss, port isolation and insertion loss response of the crossover were simulated (Figure 5-4 and Figure 5-5). Ideal performances (return loss, port isolation and insertion loss) were observed at both f_1 and f_2, as expected. An operating bandwidth of approximately 30MHz was found based on a minimal port isolation of 20dB. On the other hand, an operating bandwidth of roughly 70MHz was attained based upon a maximum insertion loss of 0.5dB.

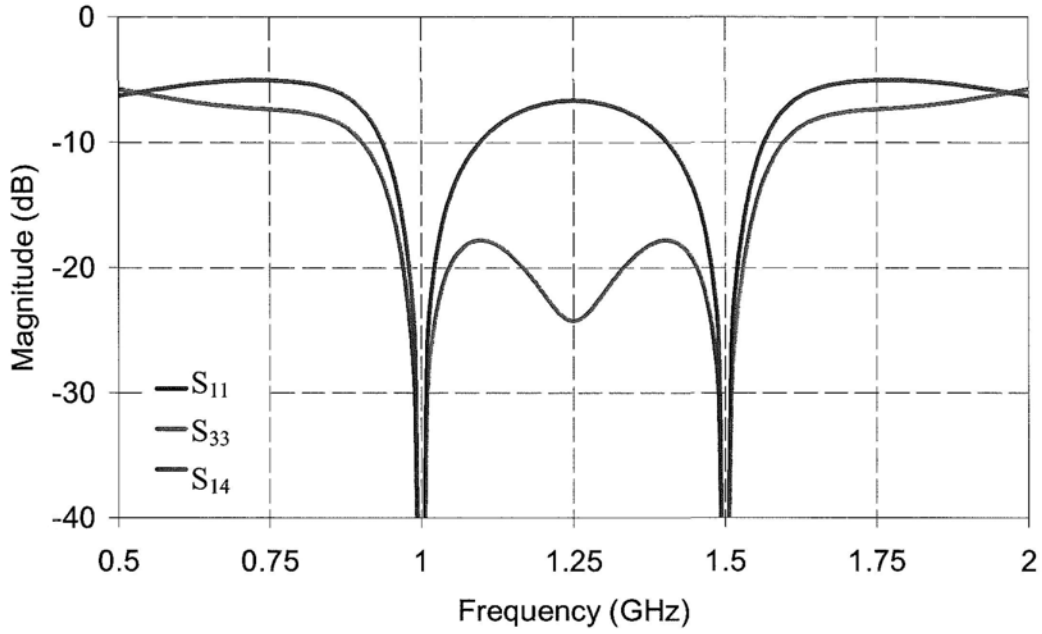

Figure 5-4: Simulated return loss and port isolation.

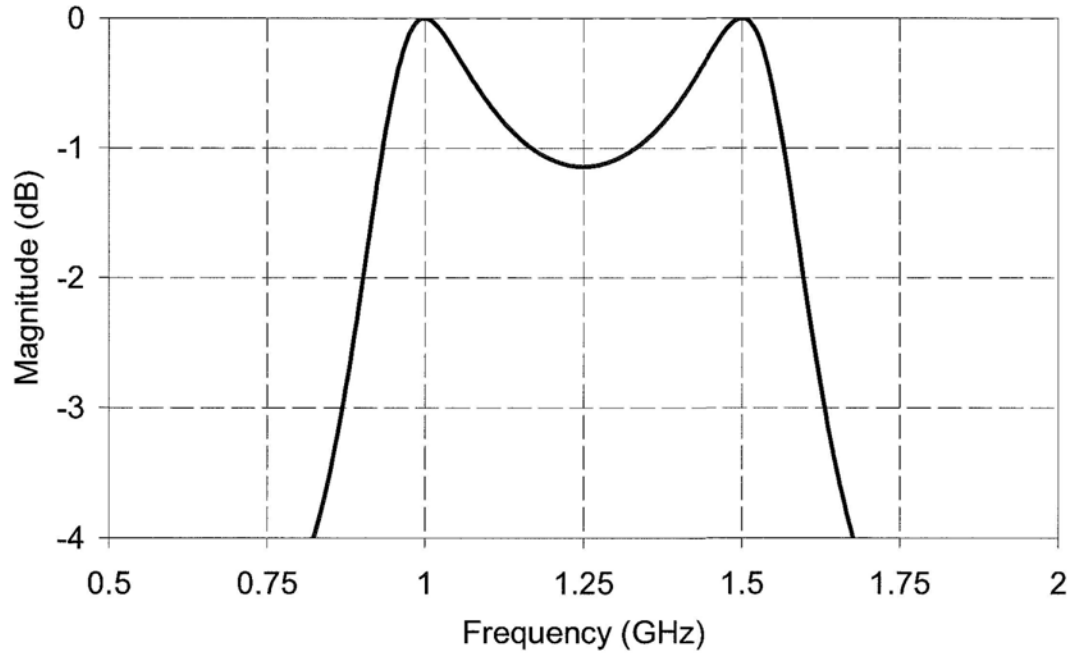

Figure 5-5: Simulated insertion loss.

5.3 Experimental results

A crossover junction operating at 800 MHz and 1.2 GHz (i.e. $f_2/ f_1 = 1.5$) was prototyped and characterized. This circuit was fabricated using microstrip on Duroid substrate. For $y_2 = 0.85$, the values of Z_A, Z_B, Z_1 and Z_2 were found to be 40.1Ω, 31.9Ω, 69.9Ω and 48.3Ω, respectively. Figure 5-6 shows the top view of the fabricated circuit. The area of core design is approximately $\lambda g/4 \times \lambda g/4$.

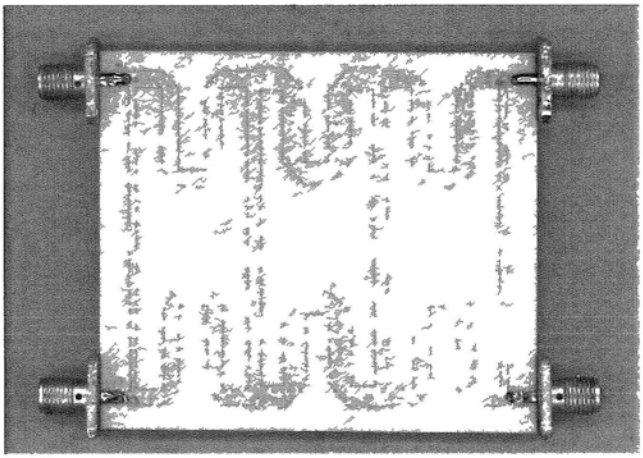

Figure 5-6: Photograph of the fabricated crossover junction.

Figure 5-7 and Figure 5-9 give the measured performance of the prototype. It is seen that dual-band operation has been achieved with a slight deviation in center frequencies (790 and 1195 MHz). Regarding the two frequency bands, the circuit was found to exhibit an insertion loss of 0.4 ± 0.1 dB and minimum return loss and port isolation of 20dB, over an operating bandwidth of approximately 35 MHz. It is believed that the small discrepancies between the simulated and measured results were mainly caused by the junction discontinuities, the substrate effect and the

tolerances of the in-house fabrication process.

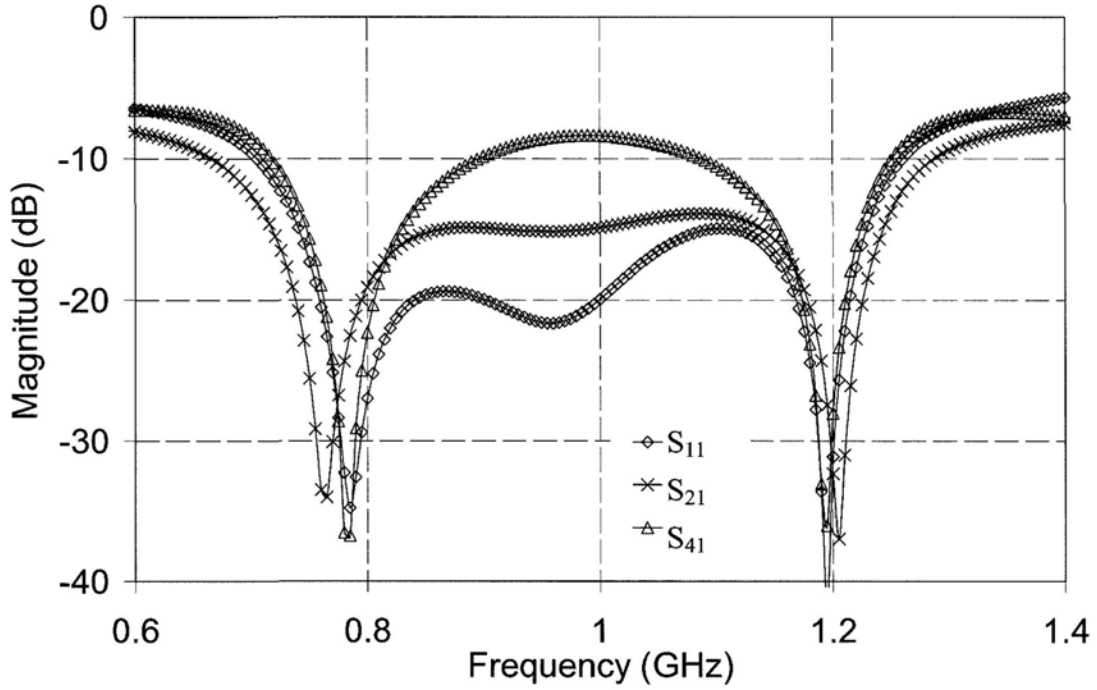

Figure 5-7: Measured return loss and port isolation (crossover).

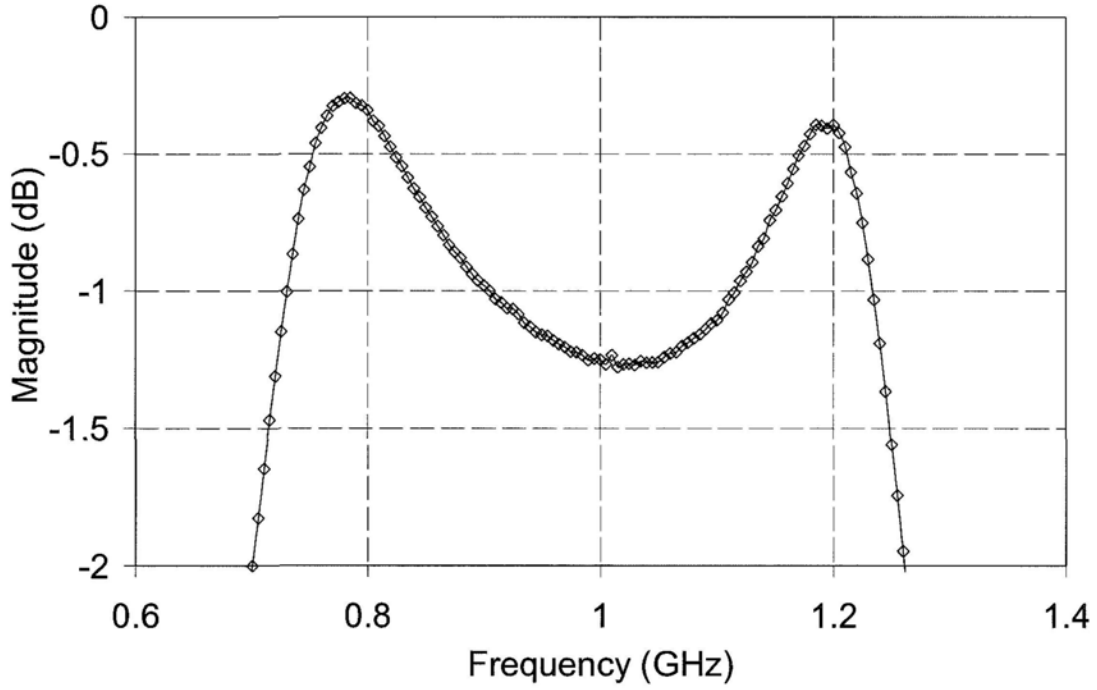

Figure 5-8: Measured insertion loss (crossover).

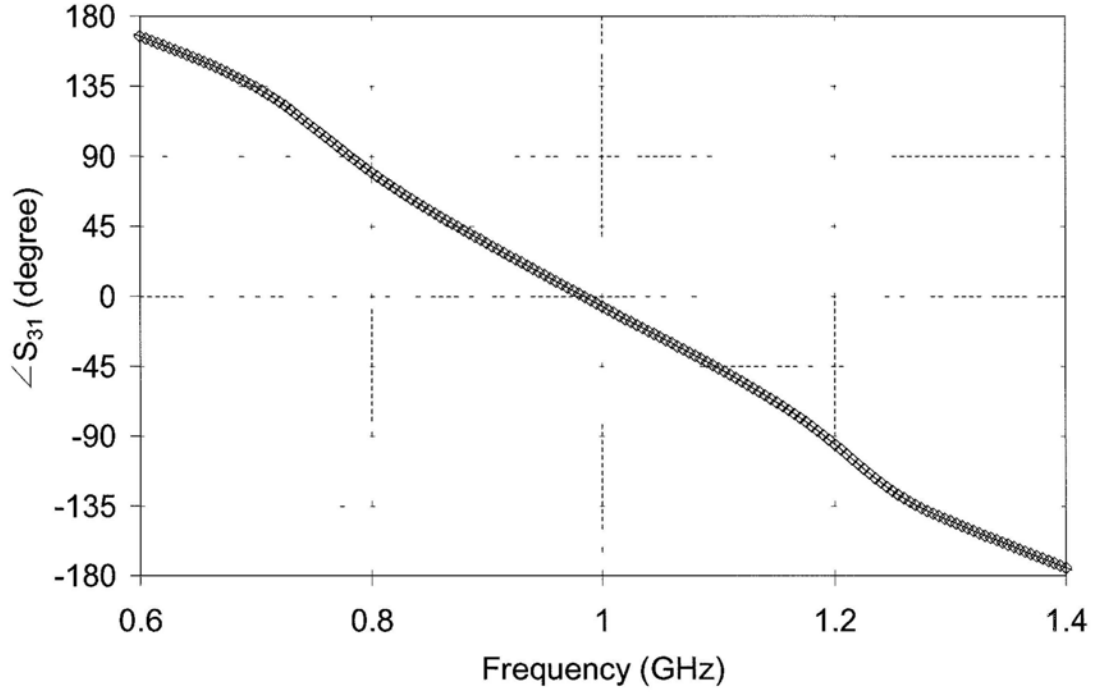

Figure 5-9: Measured phase response (crossover).

5.4 Summary

A first planar dual-band crossover junction is proposed in this section. It is structured as tri-section branch line coupler. With proper selection of line impedance, dual band frequency response is attained. The frequency ratio (f_2 / f_1) of the design is up to 1.8. A dual band cross over junction operating at 800 MHz and 1.2 GHz (i.e. f_2/ f_1 = 1.5) was prototyped and characterized and measurement is agreed with the simulated results. It features low insertion loss, high port isolation and it is useful in dual band applications with small working bandwidth.

Chapter 6. Conclusion and Recommendation for Future Work

Microwave passive couplers play a major role in wireless communication systems as they can provide power combining, power splitting and power diversion with designated phase relationship. Hence, these devices are widely used in power amplifier module, mixer design and antenna array module. Planar realization is desirable due to its low fabrication cost, simplicity in structure as well as popularity. Advanced techniques for size miniaturization and bandwidth enhancement of passive devices have been thoroughly studied in the past decades. Nonetheless, modern wireless systems demand multi-band and multi-mode operation, and hence, the development of new devices capable of meeting these requirements, has expanded substantially in recent years.

Three new types of dual-band passive devices have been described in this thesis: Rat-race coupler, power divider and crossover junction. These circuits are the first batch of passive couplers made available for dual-band operation, though they are limited in performances in bandwidth, awaiting further improvement.

1. Dual-band rat-race coupler: Three different topologies of dual-band rat-race couplers have been proposed. They are similar in structure. The first design is the largest in size. It can offer dual-band operation with a large value of f_2/f_1 (>2). The second design operates with f_2/f_1 of less than 1.75. Its major drawback is the requirement of ground vias for construction. The third design is small in size and simple in structure (no via connection). The range of f_2/f_1 is from 1.7 to 2.9. For all proposed topologies, explicit closed-form equations are made available for the evaluation of circuit parameters (line impedance). The presence of shunt stubs also serve to provide transmission zeros for inter-band rejection. These designs are found to exhibit low insertion loss, good return loss and port isolation.
2. Dual-band power divider: this is the first fully distributed design with ideal port isolation at both centre frequencies. For dual-band operation, a newly proposed dual-band quarter-wavelength impedance transformer is embedded in a conventional Wilkinson power divider and, with the insertion of a shunt stub at the input port. Either short or open-circuited stub may be used depending on the range of f_2/f_1 to be covered.
3. Dual-band crossover junction: It can be also regarded as a 0-dB coupler and is evolved from a trisection branch-line coupler. By the proper selection of line impedances, the design can be made to operate as either a wide-band or dual-band

crossover with compact size. It can offer low insertion loss and high port isolation performance but with a small operating bandwidth.

All the proposed designs can easily be implemented in microstrip with line impedance ranging from 20 Ω to 100 Ω. Other transmission line structures may also be considered including strip-line, CPW, etc.

Although the proposed dual-band circuits can eliminate the use of wide-band devices and occupy a smaller substrate area, they are narrow in bandwidth (a few %) and do not operate at large value of f_2/f_1 (e.g. > 3). Advanced designs, capable of operating with a wide bandwidth and large frequency band ratio (f_2/f_1), without extreme line impedance, and therefore, the future research towards the development of low cost, miniaturized, multi-band RF frontend.

Reference List

[1] D. M. Pozar, "Microwave Engineering," 2nd edition, John Wiley & Sons. Inc., New York, 1998.

[2] Y. C. Chiang, and C. Y. Chen, "Design of lumped element quadrature hybrid," *IEE Electronics Letters*, vol. 34, no. 5, pp. 465-467, 5th March 1998.

[3] R. K. Settaluri, G. Sundberg, A. Weisshaar, and V. K. Tripathi, "Compact folded line rat-race hybrid couplers," *IEEE Microwave and Wireless Component Letters*, vol. 10, no.2, pp. 61-63, Feb. 2000.

[4] K. W. Eccleston, and S. H. M. Ong, "Compact planar microstripline branch-line and rat-race couplers," *IEEE Trans. Microwave Theory Tech.*, vol. 51, no. 10, pp. 2119–2125, Oct. 2003.

[5] D. I. Kim, and Y. Naito, "Broad-band design of improved hybrid-ring 3-dB directional couplers," *IEEE Trans. Microwave Theory & Tech.,* vol. 30, no. 11, pp. 2040-2046, Nov. 1982.

[6] R. W. Vogel, "Analysis and design of lumped- and lumped-distributed-element directional couplers for MIC and MMIC applications," *IEEE Trans. Microwave Theory & Tech.*, vol. 40, no. 2, pp. 253-262, Feb. 1992.

[7] C.-H. Ho; L. Fan; K. Chang, "Broad-band uniplanar hybrid-ring and branch-line couplers," *IEEE Trans. Microwave Theory & Tech.*, vol. 41, no. 12, pp. 2116-2125, Dec. 1993.

[8] Kwok-Keung M. Cheng, and Fai-Leung. Wong, "A novel approach to the design and implementation of dual-Band, compact, planar, 90° branch-line coupler", *IEEE Trans. Microwave Theory Tech.*, vol. 52, pp. 2458–2463, Nov. 2004.

[9] Myun-Joo Park, "Dual-band, unequal length branch-line coupler with center-tapped stubs", *IEEE Microwave and Wireless Component Letters*, vol. 19, no.10, pp. 617-619, Oct. 2009.

[10] Hyunchil Kim, Byungje Lee and Myun-Joo Park, "Dual-band branch-line coupler with port extensions", *IEEE Trans. Microwave Theory Tech.*, vol. 58, pp. 651-655, Mar. 2010.

[11] Ching-Luh Hsu, Chin-Wei Chang, Jen-Tsai Kuo, "Design of dual-band microstrip rat race coupler with circuit miniaturization," *Microwave Symposium, 2007. IEEE/MTT-S International*, pp.177-180, 3-8 June 2007.

[12] Yi-Chyun Chiou, Jen-Tsai Kuo, Chi-Hung Chan, "New miniaturized dual-band rat-race coupler with microwave C-sections," *Microwave Symposium Digest, 2009. MTT '09. IEEE MTT-S International*, pp.701-704, 7-12 June 2009.

[13] Kuo-Sheng Chin, Ken-Min Lin, Yen-Hsiu Wei; Tzu-Hao Tseng, Yu-Jie Yang, "Compact dual-band branch-line and rat-race couplers with stepped-impedance-stub lines", *IEEE Microwave Theory and Techniques,* vol.58, no.5, pp.1213-1221, May 2010.

[14] S. Srisathit, M. Chongcheawchamnan, and A. Worapishet, "Design and realization of dual-band 3 dB power divider based on two-section transmission-line topology," *IEE Electronics Letters*, vol. 39, no. 9, pp. 723-724, 1st May 2003.

[15] L. Wu, H. Yilmaz, T. Bitzer, A. Pascht, and M. Berroth, "A dual-frequency Wilkinson power divider: for a frequency and its first harmonic," *IEEE Microwave and Wireless Components Letters*, vol. 5, no. 2, pp. 107-109, Feb. 2005.

[16] L. Wu, SZ. Sun, H. Yilmaz, and M. Berroth, "A dual-frequency Wilkinson power divider," *IEEE Trans. Microwave Theory Tech.*, vol. 54, no. 1, pp. 278–284, Jan. 2006.

[17] Kwok-Keung M. Cheng, and Fai-Leung. Wong, "A novel rat race coupler design for dual-band applications", *IEEE Microwave and Wireless Components Letters,* vol. 15, no. 8, pp. 521–523, Aug. 2005.

[18] Fai-Leung Wong and Kwok-Keung M. Cheng, "A novel rat race coupler design for dual-band applications", *IEEE Asia-Pacific Microwave Conference Proceedings,* vol. 2, pp. 667-670, Yokohama, Japan, Dec 2006.

[19] Kwok-Keung M. Cheng, and Fai-Leung Wong, "Dual-band rat-race coupler design using tri-section branch-line", *IEE Electronic Letters,* vol. 43, no. 6, pp. 41-42, March. 2007.

[20] Kwok-Keung M. Cheng, and Fai-Leung Wong, "A new Wilkinson power divider design for dual band application", *IEEE Microwave and Wireless Components Letters,* vol. 17, no. 9, pp. 664-666, Sept. 2007.

[21] Fai-Leung Wong and Kwok-Keung M. Cheng, "A novel, planar and compact crossover design for dual-band applications", *IEEE Trans. Microwave Theory Tech.*, accepted.

[22] Wilkinson, E. J., "An N-way hybrid power divider," Microwave Theory and Techniques, IRE Transactions on, vol.8, no.1, pp.116-118, January 1960.

[23] Jeng-Sik Lim, Sung-Won Lee, Chul-Soo Kim, Jun-Seek Park, Dal Ahn, Sangwook Nam, "A 4.1 unequal Wilkinson power divider," *IEEE Microwave and Wireless Components Letters,* vol.11, no.3, pp.124-126, Mar 2001.

[24] Seongmin Oh, Jae-Jin Koo, Mun-Su Hwang, Chunseon Park, Yong-Chae Jeong, Jong-Sik Lim, Kwan-Sun Choi, Dal Ahn, "An unequal Wilkinson power divider with variable dividing ratio," *Microwave Symposium, 2007. IEEE/MTT-S International*, pp.411-414, 3-8 June 2007.

[25] Zhu, Y.-Z., Zhu, W.-H., Zhang, X.-J., Jiang, M., Fang, G.-Y., "Shunt-stub Wilkinson power divider for unequal distribution ratio," *IET Microwaves, Antennas & Propagation,* vol.4, no.3, pp.334-341, March 2010.

[26] Eccleston, K.W., "N-way microwave power divider using two-dimensional meta-materials," *IEE Electronics Letters* , vol.42, no.15, pp. 863- 864, 20 July 2006.

[27] Eccleston, K.W., Junyao Zong, "Implementation of a microstrip square planar N-way metamaterial power divider," *IEEE Microwave Theory and Techniques,* vol.57, no.1, pp.189-195, Jan. 2009.

[28] Collado C., Grau Alfred, and De Flaviis F., "Dual-band butler matrix for WLAN systems," in *IEEE MTT-S Int. Dig.*, June 2005, pp. 2247–2250.

[29] J. S. Wight, W. J. Chudobiak, and V. Makios, "A microstrip and stripline crossover structure," *IEEE Trans. Microwave Theory & Tech.*, vol. 24, no. 5, pp. 270, May 1976.

[30] D. V. Kholodniok and I. Vendik, "A novel type of 0-dB diecrtional coupler for microwave integrated circuits," *Proc. 29th Eur. Microwave Conf.*, Nov. 1999, pp. 341–344.

[31] D. V. Kholodniok, G. Kalinin, E. Vernoslova, and I. Vendik, "Wideband 0-dB branch-line directional couplers," in *IEEE MTT-S Int. Dig.*, June 2000, pp. 1307–1310.

[32] Y. Chen and S. P. Yeo, "A symmetrical four-port microstrip coupler for crossover application," *IEEE Trans. Microwave Theory & Tech.,* vol. 55, no. 11, pp. 2434-2438, Nov. 2007.

[33] Y. C. Chiou, J. T. Kuo, and H. R. Lee, "Design of compact symmetric four-port crossover junction," *IEEE Microwave and Wireless Components Letters*, vol. 19, no. 9, pp. 545–447, Sept. 2009.

[34] R. E. Collin, Foundations for Microwave Engineering, 2nd ed. McGraw-Hill, New York, 1992.

[35] A. S. Mohra and M. A. Alkanhal, "Dual band Wilkinson power dividers using T-sections," *Journal of Microwave and Optoelectronic Electromagnetic Applications*, vol. 7, no. 2, pp. 83-90, Dec. 2008.

[36] H. Zhang and K. J. Chen, "A stub tapped branch-line coupler for dual-band operations," *IEEE Microwave and Wireless Components Letters*, vol. 17, no. 2, pp. 106-108, Feb. 2007.

[37] S. Y. Yuan *et al.*, "An extremely compact dual-band branch-line coupler," *IEEE Microwave Optical Technology Letters*, vol. 49, no. 12, pp. 3011-3014, Dec. 2007.

[38] Myun-Joo Park and Byungje Lee, "A dual band Wilkinson power divider," *IEEE Microwave and Wireless Components Letters*, vol. 18, no. 2, pp. 85-87, Feb. 2008.

[39] Kwok-Keung M. Cheng, and Carlos Law, "A novel approach to the design and implementation of dual-band power divider", *IEEE Trans. Microwave Theory Tech.*, vol. 56, no. 2, pp. 487–492, Feb. 2008.

[40] C. Monzon, "A small dual-frequency transformer in two sections," *IEEE Trans. Microwave Theory & Tech.*, vol. 51, no. 4, pp. 1157-1161, April 2003.

[41] Karun Rawat and F. M. Ghannouchi, "A design methodology for miniaturized power dividers using periodically loaded slow wave structure with dual-band applications", *IEEE Trans. Microwave Theory Tech.*, vol. 56, no. 2, pp. 487–492, Feb. 2008.

[42] Jia-Sheng Hong and Lancaster M. J., "Theory and experiment of novel microstrip slow-wave open-loop resonator filters", *IEEE Trans. Microwave Theory Tech.*, vol. 45, no. 12, pp. 2358-2365, Dec. 1997.

[43] Ching Kuo Wu, Hsien-Shun Wu and Ching-Kuang Cliver Tzuang, "Electric-magnetic-electric slow-wave microstrip line and bandpass filter of compressed size", *IEEE Trans. Microwave Theory Tech.*, vol. 50, no. 8, pp. 1996-2004, Aug. 2002.

[44] Pei-Ling Chi, Waterhouse R and Itoh T., "Antenna miniaturization using slow wave enhancement factor from loaded transmission line models", *IEEE Trans. Antennas and Propagation*, vol. 59, no. 1, pp. 48-57, Jan. 2011.

[45] Yi-Chyun Chiou, Shih-Wei Lai and Jen-Tsai Kuo, "Analysis and design of double-ring crossover junction with arbitrary diagonal port impedances", *IEEE Asia-Pacific Microwave Conference Proceedings,* vol. 2, pp. 2092-2095, Singapore, Dec 2009.

Author's Publication List

1. **Fai-Leung Wong**, and Kwok-Keung M. Cheng, "A Novel Planar Branch-Line Coupler For Dual-Band Applications", *IEEE MTT-S International Microwave Symposium Digest,* vol. 2, pp.903-906, Texas, U.S., June 2004.
2. Kwok-Keung M. Cheng, and **Fai-Leung Wong**, "A Novel Approach to the Design and Implementation of Dual-Band, Compact, Planar, 90° Branch-Line Coupler", *IEEE Trans. Microwave Theory Tech.,* vol. 52, pp. 2458–2463, Nov. 2004.
3. Kwok-Keung M. Cheng, and **Fai-Leung Wong**, "A Novel Rat Race Coupler Design For Dual-Band Applications", *IEEE Microwave and Wireless Components Letters,* vol. 15, no. 8, pp. 521–523, Aug. 2005.
4. **Fai-Leung Wong** and Kwok-Keung M. Cheng, "A Compact Rat Race Coupler Design For Dual-Band Applications", *IEEE Asia-Pacific Microwave Conference Proceedings,* vol. 2, pp. 667-670, Yokohama, Japan, Dec 2006.
5. Kwok-Keung M. Cheng, and **Fai-Leung Wong**, "Dual-band rat-race coupler design using tri-section branch-line", *IEE Electronic Letters,* vol. 43, no. 6, pp. 41-42, March. 2007.
6. Kwok-Keung M. Cheng, and **Fai-Leung Wong**, "A New Wilkinson Power Divider Design For Dual Band Application", *IEEE Microwave and Wireless Components Letters,* to be published, Sept. 2007.
7. Ho-Yan Yim, **Fai-Leung Wong** and Kwok-Keung M. Cheng, "A New Synthesis Method for Dual-Band Microwave Filter Design with Controllable Bandwidth", *IEEE Asia-Pacific Microwave Conference Proceedings,* pp. 1791-1794, Bangkok, Thailand, Dec 2007.
8. **Fai-Leung Wong** and Kwok-Keung M. Cheng, "A Novel, Planar and Compact Crossover Design for Dual-band Applications", *IEEE Trans. Microwave Theory Tech.*, vol. 59, pp. 568-573, Mar. 2011.

Appendix I – Transformation between S- and ABCD-parameters of two-port network

$$S_{11} = \frac{A + \frac{B}{Z_0} - CZ_0 - D}{\Delta}$$

$$S_{22} = \frac{-A + \frac{B}{Z_0} - CZ_0 + D}{\Delta}$$

$$S_{21} = \frac{2}{\Delta}$$

$$S_{12} = \frac{2(AD - BC)}{\Delta}$$

$$\Delta = A + \frac{B}{Z_0} + CZ_0 + D$$

$$A = \frac{(1 + S_{11})(1 - S_{22}) + S_{12}S_{21}}{2S_{21}}$$

$$B = Z_o \frac{(1 + S_{11})(1 + S_{22}) - S_{12}S_{21}}{2S_{21}}$$

$$C = \frac{(1 - S_{11})(1 - S_{22}) - S_{12}S_{21}}{2S_{21}Z_o}$$

$$D = \frac{(1 - S_{11})(1 + S_{22}) + S_{12}S_{21}}{2S_{21}}$$

Appendix II –ABCD- parameters of several two-port networks

Circuit	ABCD Parameters
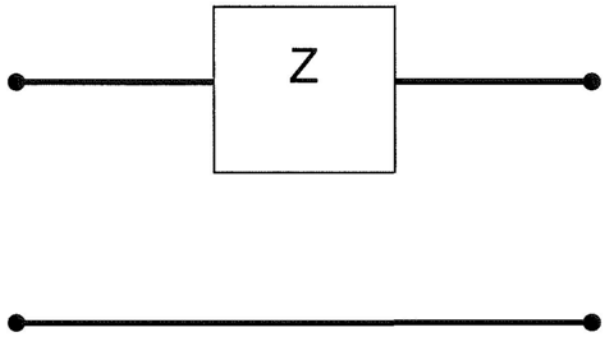	$\begin{bmatrix} A & B \\ C & D \end{bmatrix} = \begin{bmatrix} 1 & Z \\ 0 & 1 \end{bmatrix}$
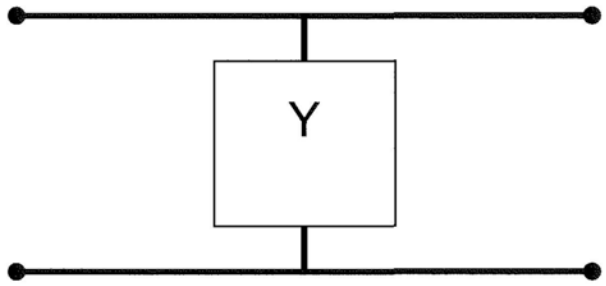	$\begin{bmatrix} A & B \\ C & D \end{bmatrix} = \begin{bmatrix} 1 & 0 \\ Y & 1 \end{bmatrix}$
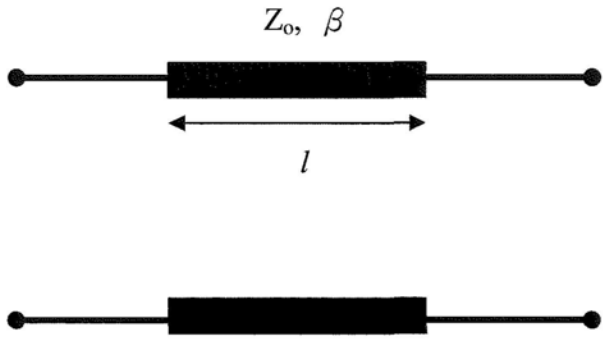	$\begin{bmatrix} A & B \\ C & D \end{bmatrix} = \begin{bmatrix} \cos\beta l & jZ_o \sin\beta l \\ jY_o \sin\beta l & \cos\beta l \end{bmatrix}$